

The role of cardiomyocyte calcium handling for the impaired contractile function after myocardial infarction in diabetic and non- diabetic hearts

Inaugural dissertation

for the attainment of the doctoral degree
in the Faculty of Mathematics and Natural Sciences
at the Heinrich Heine University Düsseldorf

presented by

Tanu Srivastava
from India

Düsseldorf, September 2023

from the Institute for Pharmacology
at the Heinrich Heine University Düsseldorf

Published by permission of the
Faculty of Mathematics and Natural Sciences
at Heinrich Heine University Düsseldorf

Supervisor: Prof. Dr. Joachim P. Schmitt
Co-supervisor: Prof. Dr. Jörg Breitzkreutz
Date of the oral examination: 05/02/2024

Table of Contents

1	Introduction.....	1
1.1	Myocyte Ca^{2+} cycle.....	1
1.1.1	Effects of β -adrenergic receptor stimulation on myocyte Ca^{2+} cycling.....	1
1.1.2	Excitation-contraction coupling (ECC) in Cardiac Muscle.....	3
1.1.3	Regulators of the Ca^{2+} cycle	4
1.2	Sarcomere function of cardiomyocytes	8
1.3	Acute myocardial infarction	10
1.4	Ischemic area, peripheral area, and non-ischemic area.....	12
1.4.1	Ischemic Area	13
1.4.2	Non-ischemic area (remote area)	14
1.5	Interaction of Ca^{2+} homeostasis and myocardial ischemia-reperfusion.....	15
1.5.1	Ca^{2+} homeostasis in myocardial ischemic injury	15
1.5.2	Ca^{2+} homeostasis in myocardial reperfusion injury	16
1.5.3	Sarcomere function in myocardial I/R injury.....	17
1.5.4	Myocardial dysfunction in the RM	18
1.6	Period after myocardial infarction	18
1.7	Experimental models for I/R	19
1.7.1	Ischemia induction with closed thorax.....	19
1.8	Type II diabetes mellitus is a risk factor for myocardial infarction	20
1.8.1	Diabetes mellitus.....	22
1.8.2	Mouse model for diabetes mellitus type II.....	23
1.9	Diet-induced obesity (DIO)	23
1.10	Ischemic conditioning.....	25
1.10.1	Ischemic conditioning of the heart.....	25
1.10.2	Remote ischemic conditioning	26
1.11	Questions	28
2	Material and Methods.....	30
2.1	Animal testing	30
2.1.1	Animals used.....	30
2.1.2	Initiation of myocardial infarction.....	30
2.2	Measurements on isolated cardiomyocytes	33
2.2.1	Isolation of cardiomyocytes by retrograde perfusion.....	33
2.2.2	Measurement of the myocyte Ca^{2+} cycle	37
2.2.3	Measurement of sarcomere length	41
2.2.4	Evaluation of Ca^{2+} transients and sarcomere function	42
2.3	Protein analysis	45
2.3.1	Work steps	45

2.3.2	Production of the heart lysates	45
2.3.3	Quantitative detection of the amount of protein using the BCA method	46
2.3.4	Polyacrylamide gel electrophoresis (SDS-PAGE)	47
2.3.5	Western blot.....	48
2.3.6	Western Blot Imaging.....	49
2.4	Statistics	50
3	Results	51
3.1	Diabetes mellitus type II	51
3.1.1	Size and velocity of intracellular Ca^{2+} cycle.	51
3.1.2	Sarcomere function	54
3.1.3	Expression of Ca^{2+} regulatory proteins in the remote myocardium.....	57
3.1.4	Activity measurement of regulators of myocytic Ca^{2+} cycle.	59
3.2	Diet-induced obesity (DIO)	62
3.2.1	Size and velocity of intracellular Ca^{2+} cycle.	63
3.2.2	Sarcomere function	65
3.3	RIC dialysates	68
3.3.1	Effects of plasma dialysates without hypoxia on myocyte Ca^{2+} cycling	68
3.3.2	Effects of plasma dialysates from humans before and after RIC on myocyte sarcomere function of cardiomyocytes without hypoxia	70
3.3.3	Effects of hypoxia on cardiomyocyte Ca^{2+} cycling	72
3.3.4	Effects of hypoxia on sarcomere function	74
3.3.5	Effects of plasma dialysates from humans before and after RIC on myocyte Ca^{2+} cycling after transient hypoxia	76
3.3.6	Effects of plasma dialysates on myocyte sarcomere function of cardiomyocytes after transient hypoxia	78
4	Discussion	81
4.1	Diabetes mellitus type II	81
4.1.1	Slowed intracellular Ca^{2+} kinetics in <i>remote</i> cardiomyocytes of db/db mice 10 days after I/R	81
4.1.2	Preserved sarcomere function in <i>remote</i> cardiomyocytes of db/db mice 10 days after I/R.	84
4.1.3	Unchanged protein expression of regulators of the myocyte Ca^{2+} cycle.	84
4.1.4	Unchanged activity of regulators of the Ca^{2+} cycle.	85
4.2	Diet-induced obesity	86
4.2.1	Changed myofilament Ca^{2+} kinetics in high-fat diet-induced obesity mouse cardiomyocytes.	87
4.2.2	Changed sarcomere function.....	88
4.3	RIC dialysates	88
4.3.1	Dialysates from blood samples post remote IPC enhance Ca^{2+} cycling and sarcomere contraction and relaxation in cardiomyocytes without hypoxia.....	89

4.3.2	Hypoxia and reoxygenation impair cardiomyocyte Ca^{2+} cycling and sarcomere function	90
4.3.3	Dialysates from blood samples post remote RIC enhance Ca^{2+} cycling in cardiomyocytes after hypoxia	90
4.3.4	RIC dialysates did not enhance sarcomere function of cardiomyocytes after hypoxia in the used experimental model	91
5	Outlook	92
6	Summary	94
7	Zusammenfassung	95
8	Abbreviation	96
9	List of Figures	98
10	List of Tables	101
11	References	102
12	Resume	113
13	Acknowledgement	114

1 Introduction

1.1 Myocyte Ca^{2+} cycle

Calcium ions (Ca^{2+}) have an important role in signal transduction pathways where they act as intracellular second messenger, involved in many functional regulatory processes (e.g., blood clotting, coagulation factors, bone mineralization, mitochondrial function etc.) [1]. Especially, they are responsible for triggering contraction of all muscle cell types. Ca^{2+} regulates the electromechanical coupling of excitation and contraction in cardiomyocytes [2]. If the concentration of Ca^{2+} in the cytosol increases, cardiac myocytes contract and if cytosolic Ca^{2+} concentration decreases relaxation is initiated. Electrophysiological signaling by Ca^{2+} in ventricular cardiomyocytes is shown in Figure 1.1.

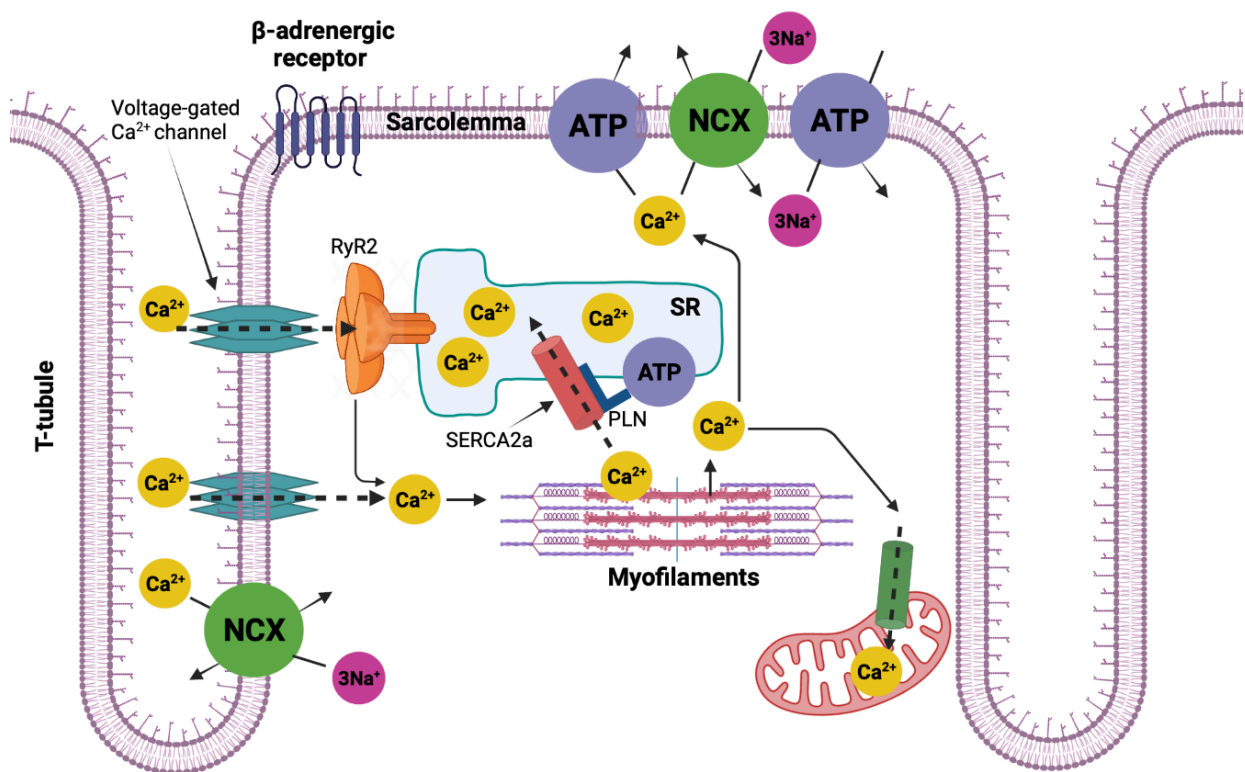


Figure 1.1: Schematic representation of the myocyte Ca^{2+} cycle in a ventricular cardiomyocyte. T-tubule = transverse tubule; ATP = adenosine triphosphate; Ca^{2+} = calcium ion; Na^+ = sodium; NCX = sodium-calcium exchanger; PLN = phospholamban; RyR2 = ryanodine receptor 2; SERCA2a = sarco/endoplasmic reticulum calcium ATPase 2a; SR = sarcoplasmic reticulum.

1.1.1 Effects of β -adrenergic receptor stimulation on myocyte Ca^{2+} cycling

The β -adrenergic is a prototypical Gs-coupled receptor. When an agonist binds to the receptor, it results in activation of the Gs-protein, subsequent activation of adenylate cyclase (AC), following the elevation of the intracellular level of cyclic adenosine monophosphate (cAMP), and the successive activation of protein kinase A (PKA) (Figure 1.2). PKA phosphorylates a set of key

regulatory proteins that control the excitation–contraction coupling cycle, such as sarcoplasmic ryanodine receptors (RyR2), sarcolemmal L-type Ca^{2+} channels, and phospholamban (PLN), which together coordinate calcium cycling kinetics, thereby significantly increasing contraction and relaxation of sarcomeres [3], [4]. cAMP induces phosphorylation of LTCC and RyR2 to increase the amount of intracellular Ca^{2+} necessary for heart contractility.

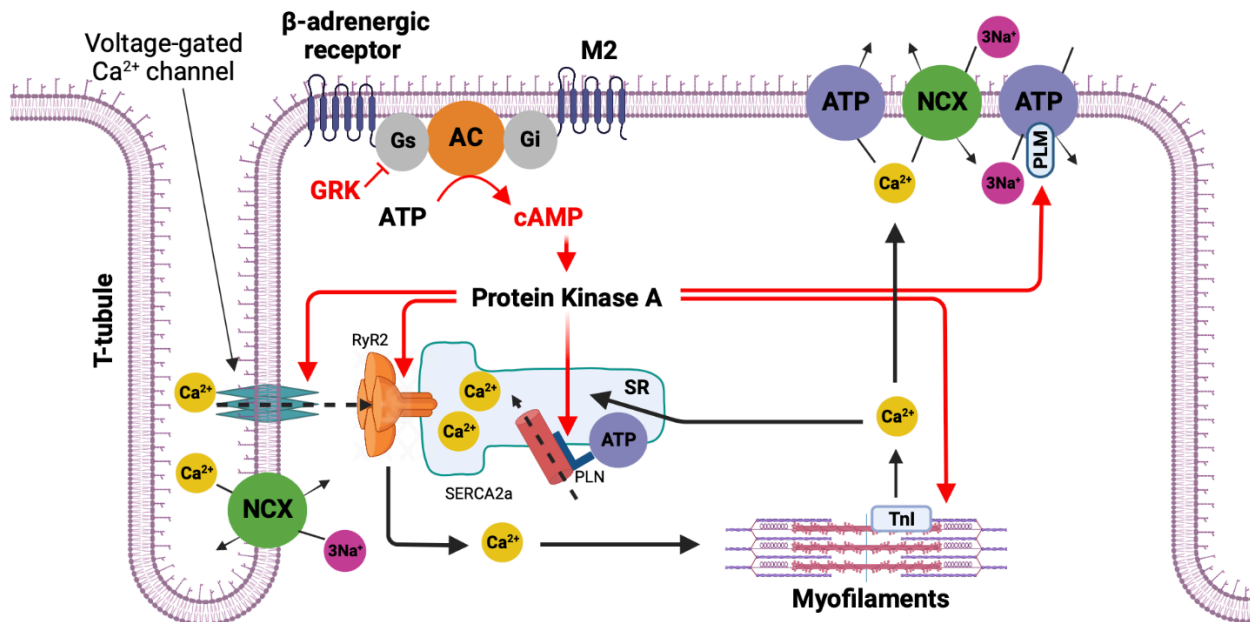


Figure 1.2: PKA signaling pathways in cardiac myocytes. T-tubule = transverse tubule; M2 = M2-cholinoceptors; Gs = stimulatory G proteins; AC = adenylyl cyclase; Gi = inhibitory G proteins; HCN = hyperpolarization-activated cyclic nucleotide-gated ion channels; NCX = sodium-calcium exchanger; ATP = sarcolemmal $\text{Na}^{+}/\text{K}^{+}$ -ATPase or sarcoplasmic reticulum Ca^{2+} ATPase; PLM = phospholamban; RyR = ryanodine receptor; PLN = phospholamban; GRK = G protein coupled receptor kinase; TnI = troponin-I.

PLN is a prime regulator of the sarcoplasmic reticulum Ca^{2+} ATPase (SERCA2a). Phosphorylation of PLN at serine 16 (Ser16) by PKA relieves its inhibition of SERCA2a, which greatly stimulates the rate and amount of cytosolic Ca^{2+} resequenced into the SR. This enhances myocardial relaxation and SR loading, which in turn generates larger Ca^{2+} transients and force during systole. PKA-dependent phosphorylation of the myofibrillar proteins troponin I (TnI) and cardiac myosin-binding protein C decreases myofibrillar Ca^{2+} sensitivity and thereby accelerates the relaxation of myofilaments. Phospholamban is another downstream target of PKA.

Phosphorylation of PLN may not only occur in a PKA-dependent manner via β -adrenergic stimulation. PLN is also phosphorylated at elevated Ca^{2+} concentration via CaMKII [5]. At elevated Ca^{2+} concentration, CaMKII becomes active and phosphorylates PLN at the threonine17 (Thr17) phosphorylation site [5]. However, this phosphorylation has no known physiological effects. The PLN phosphorylation is reversed via protein phosphatase 1 (PP1). PP1 is a ubiquitous eukaryotic enzyme and is one of the most important phosphatases at the SR. Its activity is regulated via inhibitor-1 (I-1) [6]. The activity of I-1 is increased by phosphorylation of PP1 at threonine35 (Thr35) by PKA, whereas it decreases after PKC-dependent Ser67 phosphorylation. I-1

inactivates PP1 and thereby increases the phosphorylation state of PLN [7]. However, PP1 not only dephosphorylates PLN at Ser16, but also protein phosphatase 2a (PP2a) dephosphorylates PLN.

1.1.2 Excitation-contraction coupling (ECC) in Cardiac Muscle

Excitation-contraction coupling (ECC) explains the importance of myocyte calcium cycling measurements. ECC is the process whereby an action potential (electrical impulse) triggers a myocyte to contract, followed by subsequent relaxation. When the cell stimulates the wave of depolarization i.e., an action potential, it triggers the entire process. The action potential comes down from a neuron or electrical synapse with the electricity traveling from the pacemaker cells into the contractile fibers through the gap junctions. Some of the calcium and sodium from pacemaker cells will travel into the contractile cell.

At this point, the process will trigger the opening of voltage-gated sodium and calcium channels that are found within the cell membrane, and an action potential is generated along the sarcolemma. As the action potential travels down the membrane from both sides, it's going to encounter the voltage-gated calcium channels which are L-type calcium channels. So, when the action potential hit this voltage-gated calcium channel, the channel opens and Ca^{2+} is introduced into the cytosol of cardiomyocytes during systole [8]. Ca^{2+} can stimulate muscle contraction alone, but it has a more important role. L-type Ca^{2+} channels form functional units with ryanodine receptors 2 (RyR2). Inflowing Ca^{2+} binds to the RyR2 and causes the RyR2 to open. So, the calcium from extracellular fluid enters the cell to activate RyR2. RyR2 then releases calcium from Sarcoplasmic Reticulum (SR) which is the storehouse for calcium, and this is referred to as calcium-induced calcium release resulting in the interaction of calcium with protein myofilaments to trigger the contraction [9].

This Ca^{2+} influx, which increases the intracellular Ca^{2+} concentration from 10^{-7} to 10^{-5} mol/l, in turn, activates the myofilaments. In each contracting unit or sarcomere, actin and myosin filaments are exposed which cannot interact in the absence of calcium. This is because the myosin-binding site on the actin filament is all covered by a rod-shaped protein called tropomyosin. The calcium-sensitive complex called troponin is attached to the end of each tropomyosin molecule. Ca^{2+} binds to the N-terminus of troponin C (TnC), causing TnC to bind to the C-terminus of troponin I (TnI) and thus pulling TnI away from its binding site to actin. Tropomyosin (Tm) and troponin T (TnT) together form a complex and slide into the cleft between myosin and actin, resulting in the myosin head binding to actin [10]. Contraction of the sarcomeres occurs (Figure 1.6).

During diastole, most of the intracellular Ca^{2+} is transported back into the SR via the sarco/endoplasmic reticulum calcium ATPase (SERCA2a) calcium pump [11]. It resides in the SR membrane within cardiomyocytes. A small amount of Ca^{2+} is also released from the cell in this process via the sarcolemmal sodium-calcium exchanger (NCX), and sarcolemmal calcium

ATPase (PMCA) [1]. NCX is an antiporter membrane protein and is considered one of the most important cellular mechanisms that remove calcium from the cells. It uses the energy that is stored in the electrochemical gradient of sodium (Na^+) in exchange for the counter transport of calcium ions (Ca^{2+}) which allows Na^+ to migrate down its gradient across the plasma membrane. Bers et al. have shown that in human cardiomyocytes, SERCA2a pumps approximately 70% of cytosolic Ca^{2+} back into the SR [11]. 28% leaves the cell by the means of the sodium-calcium exchanger via sarcolemma. In contrast, only about 2 % is transported by the mitochondrial calcium uniporter and the PMCA.

On the other hand, the ratio of Ca^{2+} transport looks different in rats and mice. Here, SERCA2a pumps up to 92 % of the Ca^{2+} from the cytosol back into the SR. NCX eliminates only 7% and transport 1% out of the cell via the PMCA and into the mitochondria via the mitochondrial calcium uniporter [12]. Re-excitation may occur once the cytosolic Ca^{2+} reaches its basal initial concentration, which leads to contraction and Ca^{2+} release [13]. In general, the amount of Ca^{2+} entering in the cytosol correlates with the force of contraction.

1.1.3 Regulators of the Ca^{2+} cycle

In cardiomyocytes, SERCA2a and RyR2 are the important regulators of the Ca^{2+} cycle along with many others such as L-type Ca^{2+} channels (LTCC), sodium-calcium exchanger (NCX), plasma membrane Ca^{2+} ATPase (PMCA), mitochondrial Ca^{2+} uniporter (MCU). On depolarization of the cell membrane, LTCC (also known as dihydropyridine receptors) in the plasma membrane are activated. It functions as a rapidly activated Ca^{2+} channel and the influx of Ca^{2+} through this channel induces Ca^{2+} release from the SR. The NCX and PMCA are together the main regulators of intracellular Ca^{2+} concentrations. They are membrane proteins that function to remove Ca^{2+} from the cell. Because of the essential role in Ca^{2+} regulation, they have enormous influence on contractility. MCU is a transmembrane protein that allows the calcium ions from a cell cytosol to pass into mitochondria. Ca^{2+} is balanced through the MCU in conjunction with NCX.

Other Ca^{2+} regulators that bind to SERCA2a or PLN are S100A1, and HS-1 associated protein X-1 (HAX-1). These Ca^{2+} regulators interact with SERCA2a and PLN. S100A1 is highly expressed in human myocardium and is found in the SR, myofilaments, and mitochondria. In addition, it is thought to facilitate the coupling of excitation and contraction. S100A1 has positive inotropic effects on cardiac function and cardiac contractility improves when S100A1 is overexpressed in cardiomyocytes. Another non-negligible protein that indirectly regulates Ca^{2+} kinetics, is HAX-1. It is a mitochondrial protein that is ubiquitously expressed. PLN can interact simultaneously with SERCA2a and with HAX-1. However, when PLN is phosphorylated after β -adrenergic stimulation, binding to HAX-1 is weakened. This may be because HAX-1 binds to both phosphorylation sites Ser16 and Thr17. It is suggested that HAX-1 thereby regulates the activity and conformation of PLN and thus indirectly affects Ca^{2+} kinetics. Also, when Ca^{2+} concentration is increased, this

attenuates the interaction of PLN to HAX-1, and PLN-HAX-1 interaction increases cardiomyocyte survival.

1.1.3.1 Ryanodine receptor 2 (RyR2)

The Ryanodine receptor 2 (RyR2) complex is composed of homotetrameric RyR2 and FK506-binding proteins (FKBP) anchored in the SR which is found in 1:4 stoichiometric ratio (Figure 1.3) [14]. Its activation occurs mainly via Ca^{2+} , which in turn releases the Ca^{2+} from the SR by opening of the receptor. Given its importance for cardiac function, RyR2 channel is highly regulated and can be affected by the interaction of RyR2 with different molecules such as ATP, Zinc, and a multitude of small regulatory proteins. FK506-binding proteins (FKBPs) are some of the most studied regulatory proteins, which are cis-trans peptidyl-prolyl isomerases. The FKBP is expressed in cardiomyocytes and act as essential RyR2 regulators. FKBP12 subtype correspond to low and FKBP12.6 subtype corresponds to high RyR2 affinity. Reportedly, RyR2 activity is inhibited by FKBP12.6 and not FKBP12. FKBP12.6 and RyR2 association keeps RyR2 closed, preventing calcium release from the SR, thereby, ensuring heart relaxation [15]. PKA, Ca^{2+} -calmodulin-dependent protein kinase II (CaMKII), and phosphatases are involved in RyR2 phosphorylation.

The RyR2 has several phosphorylation sites which regulate its opening probability. After β -adrenergic stimulation, RyR2 is phosphorylated at serine2808 (Ser2808) by protein kinase A (PKA). PKA-induced RyR2 phosphorylation (Ser2808) promotes FKBP12.6 and RyR2 dissociation, thereby opening RyR2 and promoting calcium-activated calcium release [16]. The reduction of PP1 and PP2A levels may be responsible to cause this process. In addition, calcium-calmodulin-dependent protein kinase II (CaMKII) can also phosphorylate RyR2 at Ser2808, and it has its own phosphorylation site at Ser2814. CaMKII is a serine/threonine specific protein kinase that is regulated by the Ca^{2+} /calmodulin complex and is also important for Ca^{2+} homeostasis and reuptake in cardiomyocytes [17]. CaMKII (Ser2814) causes RyR2 phosphorylation which is more critical than that by PKA. Importantly, RyR2 can be stabilized by FKBP12.6, thereby preventing excessive release of Ca^{2+} by RyR2 and intracellular calcium homeostasis imbalance.

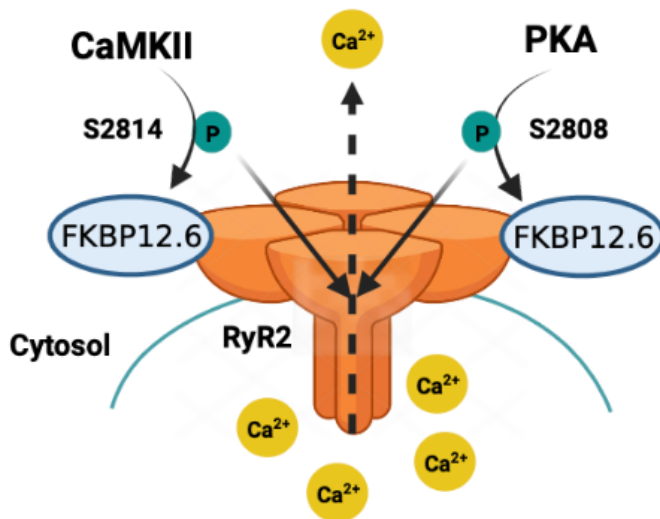


Figure 1.3: Release of Ca^{2+} from the SR into the cytosol via RyR2. RyR2 modulation by phosphorylation. S2814 is the site phosphorylated by CaMKII, and S2808 by PKA. PKA phosphorylation of S2808 dissociates FK506, which destabilizes the closed state of the channel and induces subconductance states, eliciting calcium leak. The deleterious effect is caused when Ca^{2+} leak from the SR. CaMKII phosphorylation of S2814 does not dissociate FK506 but also causes calcium leak. Ca^{2+} = calcium ion; RyR2 = ryanodine receptor 2.

1.1.3.2 Sarco/endoplasmic reticulum calcium ATPase (SERCA)

SERCA is a transmembrane protein that resides in the SR membrane of the myocytes and pumps Ca^{2+} from the cytosol back into the SR using energy from adenosine triphosphate (ATP). Phospholamban (PLN) regulates the activity of SERCA2a (Figure 1.4). PLN is a mini-membrane protein that regulates the Ca^{2+} pump in cardiac cells and consists of a dynamic pentamer-monomer equilibrium [18]. The pentamer in turn consists of five identical subunits, the monomers, and SERCA2a is reversibly inhibited by the PLN monomer in the unphosphorylated state by decreasing the affinity of SERCA2a for Ca^{2+} [19], [20]. In this process, the PLN monomer binds to a binding pocket of SERCA2a. When Ca^{2+} is bound there, the pocket is closed. This explains the ability of a high Ca^{2+} concentration to eliminate the binding between SERCA2a and PLN. SERCA2a and PLN monomers are both anchored in the SR [21]. SERCA/PLN inhibitory interactions are relaxed upon β -adrenergic stimulation, which unleashes cAMP-dependent protein kinase A (PKA) to phosphorylate PLN's cytoplasmic domain at Ser16, enhancing Ca^{2+} transport by SERCA and augmenting heart muscle contractility [5]. More Ca^{2+} can be reabsorbed into the SR from the cytosol via SERCA2a. Relaxation of the cardiomyocyte also occurs without any β -adrenergic stimulation or phosphorylation [1].

However, phosphorylation of PLN may not only occur in a PKA-dependent manner via β -adrenergic stimulation. PLN is also phosphorylated at elevated Ca^{2+} concentration via CaMKII [5]. At elevated Ca^{2+} concentration, CaMKII becomes active and phosphorylates PLN at the threonine17 (Thr17) phosphorylation site [5]. However, this phosphorylation has no known physiological effects. Intracellular calcium cycling is enhanced by β -adrenergic stimulation of cardiac myocytes. Upon β -adrenergic stimulation, adenylate cyclase (AC) becomes active through activation of the G_s protein-coupled receptor. This leads to an increased production of cyclic adenosine monophosphate (cAMP), which causes the PKA to inhibit PLN at its phosphorylation site Ser16 [3], [4]. The PLN phosphorylation is reversed via protein phosphatase

1 (PP1). PP1 is a ubiquitous eukaryotic enzyme and is one of the most important phosphatases at the SR. Its activity is regulated via inhibitor-1 (I-1) [6]. The activity of I-1 is increased by phosphorylation of PP1 at threonine35 (Thr35) by PKA, whereas it decreases after PKC-dependent Ser67 phosphorylation. I-1 inactivates PP1 and thereby increases the phosphorylation state of PLN [7]. However, PP1 not only dephosphorylates PLN at serine16 (Ser16), but also protein phosphatase 2a (PP2a) dephosphorylates PLN.

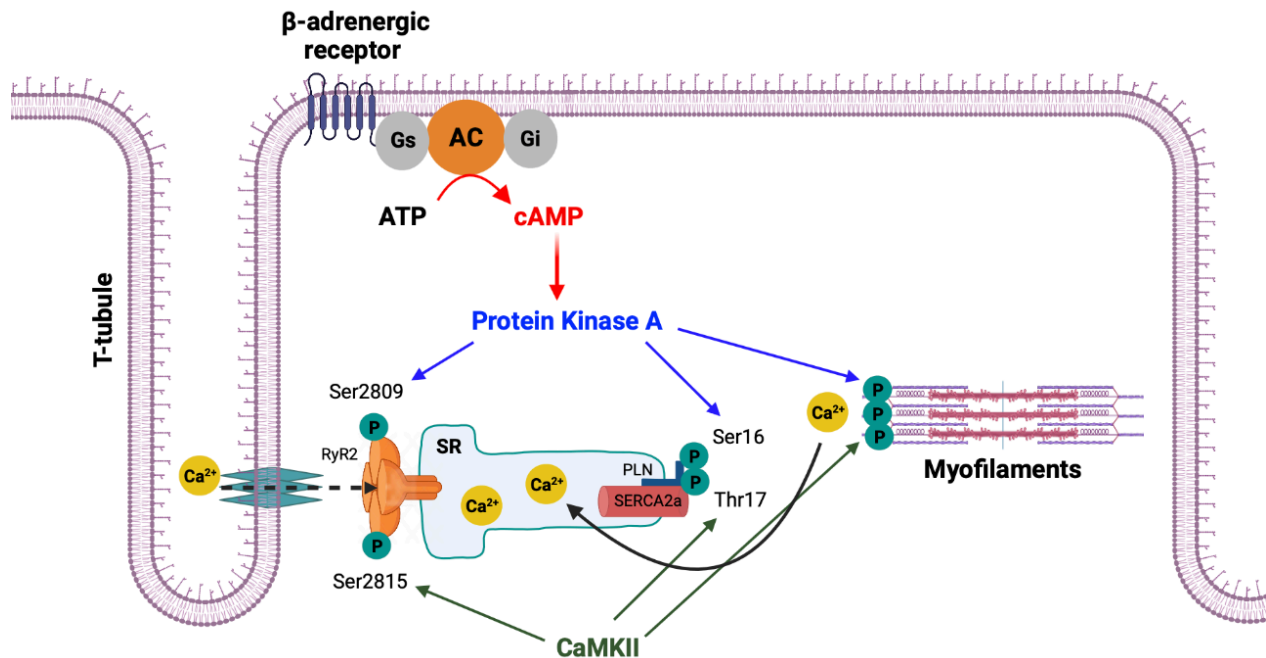


Figure 1.4: Illustration of SERCA2a and PLN monomer. Activation of PKA and CaMKII by β -adrenergic receptor stimulation and phosphorylation of their targets. Gs = stimulatory G proteins; AC = adenylyl cyclase; cAMP = cyclic adenosine monophosphate; PKA = protein kinase A; SR = sarcoplasmic reticulum; PLN = phospholamban; SERCA2A = sarco/endoplasmic reticulum calcium ATPase 2a; RyR = ryanodine receptor; CaMKII = Ca^{2+} and calmodulin-dependent kinase II; Ca^{2+} = calcium ion.

1.2 Sarcomere function of cardiomyocytes

A sarcomere is referred to as the smallest functional unit of striated muscle tissue and is the repeating unit between two Z-lines. The distance between Z-lines (i.e., sarcomere length) ranges from about 1.6 to 2.2 μm in human hearts [22]. Each sarcomere consists of long, fibrous contractile proteins as filaments which serve as the basis for the sliding filament theory that slides past each other when muscle contracts or relaxes.

The major contractile proteins are thick and thin filaments – myosin and actin, respectively. Physical and chemical interactions between the myosin and actin are responsible for shortening the sarcomere, and therefore the myocyte contract during the process of excitation-contraction coupling. Myosin is a protein with a molecular weight of approximately 470 kDa [22]. Each myosin contains two heads that interact with a binding site on actin. These heads are the site of the myosin ATPase, an enzyme that hydrolyzes ATP required for actin and myosin cross-bridge formation.

The thin filaments comprise three different types of protein: actin, troponin, and tropomyosin. Together, these are known as regulatory protein complexes. Actin is a globular protein arranged as a repeating unit chain, that forms filaments to provide cells with mechanical support and driving forces for movement. The other two regulatory proteins are troponin and tropomyosin. Tropomyosin is a rod-shaped protein, interdigitated between the actin strands. Tropomyosin attaches to the troponin protein complex at regular intervals [22]. The troponin complex is composed of three subunits: troponin-C (TN-C), which is a Ca^{2+} binding protein during ECC, troponin-T (TN-T), which binds to the tropomyosin and helps position it on actin; and troponin-I (TN-I), which prevents the myosin from binding to actin [23]. TN-I is used as a diagnostic marker for myocardial infarction [24].

After myosin and actin, titin is the third most abundant protein in muscle, greater than 1 μm in length, that functions as a molecular spring and is responsible for the passive elasticity of muscle [25], [26]. The Z line is connected to the M line in the sarcomere by titin. At the Z line, the protein contributes to force transmission and resting tension in the I band region [27]. It contributes to the passive stiffness of muscle by limiting the range of motion of the sarcomere in tension.

A sarcomere in turn extends from one Z-disk to the next. For various structural and mechanical reasons, the sarcomere length in the cardiac myocytes does not normally exceed 2.2 μm , shortening by about 0.4 μm during contraction. The thick filaments overlap with the thin actin filaments in the A band of the sarcomere. The M-band is in the middle of the sarcomere which is the attachment site for the thick filaments (Figure 1.5).

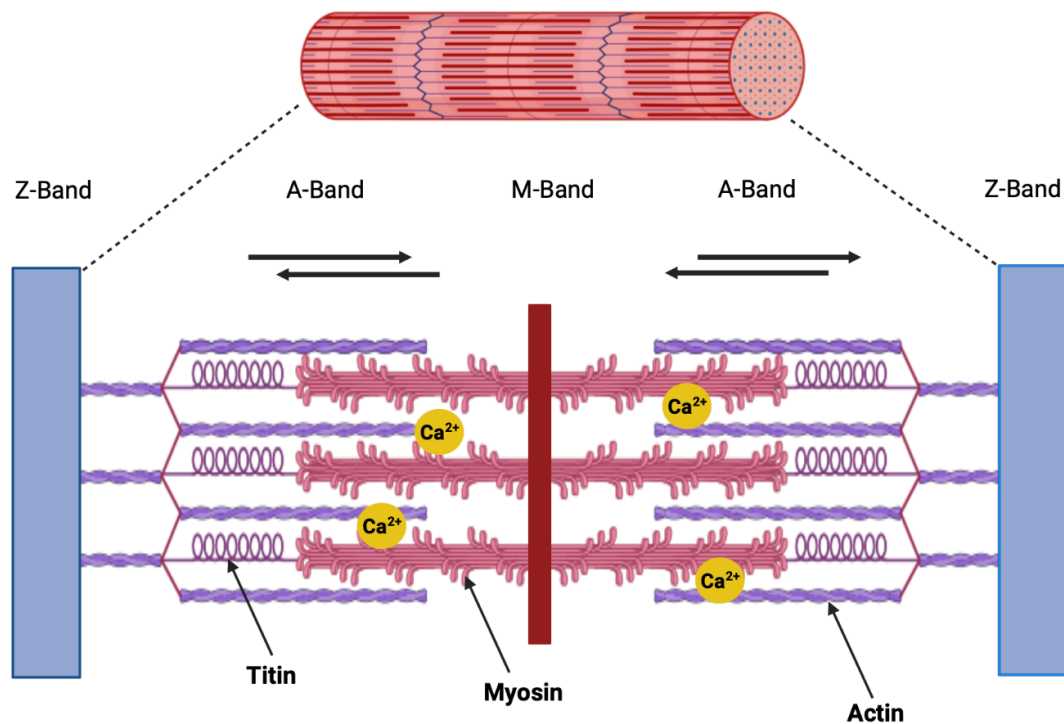


Figure 1.5: Representative sarcomere unit, schematic representation. Schematic diagram showing the main constituent of the sarcomere that have different functions during the contraction. The Z-band defined the boundaries of the sarcomere. Its main purpose is to anchor the thin (or actin) filaments. In the middle part of the sarcomere, known as the M-band, the myosin filaments interconnect and move antiparallel to both sides of the sarcomere. The A-band constitutes myosin filaments crosslinked at the center by the M-band assembly. Thin actin-containing filaments are tethered at their pointed end at the Z-band and interdigitate with the thick filaments in the A-band. Titin molecules anchor in the Z-band and extend to the M-line region of the sarcomere. Ca^{2+} = calcium ion

During systole, actin is bound to the myosin head, thus resulting in interlocking with the thick filament. The binding of actin and myosin is caused by an increase in intracellular Ca^{2+} concentration in the cardiomyocyte (Figure 1.6). In the end, myosin is attached to titin via myosin-binding protein C, which offers an elastic link to the next Z-disc. As already mentioned in connection with the myocytic Ca^{2+} cycle in chapter 1.1, Ca^{2+} binds to troponin C. This leads to a conformational change in the troponin complex by which troponin I now binds to troponin C. This frees up binding sites, that allows the myosin heads to bind to actin. The troponin complex resumes its inactivated position when Ca^{2+} is removed from the TN-C, thereby inhibiting myosin-actin binding [28]. The myosin head fastens, consuming ATP, and actin is pulled toward the center of the sarcomere. The thick and thin filaments overlay in the process. The heart regulates its force of contraction with the changes in sarcomere length. When a myocyte is stretched, the sarcomeres within the myofibrils are also stretched. With the increased sarcomere length, the force of contraction (i.e., tension development by the muscle fiber) increases and sarcomere length reaches to a maximum of approximately $2.2\ \mu\text{m}$. A small change in sarcomere length can produce large changes in tension development. The changes in active tension caused by changes in sarcomere lengths are related to changes in the number of actin and myosin cross bridges formed. Moreover, stretching the sarcomere increases TN-C affinity for Ca^{2+} , thereby leading to increased tension development [29]. With decrease in the concentration of intracellular Ca^{2+} , myocardial

relaxation occurs. The binding of the myosin head to actin ceases when Ca^{2+} dissociates from the binding site to troponin C. Troponin I is phosphorylated by PKA, which reduces the Ca^{2+} sensitivity of myofilaments. The phosphorylation state of troponin I plays an important role in the regulation of force development and myocyte relaxation.

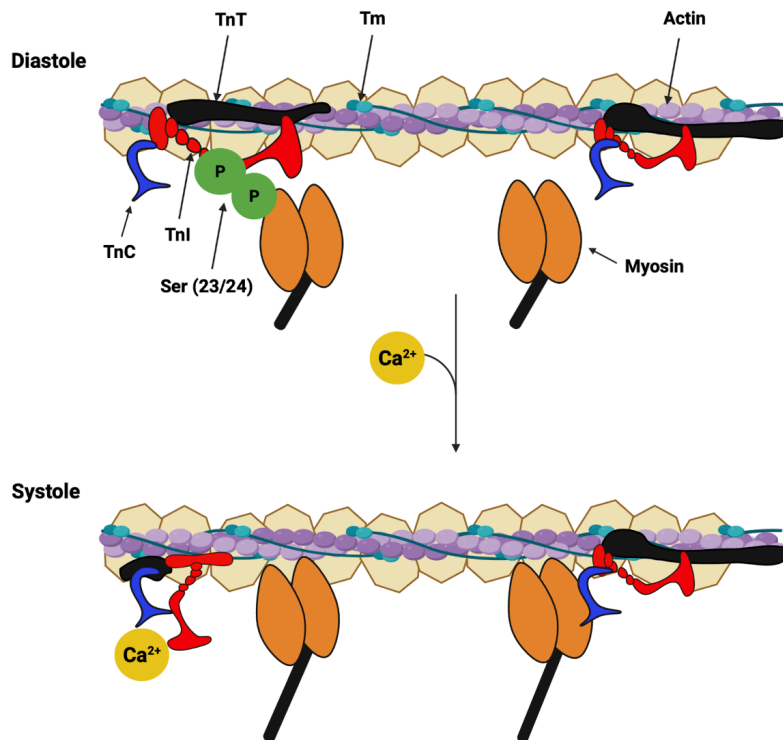


Figure 1.6: Myofilaments during diastole and systole. When Ca^{2+} binds to troponin C, a conformational change takes place by which troponin I now binds to troponin C. This frees up binding sites, allowing the myosin heads to bind to actin. The myosin head buckles, and actin is pulled toward the center of the sarcomere. The thin and thick filaments overlap in the process. With decrease in intracellular Ca^{2+} concentration, myocardial relaxation occurs. Ca^{2+} dissociates from the binding site to troponin C, and the binding of the myosin head to actin ceases. Troponin I is phosphorylated, which reduces the Ca^{2+} sensitivity of myofilaments. Ca^{2+} = calcium ion; TnC = troponin C; TnI = troponin I; Tm = tropomyosin; TnT = troponin T.

1.3 Acute myocardial infarction

Acute myocardial infarction is termed as myocardial necrosis (death of small areas of tissue) which results from acute obstruction of a coronary artery. It is usually manifested by chest pain, which travels from left arm to neck, shortness of breath, abnormal heartbeating, anxiety, and sweating. Myocardial infarction (heart attack) is known as an irreversible injury to the myocardium (heart tissue) caused by prolonged myocardial ischemia and hypoxia [30]. Occlusion of a blood vessel occurs during MI which is generally triggered by an atherosclerotic plaque [31]. The most common risk factors include diabetes, arterial hypertension, elevated levels of inflammatory markers, obesity, abnormal cholesterol levels, smoking, family history, genetics, and an unhealthy diet.

Atherosclerosis is characterized by the accumulation of lipids in the vessel walls due to the elevation of cholesterol levels, resulting in inflammatory responses. Typically, MI is caused by

plaque rupture. Plaque is composed of calcium, fat, cholesterol, and other substances found in the blood. Most people with early (less than 50 percent narrowing) ischemic heart disease do not experience symptoms or limitation of blood flow. However, as atherosclerosis progresses, especially if left untreated, symptoms may occur [32]. Here, activation of platelets results in a thrombus formation that occludes the vessel either at the plaque site or further distally if the thrombus has broken open and ruptured. The left ventricle (LV) is predominantly affected by myocardial infarction (MI), but the damage may extend into the right ventricle (RV) or the atria. MI is one of the major causes of death in the developed world, with prevalence approaching three million people worldwide [33].

Considering that the prevalence of CHD is increasing in both developed and developing countries, therefore, cardioprotection by timely reperfusion is urgently needed with the aim of reducing infarct size as the main determinant of evolving heart failure and improving the prognosis of patients with acute myocardial infarction [34]. Usually, too much time passes before patients are treated post-MI which is one of the reasons for the high mortality. Currently, regeneration of dead heart tissue by cell division is not possible. Therefore, the goal must be to ensure reperfusion of the undersupplied myocardium as quickly as possible. A 2020 study report by the World Health Organization mentioned coronary heart disease, responsible for 16% of the world's total deaths as the most frequent cause of death globally in 2019, closely followed by stroke and chronic respiratory diseases (Figure 1.7) [35]. The biggest rise in mortality since 2000 has been ischemic heart disease, which has grown from 2 million to 8.9 million deaths in 2019.

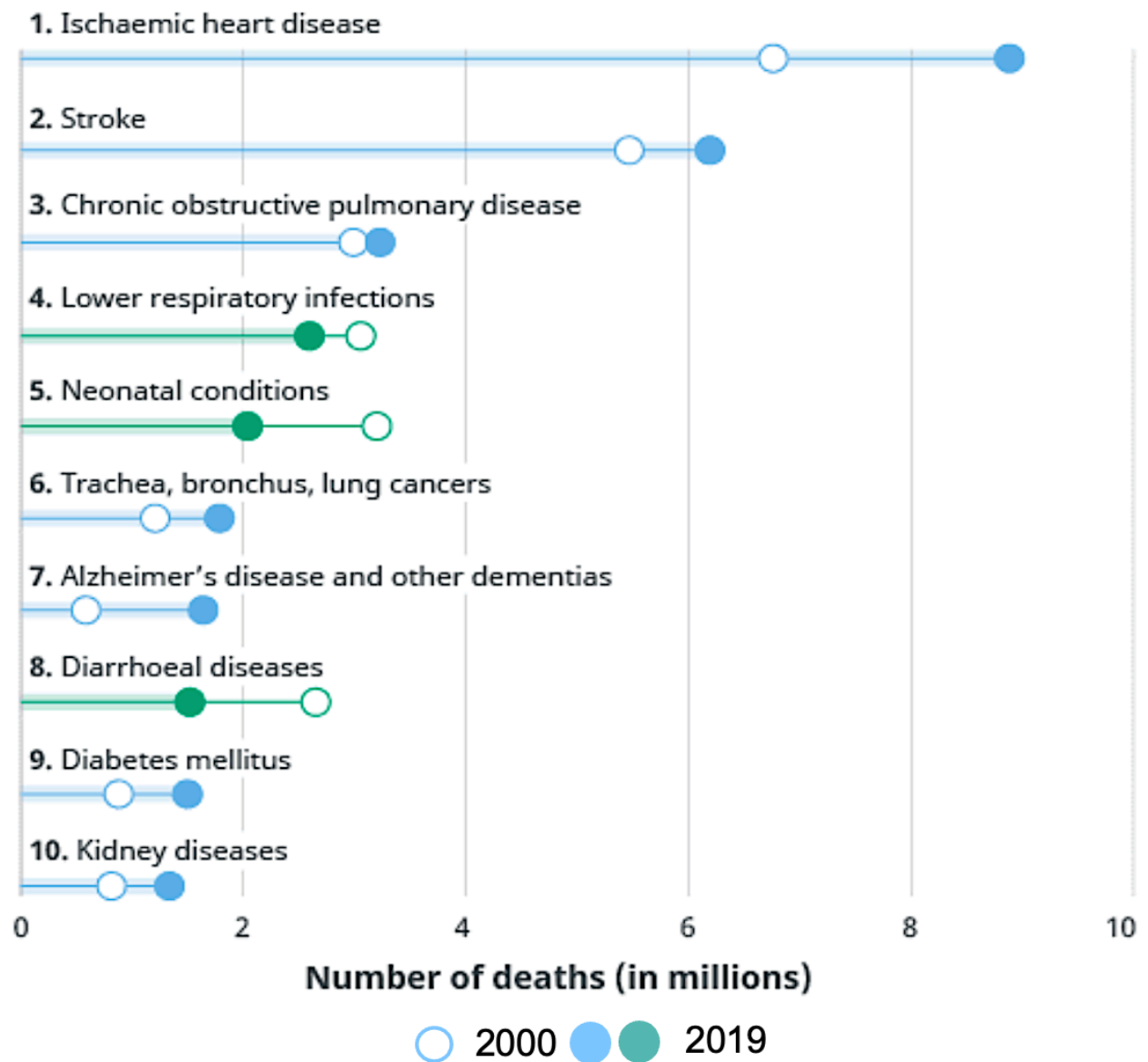


Figure 1.7: The 10 most frequent causes of death in 2019 – WHO

1.4 Ischemic area, peripheral area, and non-ischemic area

After ischemia has occurred and reperfusion has been initiated, the heart is divided into three regions: the ischemic area, the peripheral areas, and the non-ischemic area. These three regions are briefly characterized below (Figure 1.8).

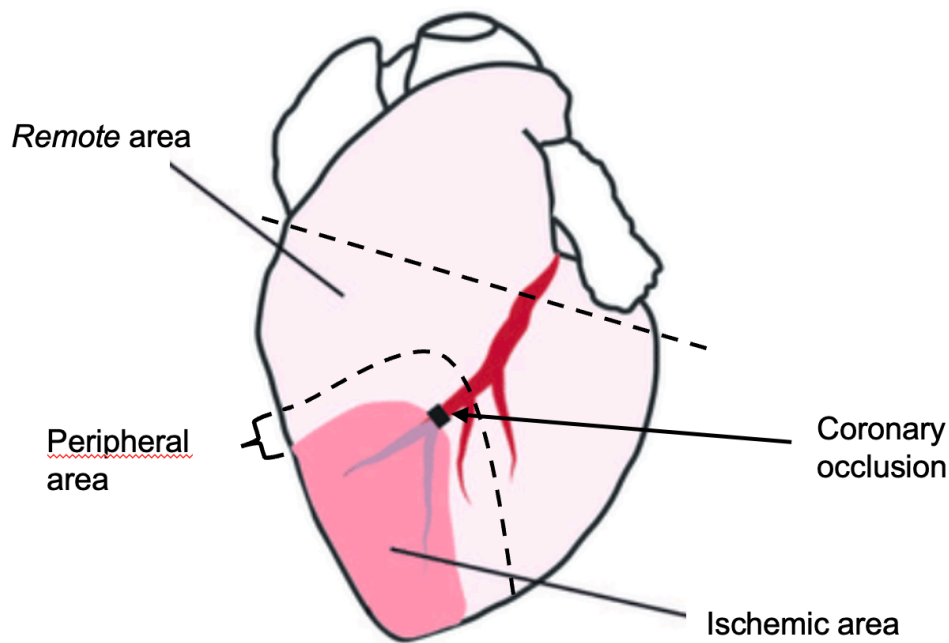


Figure 1.8: Schematic division of the heart into *remote* area, *peripheral* area, and *ischemic* area.

1.4.1 Ischemic Area

Ischemia is the condition in which the blood flow and thus oxygen is reduced or restricted to heart muscle. During left anterior coronary artery (LAD) occlusion, blood flow to the ischemic tissue is stopped. Cells in this tissue region, for example cardiomyocytes, enter an anaerobic state. Necrosis and apoptosis of cardiomyocytes in the ischemic area occur.

After ischemia has occurred, reestablishment of blood flow is important to salvage ischemic tissues and thereby oxygenation as quickly as possible to reduce infarct size, preserve contractile function, and avert high cell loss [36]. Sodium and hydrogen ions that get accumulated in the cardiomyocyte during the ischemic phase are removed resulting in the normalization of pH. The complement system is activated because of the preceding acidosis and hypoxia. Stimulation of leukocytes and endothelial cells occurs. Activated leukocytes then release interleukins and reactive oxygen species (ROS) in the ischemic myocardium. ROS are defined as the byproducts of the normal metabolism of oxygen, and sometimes are actively generated that play role in cell signaling and homeostasis.

For example, leukocytes produce increased nitric oxide (NO). This reacts with superoxide to form peroxynitrite, a highly toxic oxidant [37]. The increase in hydrogen peroxide and ROS during the reperfusion phase leads to peroxidation of lipids and oxidation of sulfhydryl groups [38]. For instance, phospholipids of membranes become instable, when ROS reacts to these membranes. There is an influx of water into the cell interior. As a result, the cells swell and the cell membrane ruptures. In addition, mechanical instability and hypercontracture of cardiomyocytes occur (for more details, refer chapter 1.2) [39]. ROS interact mainly with tyrosine residues and alter the activities of important proteins and enzymes [38].

Histologically, cardiomyocytes die in the ischemic area, and the cell nuclei condense and finally dissolve. Cell death begins in the inner layers of the heart after 30 to 45 minutes of coronary artery occlusion, and spreads to the outer layers as it progresses. Coronary blood flow is interrupted by coronary artery occlusion and deprives the affected parts of the heart of adequate oxygen and nutrients. Due to oxygen radicals, the cell membrane of the cardiomyocytes becomes unstable and due to water influx, the cell swells, and the cell membrane partially dissolves [39]. Production of aerobic energy by mitochondria in cardiomyocytes is impaired. Cardiomyocytes are flooded with Na^+ and Ca^{2+} . Activated proteases causes destruction in the cell membrane, and eventually cell death occurs [40]. However, the causes of this death at the cellular and sub-cellular levels have not been fully elucidated to date.

Ischemia is also responsible for alterations in contractile function. Force development drops dramatically when the beating heart is in the ischemic state. Contractile dysfunction occurs if the ischemic state lasts longer than 20 minutes. The muscle damage cannot be completely restored by subsequent reperfusion. However, reperfusion of the undersupplied ischemic tissue, which is initiated as soon as possible after ischemia, itself paradoxically causes further damage, threatening function and viability of the heart potentially leading to heart failure [41], [42].

1.4.2 Non-ischemic area (remote area)

The non-ischemic area, often referred to as the remote area, is the tissue that is not affected by ischemia [43]. It continues to receive blood and nutrients and is responsible for the contractile function of the cardiac pump. The remote area plays a functional role for cardiac output and the blood supply of the body. This tissue is separated from the ischemic area by the peripheral area and not directly adjacent to the infarct area. The nuclei of cardiomyocytes in the ischemic area are compacted and nucleus dissolution occurs due to apoptosis [44]. In contrast, the non-ischemic tissue is morphologically indistinguishable from healthy myocardium, and the nuclei have not dissolved.

Ischemic area releases metabolites or free oxygen radicals which reaches to more distant, healthy areas of the heart via blood flow and lead to changes there. Reactive oxygen species can interact with proteins, lipids, or sugar molecules, and thus lead to restrictions in cells. Therefore, remote tissue is also exposed to oxidative and nitrosative stress [45]. In addition, the mechanical stress on the remote myocardium of the heart is altered by the loss of function in the ischemic heart areas [46]. In the long term, it leads to conformational changes in cardiomyocytes. Following acute MI, pan-cardiac responses include the apparently unaffected remote myocardium [47]. Although macrophage and monocyte accumulation are higher in the infarcted zone, these cells are also recruited to remote myocardial tissues [47], [48]. Cytokine production from cardiomyocytes and macrophages further elicits inflammatory responses and collagen deposition which likely contribute to left ventricular (LV) remodeling [49], [50]. Early after coronary occlusion, regional

function within the remote myocardium depends, in part, on the length of time after the ischemic insult.

There is increasing evidence indicating that also remote myocardium is subjected to pathophysiological changes after MI [48]. Findings from recent studies suggest that tissue changes may also occur in remote myocardium after AMI and that these changes are associated with adverse cardiac remodeling [51], [52]. A better knowledge of the tissue changes in remote non-infarcted myocardium and their relation to adverse cardiac remodeling may help to better understand the pathophysiological mechanisms that are responsible for adverse cardiac remodeling post AMI, which in turn could be helpful to identify patients at increased risk and potential targets for therapy.

1.5 Interaction of Ca^{2+} homeostasis and myocardial ischemia-reperfusion

Ca^{2+} is a ubiquitous signal for regulating cellular function, including survival and death. A minimal amount of Ca^{2+} is necessary for the optimal physiological function of the heart. Disruption of calcium homeostasis, including decreased SR Ca^{2+} reuptake, abnormal function of calcium channels, SR Ca^{2+} leakage, or significantly decreased SERCA2a expression is associated with various types of heart diseases, including ischemic heart disease, reperfusion injury, hypertrophic cardiomyopathy, dilated cardiomyopathy, and heart failure [1]. Therefore, restoration of cardiomyocyte Ca^{2+} handling in the heart after MI may represent an interesting therapeutic strategy to improve myocardial remodeling and increase cardiac contractile function.

1.5.1 Ca^{2+} homeostasis in myocardial ischemic injury

The cardiomyocyte relies on anaerobic energy production in the ischemic state [41]. Myocardial cells have metabolic abnormalities after a period of ischemia and hypoxia, including increased anaerobic fermentation. Furthermore, intracellular H^+ aggregation causes a low intracellular pH, and intracellular Na^+ increases through H^+/Na^+ exchange (HNX). Excessive intracellular Na^+ will promote Na^+ excretion and Ca^{2+} intake by NCX, which significantly increases intracellular Ca^{2+} levels, hence, leading to Ca^{2+} overload. The impaired function of the Na^+/K^+ ATPase because of ATP depletion causes a rise in intracellular Na^+ and a fall in intracellular K^+ . Glycolysis and increased formation of lactate and protons reduces the cytosolic pH. Persistent oxygen deficiency and increasing acidosis lead to cessation of anaerobic ATP production, so that ATP-dependent processes are also terminated. When oxygen supply and blood flow to the cardiac tissue returns to normal, extracellular pH level is further increased, NCX and HNX activities are enhanced [53]. Sodium ions flowing in across the cell membrane can no longer be actively transported out of the cell. Ultimately, the NCX is activated in the opposite direction by the increased cytosolic sodium concentration. Na^+ leaves the cardiomyocyte and Ca^{2+} returns, and intracellular Ca^{2+} overload is

further aggravated. Studies have shown that HNX and NCX inhibition has a protective effect on myocardial I/R injury [54].

Moreover, SERCA2a activity decreases in the ischemic region, and therefore less cytosolic Ca^{2+} can be stored in the sarcoplasmic reticulum (SR) [55], [56]. In addition, an increased amount of Ca^{2+} is released from the SR into the cytosol. This significant increase in intracellular Ca^{2+} concentration in the cardiomyocyte activates signaling cascades, e.g., Ca^{2+} dependent proteases such as calpains, mediating severe cell damage during ischemia that may lead to cell apoptosis. Additionally, myocardial I/R produces toxic substances, such as oxygen-free radicals (OFR), in the myocardial cells. OFR can decompose cell membrane phospholipid components and damage membrane structure, which leads to increased membrane permeability and excessive extracellular Ca^{2+} influx [57]. OFR also damages to the SR membrane, eventually increasing intracellular Ca^{2+} levels and further exacerbating Ca^{2+} overload.

1.5.2 Ca^{2+} homeostasis in myocardial reperfusion injury

Cardiac ischemia causes a rapid decrease in mechanical performance and, if prolonged, myocardial cell death occurs on reperfusion. In principle, the early decline in mechanical performance could be caused either by reduced intracellular Ca^{2+} release or by reduced responsiveness of the myofibrillar proteins to Ca^{2+} . Ca^{2+} plays an essential role in maintaining ECC in cardiomyocytes, including Ca^{2+} release, recapture, and storage. Ca^{2+} homeostasis is particularly important for myocardial cell structure and function. So, it is of significance to focus on some cardiac protective reagents related to Ca^{2+} overload to treat myocardial I/R injury. Ca^{2+} levels in myocardial cells are regulated by LTCC, RyR2, SERCA, NCX, PLN, CaMKII, FKBP12.6, and mitochondria, which participate in Ca^{2+} overload during myocardial I/R injury.

Excessive intracellular calcium enters the mitochondria, resulting in mitochondrial calcium overload; this inhibits ATP production, exacerbates energy metabolism disorders, and eventually leads to myocardial cell apoptosis [58]. Sarcoplasmic Reticulum Ca^{2+} uptake is slowed during the reperfusion phase after ischemia in human atrial myocardium [59]. Here, SERCA2a activity is predicted to be reduced in continuation by ischemic damage. Animal studies have shown that cytosolic Ca^{2+} reuptake into the SR is also lower in the ventricular myocardium [60]. Moreover, it is known that after ischemia in the human myocardium, the release of Ca^{2+} from the SR into the cytosol decreases during reperfusion [61]. This is probably due to decreased number of ryanodine receptors (RyR2) [60]. Studies have shown that during myocardial I/R, the RyR2 structure gets damaged, which also accounts for many calcium leaks in SR and calcium overload.

Due to the slow rate of cytosolic Ca^{2+} accumulation of cardiomyocytes, there is a direct increase in diastolic tone and an indirect decrease in the amount of Ca^{2+} stored in the SR. Reduced Ca^{2+} sensitivity of the myofilaments further contributes to slowing down contractility [55]. In addition, the activity of the sodium-calcium exchanger (NCX) is decreased, so less Ca^{2+} can be transported out

of the cell [62]. Therefore, an overload of Ca^{2+} also occurs in the cytosol during the reperfusion phase [36]. Cardiomyocyte Ca^{2+} transport regulates cardiac contractility and relaxation. The myocyte Ca^{2+} handling is impaired in the nonischemic remote myocardium early after I/R. Ca^{2+} content of the SR is also reduced in remote myocardium due to the impaired Ca^{2+} uptake, because SR Ca^{2+} leak is not increased. During cardiac cycles, the speed reduction, and the extent of cytosolic Ca^{2+} increase and decrease were found which is associated with depressed sarcomere function [63].

1.5.3 Sarcomere function in myocardial I/R injury

During the ischemia/reperfusion phase, sarcomere function changes, characterized by reduced contractility (systolic dysfunction) and/or impaired filling (diastolic dysfunction) [64], [65]. An important role for alterations in sarcomere function is played by the overloading of the cytosol of the cardiomyocytes with Ca^{2+} during ischemia, which reduces the cardiac pump function as described in chapter 1.1. This should result in over-contraction of the sarcomeres. However, because of the prevailing acidosis and ATP deficiency, this over-contraction fails to occur. Instead, a pronounced rigor of the transverse bridges results in Ca^{2+} -independent transverse bridging between actin and myosin filaments with consequent shortening of the cardiomyocytes without over-contraction of the contractile apparatus.

There is a rapid restoration of the physiological pH of approximately 7.40 by initiating reperfusion. The oxygen is again supplied to cardiomyocytes and ATP production is resumed. The cell attempts to counteract Ca^{2+} overload by transporting Ca^{2+} into the SR via SERCA2a. Ca^{2+} is released into the cytosol once the capacity of the Ca^{2+} store is reached. This rapid succession of multiple Ca^{2+} uptakes into the SR and Ca^{2+} release into the cytosol results in Ca^{2+} oscillations [66]. These Ca^{2+} oscillations occur in the first minutes after the initiation of reperfusion. As a result, the contractile apparatus is also excessively activated and hypercontracture of the sarcomeres occurs. The cell shortens with the loss of transverse striation. Morphologically, strand breaks of the sarcomeres occur. These not only affect the cells of the ischemic area, but also have an impact on the neighboring cells of the marginal zone. Ultimately, hypercontracture can lead to cell death [67].

The increased intracellular Ca^{2+} concentrations trigger degradation processes in cytoskeletal proteins, which may result in contractile dysfunction [68]. Increased modification of the sarcomere protein titin also occurs, resulting in an increase in myocyte stiffness [69]. Functional abnormalities are also seen in the non-ischemic area as early as 30 minutes after ischemia [43]. On the other hand, increased mechanical stress on the remote myocardium is considered a cause of the impaired systolic function of the remote myocardium [70]. In addition, the adjacent muscle area is thought to be functionally impaired by non-synchronous contraction of the ischemic myocardium [71]. Asynergy in the remote area was demonstrated in the human heart four days after myocardial

infarction using echocardiography. The compensation of reduced contractility of ischemic muscle fibers is thus hampered [43].

1.5.4 Myocardial dysfunction in the RM

I/R impairs myocardial contractile function not only in the infarct zone but also in non-infarcted regions, i.e., the remote myocardium [72]. This impairment is caused by alterations to the sarcomere proteins themselves and to the regulation of their activity via beat-to-beat intracellular Ca^{2+} cycling. Studies have shown that Ca^{2+} transport kinetics of remote myocytes were slow, particularly the activity of the Ca^{2+} ATPase SERCA2a was reduced and contributed to impaired sarcomere function [73], [74]. The expansion of this non-infarcted region is believed to cause increased dynamic wall stress and leads to adverse remodeling [73]. The mechanisms underlying this encircling myocardial dysfunction are not well-known. The reduced phosphorylation state of phospholamban at its PKA-dependent site Ser16 plays a crucial role for depressed Ca^{2+} cycling of RM myocytes, resulting from increased phosphatase activity rather than from impaired PLN phosphorylation [63].

1.6 Period after myocardial infarction

Due to oxygen radical generation during ischemia, further damage to the myocardium occurs once the undersupplied tissue is reperfused after the opening of the coronary artery occlusion. However, reperfusion of the tissue is required as soon as possible after the acute event because it improves patient survival. Delay in time to reperfusion, results in significant loss of ventricular function after MI. It has been shown that infarct damage is higher without reperfusion than with reperfusion [75]. The time during reperfusion after MI is divided into three phases (Figure 1.9).

Inflammatory phase: The inflammatory phase begins 3 to 72 hours post-MI [75]. After the onset of reperfusion, most cardiomyocytes (myocardial cells) die already during the ischemic phase and shortly thereafter, i.e., within the first few minutes. Defective or dying cardiomyocytes secrete reactive oxygen species [76]. This results in the activation of inflammatory mediators, which in turn allows neutrophils to migrate into the infarcted tissue [75]. Leukocytes clear the infarcted tissue of dead cells, for example cardiomyocytes and remnants of the matrix.

Moreover, tumor necrosis factor α (TNF α) initiates apoptotic and necrotic processes in cardiomyocytes. TNF α is an inflammatory cytokine which is responsible for a diverse range of signaling events within cells, leading to necrosis or apoptosis. Approximately 48 to 72 hours after reperfusion of ischemic tissue, cell death influenced by necrosis and apoptosis reaches its maximum and does not increase further [76]. Two days after MI, there is increased differentiation of fibroblasts into myofibroblasts and activation of myofibroblasts [75]. There is also degradation of type I and type III collagen [77]. During this phase, there is not much known about the more

distant non-ischemic tissue, defined as remote area, and the behavior of the cardiomyocytes located there.

Proliferative phase: During the proliferative phase, the synthesis of inflammatory mediators ceases approximately 72 hours to 7 days after MI [75]. Increased collagen I and III are produced by activated myofibroblasts during this healing process, which ensure the maintenance of the extracellular matrix. Dead cardiomyocytes are replaced by collagen.

Maturation: 28 days after MI, fibrous tissue completely replaces the necrotic tissue which consist of apoptotic cardiomyocytes and fibroblasts [75]. Scar formation takes place. The cardiomyocytes of the adjacent tissue directly adjacent to the ischemic and the non-ischemic area changes in shape with the growth in length and hypertrophy [78]. Cardiac reconstruction with the time thickens the heart wall, resulting in the stiffness of the heart. The consequences are hypertrophy and/or dilatation until chronic heart failure.

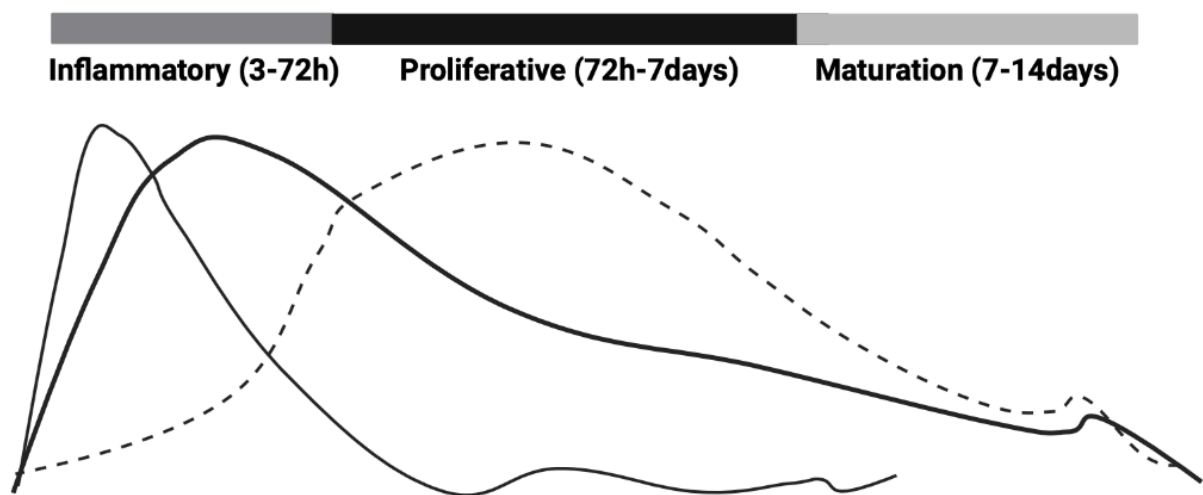


Figure 1.9: The phases of healing in reperfused mouse infarcts (1-h coronary occlusion followed by reperfusion) [75].

1.7 Experimental models for I/R

To understand the pathophysiological mechanisms after MI and to derive new therapeutic interventions from them, there are animal experimental models that can be used to mimic ischemia/reperfusion (I/R) in animals as realistically as possible to MI in humans [79]. The experimental model used in this work is briefly introduced below.

1.7.1 Ischemia induction with closed thorax

Performance of ischemia induction with the thorax closed includes the following steps: anesthetization and sedation of the experimental animal, thoracotomy with the application of LAD ligation, and convalescence of several days. Ischemia is induced with the thorax closed under anesthesia after convalescence of several days. For this purpose, the sutures are dissected free

in a tissue pocket located under the skin. When the sutures are tightened, occlusion of the LAD occurs without opening the thorax. The method of ischemia induction with the thorax closed is described in more detail in chapter 2.1.2.

Nossuli et al first described the method of closed thorax ischemia induction in mice [80]. One reason behind the development of this method was that ischemia induction in open thorax resulted in an increase in the inflammatory response not only in the ischemic and reperfused animals but also in the sham-operated animals. Surgical trauma cannot occur during MI in humans since the thorax is not open therefore, a solution was sought to mimic this in animal experiments. Thus, after several days ischemia and subsequent reperfusion are performed, when the increase in inflammatory mediators has subsided [79].

There is a decrease in inflammatory factors after three days, so appropriate convalescence is recommended to avoid confounding the results [80]. Therefore, low probability of surgical trauma and rather rarely occurring infections, which also reduces the mortality rate are the advantages of this method [30], [80]. Ischemia and reperfusion can be performed at any time and is easily reproducible. Ischemia induction with the thorax closed is more clinically relevant than the methods described in chapters 1.6.1 and 1.6.2 [30]. However, this method also has a disadvantage that direct visual control of ischemia is not possible. Occlusion of coronary artery can only be monitored with electrocardiography.

All animal models have a disadvantage that MI does not occur spontaneously in animals but is artificially induced at a certain point of time [79]. On the other hand, it usually occurs spontaneously in humans, and is mostly promoted by an unhealthy diet, too little exercise or by other factors and in some cases for years beforehand. This is difficult to replicate in experimental animals. Models have been established in which animals were fed a high cholesterol diet, for example. These models are less suitable for research projects since here the coronary arteries occlusion also occurs spontaneously and unpredictably over time.

The advantage of LAD ligation in the experimental animal is that all animals have the infarct at a defined time point, the localization of the coronary occlusion is same, resulting in comparably sized infarcts [79]. Thus, more reproducible results can be obtained. The closed-chest ischemia induction model was chosen in the present work to perform I/R. In this model, a possible postoperative infection that could influence the ischemia/reperfusion phase is prevented. Moreover, in contrast to ischemia induction with the thorax open, both cooling and desiccation of the cardiac surface are avoided, which in turn ensures similarly large infarct sizes.

1.8 Type II diabetes mellitus is a risk factor for myocardial infarction

Although there have been potential breakthroughs toward many of the extra pancreatic manifestations of diabetes, acute myocardial infarction continues to be a significant reason for

morbidity and mortality in patients with T2DM [81]. As a result, these and other factors are responsible for diabetes and increase atherosclerotic plaque formation and thrombosis, thereby contributing to myocardial infarction. The risk of recurrence of MI in T2DM patients exceeds 40%. In a scientific announcement published on April 13, 2020, in *Circulation*, the American Heart Association (AHA) stated that CAD in T2DM patients' needs to be examined more aggressively to diminish the risk of MI compared with CAD in patients without T2DM [82]–[84].

In 2019, the European Association for the Study of Diabetes (EASD) and the European Society of Cardiology (ESC) jointly issued the Guidelines on Diabetes, Pre-Diabetes, and Cardiovascular Diseases recommending that all cardiovascular disease patients should be screened for T2DM and patients with cardiovascular disease complicated by T2DM should undergo comprehensive risk factor management, including control of lipid levels, blood pressure, and serum glucose; management of antiplatelet therapy regimens and lifestyle interventions [83]. In addition to damaging blood glucose levels, patients also experience high blood pressure, high cholesterol, and obesity, all of which impair the cardiovascular system and increase their chances of having a heart attack.

A deteriorated metabolic state develops early in the diabetic patient, resulting in the alteration of the cardiac metabolism. The longer this period continues and lasts, the more advanced the damage to the myocardium. Some of the ways that how diabetes mellitus causes adverse changes in the myocardium are micro- and microangiopathies, myocardial fibrosis, altered vascular pathology, overloading of cardiac cells with Ca^{2+} , and limitations in electrophysiology. According to "Gesundheit in Deutschland aktuell" (GEDA) in 2009, only around 10% of diabetes patients had no concomitant diseases related to diabetes [85]. In contrast, about 35% of the patients over 50 years of age examined had an organ disease in addition to their diabetes, which manifested itself in cardiovascular disease, eye disease or renal insufficiency.

From past decades, it has been known that both type I and type II diabetics suffer MI more frequently [86], [87]. Moreover, death in diabetic patients after MI is twice as high as in patients without a history of diabetes [88]. Therefore, it is crucial to know the underlying causes and mechanisms to prevent the high death of diabetics after MI by targeted therapeutic measures. As with intracellular Ca^{2+} circulation in cardiomyocytes, it is known that both systolic and diastolic function of the heart is impaired in mouse models with type II diabetes mellitus [89]. One possible cause represents decreased SERCA2a activity with the consequence that the loading of the SR with Ca^{2+} is also lower. Oxidative stress plays an important role in cardiac damage of infarcted hearts and is known to induce modifications of sarcomere and Ca^{2+} handling proteins, thereby altering their function, expression, and activity. The findings indicate that these defects play a decisive role in the impairment of SERCA2a activity in T2DM hearts.

T2DM impairs electromechanical coupling and sarcomere function and thereby impedes important early adaptive remodeling processes after I/R. In addition, T2DM exacerbates the depression of

Ca^{2+} cycling in remote myocytes after I/R and prevents adaptational titin phosphorylation and cardiomyocyte stiffening. Observation of reduced chamber in T2DM animal models and T2DM patients alters phosphorylation of the sarcomeric protein titin, leading to an increment of cardiomyocyte passive tension (PT) [90]. An altered cardiomyocyte Ca^{2+} homeostasis in T2DM patients induced diastolic dysfunction. In T2DM, a decreased contractile function was related to increased cardiomyocyte Ca^{2+} efflux, reduced Ca^{2+} entry, decreased SR Ca^{2+} load, and altered expression of SR Ca^{2+} handling proteins [91]. Moreover, diabetes also affects adaptive titin modification after acute myocardial I/R.

One of the questions that the present work addresses are how diabetes affects the functional consequences of I/R on cardiomyocytes from the remote myocardium.

1.8.1 Diabetes mellitus

Diabetes mellitus is a group of metabolic disorders which is characterized by high blood sugar levels over a prolonged period. There are two types of diabetes mellitus - types I and II.

Type 1 diabetes (T1D), also defined as juvenile diabetes or insulin-dependent diabetes mellitus, is an autoimmune disease that results from the failure of the pancreas to produce very little or no insulin due to the loss of beta cells [92]. Immune-mediated destruction of beta cells in the pancreas leads to insulin deficiency and ultimately to hyperglycemia. About 10% of diabetes mellitus patients suffer from type I (T1DM) [93]. Type II diabetes (T2DM), also known as adult-onset diabetes or non-insulin-dependent diabetes mellitus, is a common chronic condition in which cells respond poorly to insulin and with the advancement in the disease, a deficiency of insulin also gets developed. Type 2 diabetes affects around 90% of all people with diabetes and is more common in older adults [93], [94]. The combination of beta-cell dysfunction and insulin resistance leads to impaired glucose homeostasis [95]. Type 1 diabetes must be controlled with Insulin injections.

Type II diabetes is often triggered by an unhealthy lifestyle, especially a lack of physical activity and an unhealthy diet, but also by hereditary factors. The treatment of Type 2 diabetes can also be done with oral antidiabetic medications, with or without insulin. Every year, approximately 500,000 people in Germany are diagnosed with T2DM [96]. The prevalence of diabetes mellitus is generally increasing.

As of 2019, approx. 463 million people (8.8% of the adult population) had diabetes worldwide, with type 2 diabetes combined in total about 90% of the cases [97]. Rates are similar in men and women. T2DM has become one of the leading chronic non-communicable diseases, and its prevalence has significantly increased globally and suggesting that rates will continue to rise [97]. Diabetes resulted in approximately 4.2 million deaths in 2019 [97]. T2DM and its complications are seriously affecting the quality of human life with the increase in the number of cases and have become a serious global public health problem. There is a prediction by World Health Organization

(WHO) that by 2030, 350 million people worldwide will have type II diabetes mellitus, twice as many as in 2003 [98]

1.8.2 Mouse model for diabetes mellitus type II

Leptin-receptor (Lepr) deficient mice (db/db) were used as the animal model for type II diabetes mellitus. The db/db mouse model of leptin receptor is currently the most widely used T2DM mouse model [99]. This leptin-receptor deficient mouse has a mutation in the gene that encodes the leptin-receptor, and leptin-receptor confers sensitivity to T2DM obesity and insulin resistance [100]. In contrast to the leptin-deficient ob/ob mouse, db/db mice are not only overweight but also develop a marked diabetic metabolic state that shortens the lifespan of the animals. The ob/ob mouse model is a much milder diabetes model.

The mice that are homozygous for the leptin-receptor mutation (db/db) exhibit a hyperglycemic syndrome like humans [101]. At four weeks of age, they develop hyperglycemia due to increased dietary intake, higher body weight in comparison with normoglycemic heterozygous db/+ mice, and a higher plasma insulin concentration. After seven weeks, they are insulin resistant and blood glucose concentration is significantly increased.

1.9 Diet-induced obesity (DIO)

Cardiovascular diseases (CVDs) continue to be the leading cause of morbidity and mortality across the world. While some genetic markers have been recognized, they explain less than 15% of the variance in the risk for these diseases [102]. It is well confirmed that external factors, such as obesity, poor diets, and sedentary lifestyles are the main contributors to CVD risk [103], [104]. Obesity contributes significantly to impaired cardiovascular function and increased CVD risk. Obesity can be considered a chronic metabolic disease characterized by excess accumulation of fat in healthy individuals. The prevalence and incidence of obesity have markedly increased worldwide during recent decades, and obesity is currently considered a global epidemic and a major public health problem that affects both developed and underdeveloped countries [105]. This condition affects approximately 30% of the world's population, indicating more than one billion people (WHO, 2000).

In addition, this event crescent makes obesity an important risk factor often associated with a reduction in life expectancy, increased mortality risk, and the development of major risk factors for numerous co-morbidities such as type II diabetes mellitus, hyperlipidemia, and cardiovascular diseases [106]. DIO mice are a model of early-stage diabetes (rather than “only” obesity). DIO shows postprandial hyperglycemia and disturbed glucose tolerance and moderate insulin resistance. Db/db mice show severe obesity, severe insulin resistance and severe hyperglycemia (even fasting hyperglycemia) with blood glucose levels around 600mg/dl due to hyperphagia and older animals show atrophy of the beta-cells in the pancreas (islet atrophy) which leads to further

progression of hyperglycemia. Db/db shows all these changes even with a regular diet (without a high-fat diet). Db/db progress to heart failure when >12 weeks old. Experimental studies have demonstrated that obesity induced by different types of high-fat and/or high-energy diets also leads to myocardial dysfunction in rodents [107]. Several factors are responsible for possible cardiac abnormalities in obese models, including intracellular calcium (Ca^{2+}) handling, and major regulatory mechanism of myocardial contraction and relaxation. The intracellular Ca^{2+} cycling proteins located in the sarcolemma and sarcoplasmic reticulum (SR), such as the L-type Ca^{2+} channel, SR Ca^{2+} -ATPase (SERCA2a), phospholamban (PLN), calsequestrin (CSQ), ryanodine receptor (RyR2), and $\text{Na}^{+}/\text{Ca}^{2+}$ exchanger (NCX), have been described as essential in the regulation of myocardial contraction and relaxation by controlling Ca^{2+} transient homeostasis [108]. These alterations contribute to reduced Ca^{2+} entry and SR Ca^{2+} reuptake, both of which are essential for normal cardiac function. Thus, changes in proteins involved in coordinating Ca^{2+} movement may contribute to contractile dysfunction, however, the mechanisms responsible for functional abnormalities in obesity have not yet been fully clarified.

Considering the lack of information regarding high-fat diet-induced obesity, heart function, and the proteins involved in myocardial Ca^{2+} handling, the aim of this work was designed to study the hypothesis that this dietary model of obesity leads to cardiac dysfunction resulting from alterations in the regulatory proteins of intracellular Ca^{2+} homeostasis. Taken together, the results will provide an understanding of the mechanisms underlying the participation of this pathway in heart function during a prolonged period of obesity.

Many experimental studies with diet-induced obesity models focus not only on the amount of fat used but also on the source, which results in diets with a predominance of saturated or unsaturated fatty acids since they are substantially linked with different outcomes [109]. In addition, research studies confirm that dietary saturated fatty acids are positively related to increased ventricular remodeling, cardiac hypertrophy, and mitochondrial and contractile dysfunction [110]. Several studies mentioned in the literature that evaluated calcium handling-related proteins and cardiac function in obesity models used high-fat diets with a predominance of unsaturated fatty acids [111]. However, Cheng et al., using a high-fat diet rich in saturated fatty acids for 8 weeks, showed that only pPLN Thr17/PLN ratio was downregulated, without having modifications in the protein levels of SERCA2a, PLN, pPLN Ser16, cardiac function, and the ratios of SERCA2a and pPLN Ser16 to total PLN [112]. There is no study that assessed all proteins associated with myocardial Ca^{2+} handling in long-term obesity caused by a high-fat diet with a predominance of saturated fatty acids.

Studies have illustrated that feeding of high-fat diets in mice increases the production of myocardial reactive oxygen species (ROS) and downregulates the insulin-responsive phosphoinositide 3-kinase (PI3K)/protein kinase B (Akt) signaling pathway, independent of hypertension and obesity [113]. This signaling dysregulation was associated with myocardial

structural pathophysiology. Other studies have previously identified a role for Akt in cardiomyocyte Ca^{2+} regulation, particularly phosphorylating key Ca^{2+} handling proteins, the L-type Ca^{2+} channel, and phospholamban [PLN; the sarcoplasmic reticulum Ca^{2+} -ATPase (SERCA2a) regulator] [114]. The activity of Ca^{2+} flux proteins is firmly regulated by both kinase and phosphatase activities, and there is some evidence that dephosphorylation of PLN and ryanodine receptors plays a role in diabetic cardiomyopathy [115]. No study to date has sought a connection between enhanced intake of high-fat diets and cardiomyocyte Ca^{2+} dysregulation in the insulin-resistant myocardium.

1.10 Ischemic conditioning

There is an improved survival of MI due to early reperfusion therapy after the acute event, however, strategies that protect the heart during ischemia are still missing in clinical practice, and that ischemic conditioning may represent a promising strategy toward this end. Ischemic conditioning, a powerful form of endogenous protection against MI by improving myocardial salvage, has been demonstrated in many animal species and in isolated human cardiomyocytes. The term 'ischemic conditioning' indicates the priming of the tissue at risk with short non-deleterious and monotonous phases of sublethal ischemia [116]. This study deals with ischemia-reperfusion injury and myocardial infarction and is based on the protection of the heart from ischemic damage. Experiments addressing the mediators of this so-called ischemia/reperfusion (I/R) injury have offered novel therapeutic strategies. However, all these approaches have not been yet favorably executed in clinical practice. As listed in animal models, the vigorous cardioprotective repercussion of ischemic conditioning undeniably proclaims more inventive research both at the experimental and clinical extents [117].

1.10.1 Ischemic conditioning of the heart

Transient ischemia and reperfusion protect the heart from subsequent I/R injury because infarct sizes are smaller. In the following years, reduction of infarct size with postconditioning has been described in most of the experimental studies and, despite the lack of complete consensus, has emerged as a promising cardioprotective intervention [118]. Postconditioning (i.e, brief cycles of ischemia-reperfusion applied immediately after reopening the culprit coronary artery) could reduce myocardial infarct size by 30% to 40%. These results are consistent with the long-held hypothesis that lethal reperfusion injury indicates an important component of the final irreversible damage to the heart. Interestingly, the ischemic stimulus works not only if the heart itself undergoes ischemia and reperfusion, but also if it is applied remote from the heart, for example to a forearm, as in our experiments. The biological effects of ischemic conditioning are supported by strong experimental data. [123] In the heart, ischemic conditioning not only reduces infarct size but also improves contractile function after I/R (Figure 1.10) [124][125].

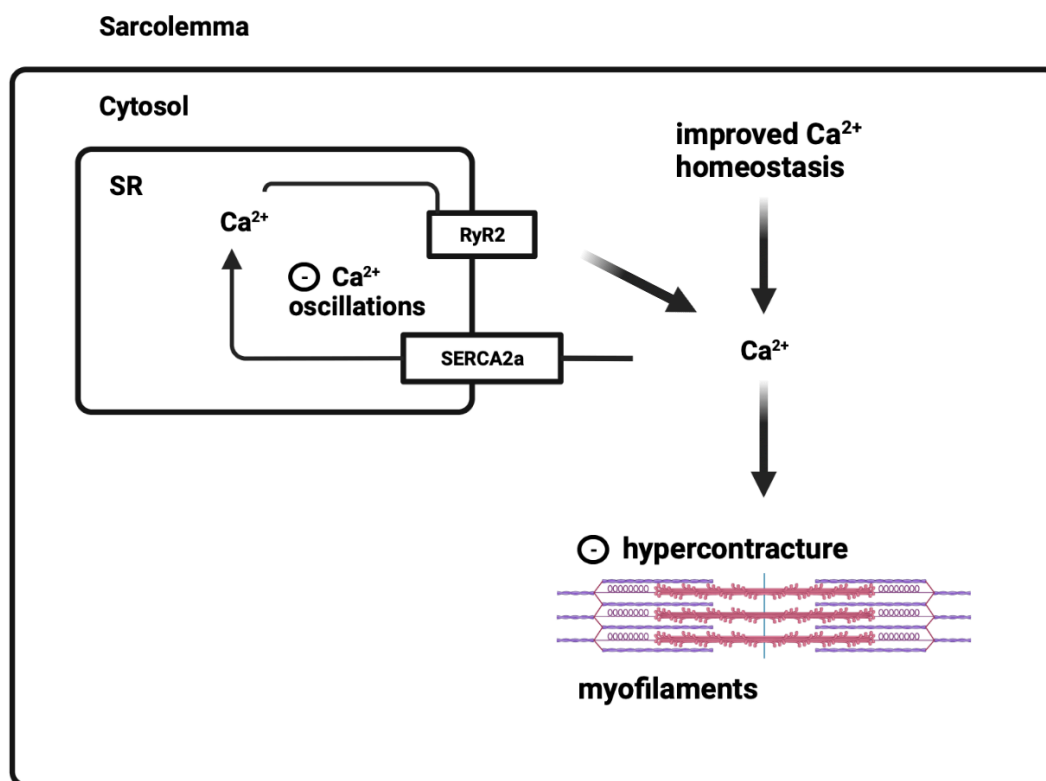


Figure 1.10: Hypothesized role of Ca^{2+} in ischemic conditioning of cardiomyocytes. Key signaling steps on subcellular level, influencing myocardial contractile function during I/R with ischemic conditioning. (–) denotes decrease; Ca^{2+} -calcium; I/R-ischemia/reperfusion; RyR2-ryanodine receptor 2; SERCA2a-sarcoplasmic/endoplasmic reticulum Ca^{2+} -ATPase; SR-sarcoplasmic reticulum.

1.10.2 Remote ischemic conditioning

Remote ischemic conditioning (RIC) is a process through which periods of intermittent ischemia, generally via the constant function of a blood pressure cuff to a limb above systolic pressure, define systemic protection against ischemia in temporally discrete vascular territories. The underlying mechanisms have not been characterized fully but have shown the involvement of neural, hormonal, and systemic inflammatory signaling cascades [119]. There might be structural changes or disorders in signal transduction between the remote organ and the effector organ (i.e., a modification in the release of the humoral factors) leading to possible loss of cardioprotection by RIC. The organ protection is somewhat mediated by the release of endogenous substances into the bloodstream because plasma from RIC-treated humans is cardioprotective [120]. This remote ischemic conditioning revealed that the RIC signal from remote tissue to the heart involves neuronal and humoral pathways that are transported via the blood from the arm to the heart. The plasma from RIC-treated humans can be dialyzed, and the dialysate applied to a heart can achieve cardioprotection. Since these to-date unknown factors also improve cardiac contractile function that is closely regulated by rapid changes of Ca^{2+} concentrations within myocytes, it's a hypothesis that a humoral factor that is induced by RIC affects cardiomyocyte Ca^{2+} homeostasis, because calcium mediates muscle contraction. The explicit nature of the circulating cardioprotective factors released by RIC remains unknown. RIC by transient limb ischemia depends on intact neural

pathways and nitric oxide-sensitive nerve stimulation to release blood-borne, hydrophobic, and small (molecular mass >15 kDa) circulating factor(s) [121]. The reduction in noncardiac complications recommends that, unlike local conditioning, RIC may have more widespread outcomes not only limited to the heart but also advantageous for thrombolysis in the treatment of stroke and for prevention of contrast medium-induced nephropathy [122].

The ischemic conditioning stimulus can be successfully applied before, during, or after the main ischemia (pre-, per-, postconditioning, Figure 1.11) [123]. Theoretically, three entities of remote ischemic conditioning (RIC) and ischemic preconditioning (IPC) can be categorized: the generation of a protective signal, the transfer of the signal to the target organ, and the response to the transferred signal resulting in cardioprotection [124]. Transient ischemic episodes of peripheral tissue enhance the tolerance of the myocardium against I/R injury. The concept of endogenous cardioprotection have been expanded to encompass the paradigms of postconditioning (with the protective stimulus applied to the heart at the time of reperfusion) and the intriguing phenomenon of remote conditioning (in which the protective trigger is applied at a remote site, either before, during, or immediately on ease of sustained myocardial ischemia). As expected, considerable effort has been invested in validating the infarct-sparing effect of preconditioning, postconditioning, and remote conditioning in multiple species and models, to gain the insight into the molecular mechanisms responsible for conditioning- induced cardioprotection. The current challenge and, indeed, the current mandate are to subsidize on this wealth of knowledge and utilize the favorable effects of myocardial conditioning to protect the human heart from ischemia-reperfusion injury [125].

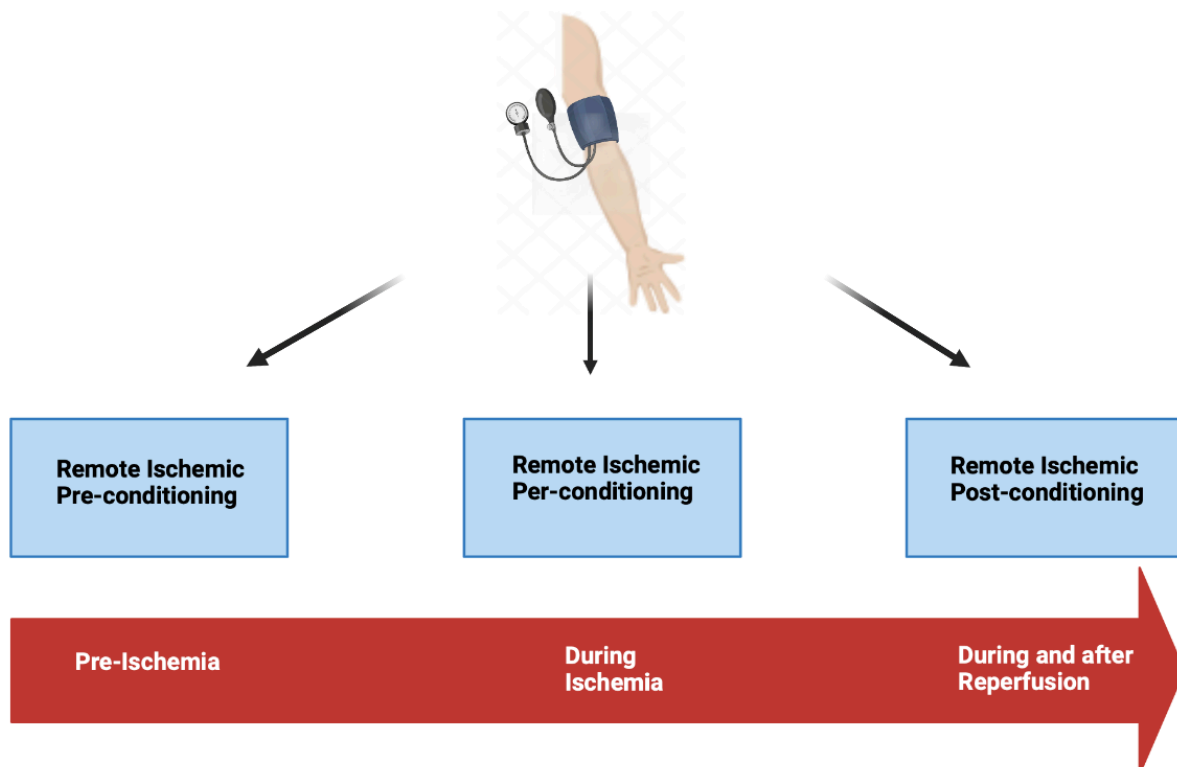


Figure 1.11: Model of remote ischemic conditioning

Experimental findings on ischemic preconditioning cannot be directly extrapolated to humans because its mechanisms differ from other animal species. Unfortunately, for both ethical and logistic reasons, no clinical study can meet the strict conditions of experimental studies on preconditioning with infarct size as the endpoint. Thus, surrogate endpoints have been used, including electrocardiographic ischemic changes, contractile function, or biochemical evidence of cell damage. As the mechanisms of ischemic preconditioning may differ from those involved in the reduction of infarct size in the experimental models, these must be considered in the evaluation of clinical studies on preconditioning. *In vitro* human studies have shown that human cardiomyocytes can be preconditioned in which confounding effects due to coronary collateral flow can be overcome. Yellon et al. showed that isolated, superfused, contracting human atrial trabeculae can be preconditioned against a combined hypoxic and substrate depletion challenge by simulated ischemia [126].

Several previous studies have used surgical ligation of the femoral vessels with or without abrogation of the femoral nerve to induce preconditioning at remote sites [127]. This confined approach was further integrated with mere visual control of ischemia and reperfusion success in the hindlimb of mice without the profit of objective and dependable quantitative measurement methods. The unique prospect of translating RIC to the clinical setting acquires from its universal availability and non-invasive nature. The latest meta-analysis of current trials indicated a clear effect of RIC on clinical outcomes [128].

However, not all studies have correspondently reported beneficial effects from RIC, and some study populations did not show any infarct-sparing effects. Another important limitation of many clinical studies reported is indicated by the extent of coronary collateral flow, which, in humans, is a major factor in the severity of myocardial ischemia during coronary occlusion, it cannot always be accurately quantified. Therefore, animal models remain the possible course of choice for molecular studies into the underlying signaling mechanisms in RIC with particular significance for mouse models considering the availability of knockout specimens. The suitable RIC stimulus in animal models should mirror the maneuver in patients, thus avoiding the drawback of blood loss, inflammation, and e.g., pain as induced by surgical techniques.

1.11 Questions

Despite the rising use and success of interventional coronary reperfusion approaches, morbidity and mortality from acute MI are still substantial. Acute MI is one of the most common causes of death both in Germany and worldwide [35]. During the first hours to days after MI, cytosolic Ca^{2+} concentration increases in the infarcted area of the myocardium, triggering apoptotic and necrotic processes. It was found that the sarcomere function is disturbed 24 hours after I/R also in the non-ischemic myocardium. The underlying causes include reduced kinetics of intracellular Ca^{2+} transport, because local Ca^{2+} concentrations in cardiac myocytes coordinate the activity of

contractile units. Disturbed calcium involves impaired activity of SERCA2a, which transports cytosolic Ca^{2+} to intracellular stores [56], [61]. SERCA2a activity also was found reduced in hearts of db/db mice, and even more severe impairment of Ca^{2+} cycling was observed in remote cardiomyocytes of this established animal model for T2DM 24 hours after I/R.

Based on these data, this thesis work investigated the following questions:

Does disturbed cardiomyocyte Ca^{2+} cycling in the remote myocardium contribute to the worse outcome of diabetic hearts after ischemic injury?

To answer these questions, this work aimed to investigate if the I/R-induced depression of cardiomyocyte Ca^{2+} cycling in the remote myocardium of db/db hearts was sustained for longer than 24 hours. To this end, myocyte Ca^{2+} handling and sarcomere function were analyzed in db/db hearts 10 days after I/R by surgical transient coronary artery occlusion. At this later timepoint, myocardial remodeling has overcome the early inflammatory phase and proliferative processes have already occurred. Thus, acute (oxidative) stress responses and immune cell accumulation due to chemokine and cytokine release as potential triggers of Ca^{2+} dysregulation early after I/R are no longer present. Analyses of expression and posttranslational modifications of Ca^{2+} regulators in heart tissue at this later time point supplemented the measurements.

To evaluate the significance of T2DM myocyte Ca^{2+} mishandling and contractile dysfunction of the heart, it was also investigated if Ca^{2+} cycling and sarcomere function were found disturbed also in an independent mouse model of chronic hyperglycemia, the DIO mice. As described in 1.9., DIO mice develop a pre-diabetic phenotype with hyperglycemia due to a diabetogenic diet, but not the fully developed metabolic phenotype as db/db mice. The comparison of both mouse models may help to identify specific causes underlying Ca^{2+} dysregulation in T2DM.

Do the cardioprotective effects of remote ischemic conditioning during ischemic injury involve cardiomyocyte Ca^{2+} handling?

It was shown that remote ischemic conditioning exerts cardioprotection via a humoral factor that can be transferred across species and is able to enhance active force production of the myocardium after hypoxia suggesting myocyte Ca^{2+} regulators as a potential target [129]. Since positive inotropic effects have been observed in human trabeculae within 1 h of treatment, freshly isolated mouse cardiomyocytes were also incubated for 1 h with plasma dialysates from human healthy volunteers with and without remote ischemic conditioning before measurements of intracellular Ca^{2+} kinetics and sarcomere function.

2 Material and Methods

2.1 Animal testing

The mouse is a well-established model organism for myocardial infarction because of its close physiological and genetic similarities to humans as well as the ease with which its genome can be manipulated and analyzed. In addition, well-characterized genetic models for T2DM exist, such as the leptin receptor-deficient db/db mouse.

The animal experiments were approved and executed according to the guidelines of the German Animal Welfare Act, in advance by the North Rhine-Westphalia State Office for Nature, Environment and Consumer Protection (LANUV) (Az. 84-02.04.2017.A145). Breeding and husbandry of the animals took place under standardized conditions and was performed at the Central Facility for Animal Research and Animal Welfare (ZETT) of Heinrich Heine University Düsseldorf, Germany.

2.1.1 Animals used

Male leptin receptor-deficient, db/db mice aged 10 to 12 weeks were studied for the type II and I/R diabetes mellitus combination. To accomplish DIO investigation, male C57BL/6 mice were fed for 9 weeks with either a standard diet (control) or a high-fat diet (HFD) and tap water. This experimental design resulted in the following two experimental groups: control and HFD.

These mice were obtained from the breeding group of Prof. Dr. J. W. Fischer from the Institute of Pharmacology and Clinical Pharmacology, Heinrich-Heine-University, Düsseldorf, Germany. C57BL/6J male mice aged 8 to 9 weeks were used for the RIC dialysates studies. These animals were obtained directly from Janvier Labs (Le Genest- Saint-Isle, France).

2.1.2 Initiation of myocardial infarction

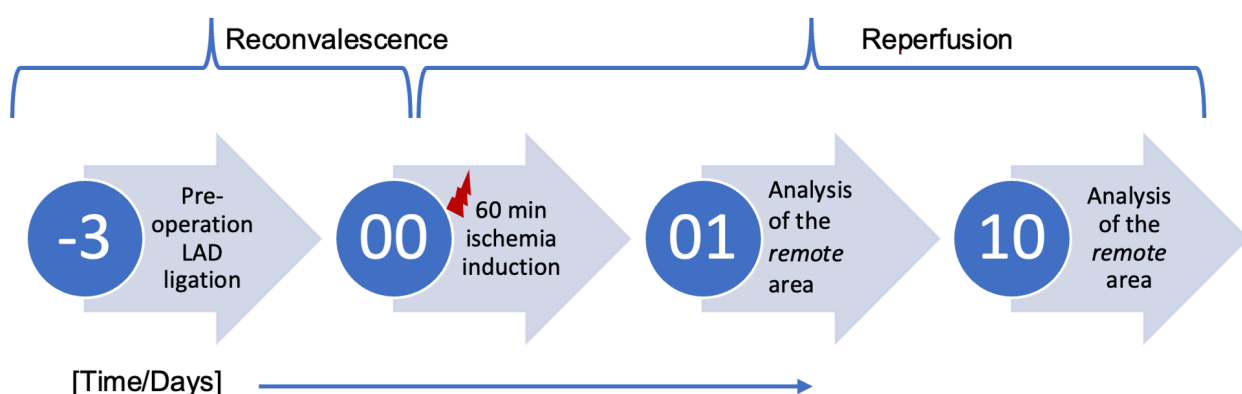


Figure 2.1: Timeline of myocardial infarction performance. LAD = left anterior coronary artery. The timing of the experimental procedure is outlined in Figure 2.1.

The preoperational LAD ligation was performed three days before ischemia induction (chapter 2.1.2.1). After the convalescence of the mice for three days, ischemia was induced for 60 minutes on day 0 (chapter 2.1.2.2). 10 homozygous (db/db) and 10 heterozygous (db/+) mice were operated but 9 db/db and 10 db/+ mice survived the procedure until 10d after I/R which were analyzed. The preoperations were performed by Prof. Dr. J.P. Schmitt. The pre-operations of the db/db mice were performed by Dr. Simone Gorreßen and Mr. Dominik Semmler.

2.1.2.1 Pre-operation

Mice were anesthetized by intraperitoneal injection using xylazine (10 mg/kg body weight) and ketamine (60 mg/kg body weight). The effectiveness of anesthesia was checked by pressing the paws and mice's tail root. The mice were placed supine on a heated hot plate (37 °C). Then they were intubated and connected to a ventilator (Minivent Microventilator, Hugo Sachs Elektronik-Harvard Apparatus GmbH, March-Hugstetten, Germany). Ventilation was performed with a stroke volume of approximately 250 µl at a ventilation rate of 140 breaths per minute with a mixture of 1/3 oxygen and 2/3 room air.

During the pre-operation, a suture loop is placed around the LAD, which later closes the vessel by tensioning it. A Leica MZ9.5 stereomicroscope (Meyer Instruments, Houston, Texas, USA) was used. After thoracotomy was performed between the 3rd and 4th ribs, the pericardium was cut. A 7-0 suture (7-0 Pro- lene™, Johnson & Johnson Ethicon, Norderstedt, Germany) was carefully passed under the LAD, 1 mm away from the tip of the left cardiac ear. The suture was cut from the needle, and both ends were threaded through a 1-mm-thick polyethylene ring (PE-10) to form a loose loop around the LAD. The thorax was closed with a suture (4-0 Prolene™, Johnson & Johnson Ethicon, Norderstedt, Germany) and the ends of the suture loop around the LAD were then passed out of the thorax to the left and right of the closure knot. The two ends were knotted and placed subcutaneously under the skin on the right side of the thorax. Finally, the skin was sutured together with a suture (5-0 Prolene™, Johnson & Johnson Ethicon, Norderstedt, Germany) and closed. After the mouse was awake again, ventilation was discontinued. For pain relief, the mice were treated subcutaneously with buprenorphine (0.05-1 mg/kg) every 8 hours for the following 2 days.

2.1.2.2 Ischemia induction with closed thorax

Prior to ischemia induction, mice were anesthetized with a mask through which isoflurane (Fluovac, Hugo Sachs Elektronik-Harvard Apparatus GmbH, March-Hugstetten, Germany) was flooded. During this procedure, the mice snouts were held in the mask and ventilated with a mixture consisting of 1/3 oxygen and 2/3 room air and an isoflurane content of 5% by volume. Suction of the isoflurane was performed with a Veterinary Fluosorber (Fluovac Harvard Apparatus, Edenbridge, Kent, UK).

After the anesthesia, animals were placed on their backs on the operating table. Here, the paws were fixed on the warming plate with adhesive tape. The body temperature of the mice was maintained at 37 to 37.5 °C throughout the duration of ischemia and monitored with an endorectally inserted probe. For occlusion control of the left anterior coronary artery (LAD), mice were connected to an electrocardiogram (ECG) (Hugo Sachs Harvard-Apparatus GmbH, March-Hugstetten, Germany) throughout ischemia induction. The ECG needles were attached to the paws.

Before the skin suture knots were carefully cut and opened, the isoflurane concentration was lowered to 2% by volume. After opening the skin, the ligature sutures were carefully dissected free from the skin pocket without applying tensile stress. The sutures were then led away to the left and right sides, respectively, and attached to a magnetic holder with adhesive tape (Figure 2.2). Under constant ECG monitoring, the suture tension was carefully increased by moving the magnetic holders apart on the operating table until the ECG showed ST-segment elevation (see chapter 2.1.2.3). To ensure 60 minutes of LAD occlusion, suture tension was checked at least every 10 minutes. For disinfection and to avoid encrustation during occlusion, the wound was treated with Betaisodona® solution (Mundipharma GmbH, Limburg, Germany) and kept moist with isotonic saline solution (Fresenius Kabi Deutschland GmbH, Bad Homburg, Germany).

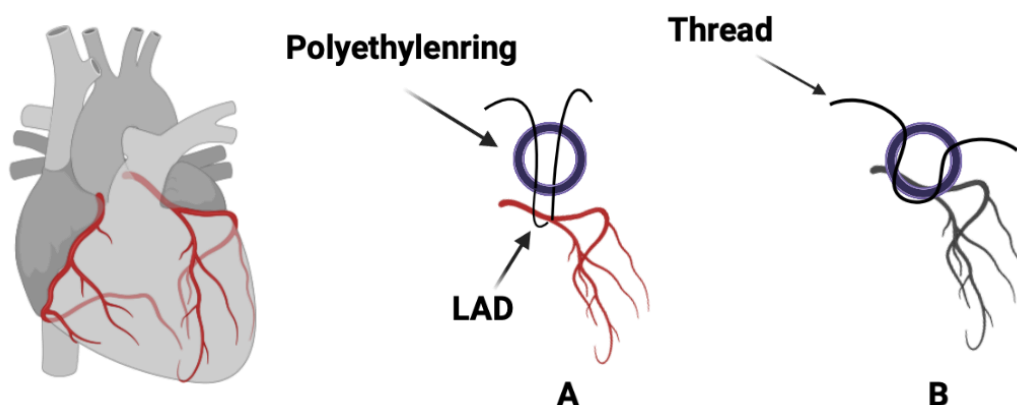


Figure 2.2: Illustration of the LAD ligation modified after Teramoto et al [130]. A: Condition at pre-operation. The suture loop is placed around the left anterior coronary artery, but no tension is yet applied to the sutures. Ligation has not yet occurred. B: Ligation of LAD. When the suture is tightened at both ends, the polyethylene ring moves downward, and the blood flow is stopped through the LAD at this point.

After 60 minutes of ischemia, both sutures were cut as close to the thorax as possible, and reperfusion was initiated. Subsequently, the skin was dressed with a Prolene filament (5-0 Prolene™, Johnson & Johnson Ethicon, Norderstedt, Germany). Anesthetization of the mice was terminated shortly thereafter. Instead of ischemia induction, the animals in the control group were anesthetized for one hour but overall underwent the same procedure.

2.1.2.3 Verification of LAD occlusion by means of ECG

Occlusion of the LAD, and induction of I/R, were monitored by ECG for 1 hour. At baseline, before the suture placed around the LAD was tightened, the basal ECG was recorded using Basic Data

Acquisition Software (BDAS; Harvard Apparatus, Holliston Massachusetts, USA). The derivation of a normal mouse ECG is shown in Figure 2.3 A. Occlusion of the LAD was evidenced by ST elevation in the ECG (Figure 2.3 B). Reperfusion of the ischemic tissue began, after the reopening of the LAD. This was evidenced a few minutes later by a slight decrease in ST elevation on the ECG (Figure 2.3 C).

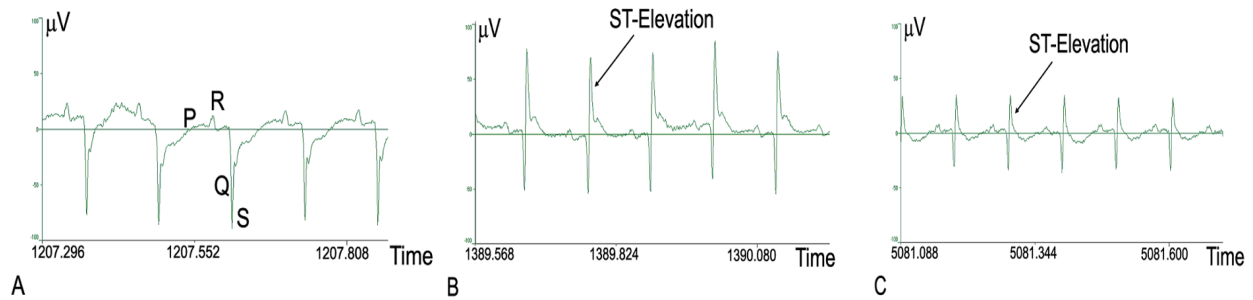


Figure 2.3: Section of a mouse electrocardiogram (ECG). A: basal ECG before ischemia induction; B: ECG with ST elevation after ischemia induction; C: ECG after reopening of the LAD and start of reperfusion.

2.2 Measurements on isolated cardiomyocytes

2.2.1 Isolation of cardiomyocytes by retrograde perfusion

Mice hearts were harvested after 1 hour of ischemia and 10 days of reperfusion. Approximately 5 to 10 minutes before the mice were killed by cervical dislocation, they were heparinized intraperitoneally with 400 U heparin sodium 25.000 (I.U./5 ml) (ratiopharm GmbH, Ulm, Germany). Then, within 5 minutes, the heart was removed from the thorax and the aorta was attached to a cannula. The cannula should be placed carefully, otherwise, it would pierce the aortic valve and the coronary arteries would be displaced, and global perfusion of the tissue via the coronary vessels would be disrupted. A syringe filled with PBS was connected to the cannula and blood was carefully flushed from the heart. The heart was then connected via the cannula to a tubing system filled with Ca^{2+} -free buffer II to flush the remaining blood from the heart.

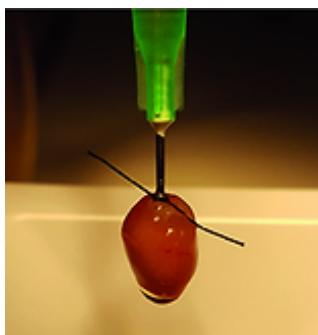


Figure 2.4: Cannulated heart. The aorta of heart is attached to a cannula with the black suture.

By maintaining a steady temperature of 37 °C, the step was further followed by six minutes of perfusion (2.2-2.4 ml/min) with a collagenase solution. The heart was then placed in a Petri dish filled with Wash Buffer I. The atria were separated like the infarcted cardiac apex and discarded.

This ensured that only cardiomyocytes were later isolated from the non-infarcted cardiac tissue. The remote myocardium was transferred in a 50 ml falcon tube together with wash buffer I and incubated for 10 minutes at 37 °C. The heart tissue was then transferred back to a Petri dish. Using fine scissors, the digested tissue was minced. The tissue pieces were then aspirated with a plastic pipette and carefully blown out again. In the process, the cardiomyocytes were dislodged from the tissue and brought into solution. Through a nylon mesh (150 µm pore size), the cell suspension was filtered, and the remaining tissue pieces were separated from the dissolved cells. To wash out the excess BDM, the cell suspension was washed three times with the washing buffers containing different concentrations of Ca^{2+} . After sedimenting the cells for ten minutes, a pellet was formed. The supernatant was removed, and wash buffer was added to the sedimented cell pellet. The cells were first washed with wash buffer I, then with wash buffer II, and finally with wash buffer III. At each washing step, the cells were carefully resuspended by inverting them. The buffers used are summarized in Table 1.

Table 1: Buffers and solutions used in the measurement on isolated cardiomyocytes (isolation of cardiomyocytes)

Buffer	Composition	
Phosphate buffered salt solution (PBS)	137 mM	Sodium chloride (NaCl)
	2.7 mM	Potassium chloride (KCl)
	1.5 mM	Potassium dihydrogen phosphate (KH_2PO_4)
	8.3 mM	di-sodium hydrogen phosphate (Na_2HPO_4) pH 7.4
Buffer I	126 mM	Sodium Chloride (NaCl)
	4.4 mM	Potassium Chloride (KCl)
	1 mM	Magnesium Chloride (MgCl_2)
	add 500 ml	DdH ₂ O (Millipore water)
Buffer II	4 mM	Sodium hydrogen carbonate (NaHCO_3)
	10 mM	(N-[2-Hydroxyethyl] piperazine-N''-[2-ethane sulfonic acid] (HEPES)
	30 mM	2,3 Butanedione monoxime (BDM)
	11 mM	Glucose

	50 ml	Buffer I
	1000 ml	DdH ₂ O (Millipore water) pH 7.3-7.35, sterile filtration, filter with 0.22 µm pore size (Filtropur S 0.2, Sarstedt Aktiengesellschaft & Co., Nümbrecht, Germany)
Buffer III	4 mM	Sodium hydrogen carbonate (NaHCO ₃)
	10 mM	HEPES
	11 mM	Glucose
	50 ml	Buffer I
	1000 ml	DdH ₂ O (Millipore water) pH 7.3-7.35, sterile filtration, filter with 0.22 µm pore size (Filtropur S 0.2, Sarstedt Aktiengesellschaft & Co., Nümbrecht, Germany)
Loading buffer	137 mM	Sodium chloride (NaCl)
	5.4 mM	Potassium chloride (KCl)
	0.5 mM	Magnesium chloride (MgCl ₂)
	10 mM	HEPES
	5.5 mM	Glucose
	1000 ml	DdH ₂ O (Millipore water) pH 7.3-7.35, sterile filtration, filter with 0.22 µm pore size
	1 M	Calcium chloride (CaCl ₂) solution (freshly added 5.0 l to 10 ml)

Perfusion buffer	137 mM	Sodium chloride (NaCl)
	5.4 mM	Potassium chloride (KCl)
	1.2 mM	Calcium chloride (CaCl ₂)
	0.5 M	Magnesium chloride (MgCl ₂)
	10 mM	(N-[2-hydroxyethyl] piperazine-N`2-ethane sulfonic acid] (HEPES)
	5.5 mM	Glucose
	500 M	Probenecid
	1000 ml	DdH ₂ O (Millipore water) pH 7.3-7.4, sterile filtration, filter with 0.22 m pore size (Filtropur S 0.2, Sarsted Aktiengesellschaft & Co., Nümbrecht, Germany)
Collagenase solution	0.4 mg/ml	Collagenase type I (300 U/mg)
	20 ml	Buffer II
	0.1 M	Calcium chloride (CaCl ₂) solution (Freshly added 5.0 l to 20 ml). The collagenase solution was always freshly prepared.
Wash buffer I	20 mg/ml	Albumin Bovine Serum Fraction V
	20 ml	Buffer II
	1 M	Calcium chloride (CaCl ₂) solution (freshly added 2.0 l).
Wash buffer II	20 mg/ml	Albumin Bovine Serum Fraction V
	10 ml	Buffer II
	1 M	Calcium chloride (CaCl ₂) solution (freshly added 2.0 l).
Wash buffer III	20 mg/ml	Albumin Bovine Serum Fraction V
	5 ml	Buffer II
	5 ml	Buffer III
	1 M	Calcium chloride (CaCl ₂) solution (freshly added 2.0 l).

2.2.2 Measurement of the myocyte Ca^{2+} cycle

2.2.2.1 Fluorescence indicator Fura-2 acetoxymethyl ester

Ca^{2+} is a dynamic secondary messenger as it plays an important role in stimulus-response reactions of cells. It fluctuates more rapidly than any other intracellular signaling substance. Tsien et al. [131] developed the membrane permanent derivative Fura-2 acetoxymethyl ester (Fura-2 AM; Thermo Fisher Scientific Inc., Waltham, MA, USA) to measure the intracellular calcium concentrations by fluorescence. When added to cells, it crosses the cell membrane unhindered into the cell interior of the intact cardiomyocyte, due to its four acetoxymethyl ester groups [131]. Once it is inside the cell, acetoxymethyl groups are removed by cellular esterases and this removal regenerates Fura-2, the pentacarboxylate calcium indicator from Fura-2 AM. Ca^{2+} binds to the released carboxyl groups.

Fura-2 is a ratiometric indicator that binds to free intracellular calcium [132]. Fura-2 emits light at 510 nm when excited at 340 and 380 nm of light, whereas the fluorescence intensity at each excitation wavelength depends on the calcium concentration (Figure 2.5). At high Ca^{2+} concentration, the fluorescence intensity excites at the wavelength of 340 to 350 nm whereas if the Ca^{2+} concentration is reduced until no more Ca^{2+} is present in the solution, then the fluorescence intensity of Fura-2 shifts to higher wavelengths of 380 to 390 nm. In addition, Fura-2 ratio allows for the correction of unequal dye loading etc.

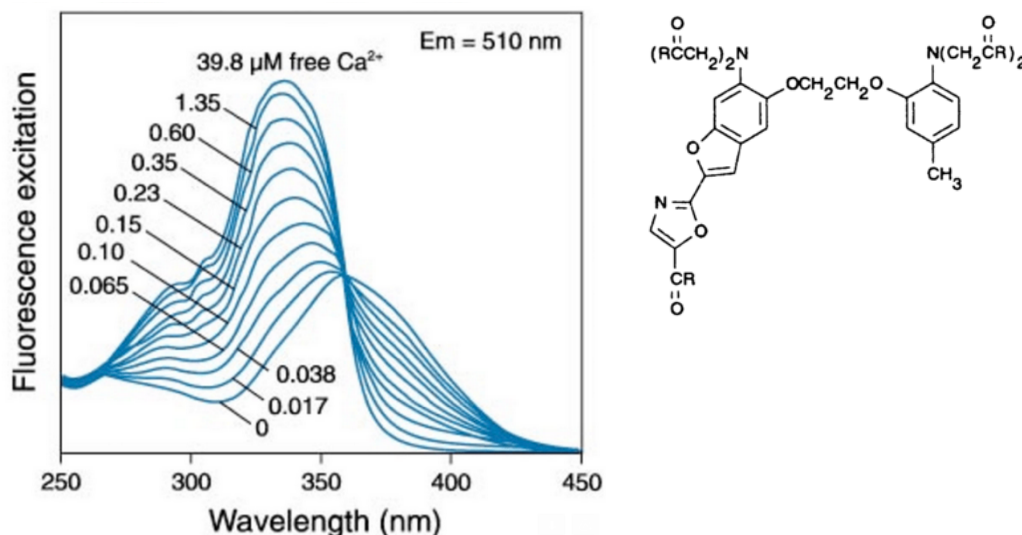


Figure 2.5: Fluorescence excitation spectra of Fura-2 at different Ca^{2+} concentrations [133]. Multiple solutions containing between 0 and 39.8 μM free $[\text{Ca}^{2+}]$, scanned between 250nm and 450nm and emission (Em) read at 510 nm. Top right structural formula of Fura-2

2.2.2.2 The β -adrenergic receptor agonist isoproterenol

Isoproterenol is a non-selective β -adrenoreceptor agonist. β -adrenergic stimulation increases the amplitude of the action potential plateau but accelerates repolarization and reduces the action potential duration. In this regard, β -adrenergic stimulation has been shown to steepen the

restitution curve in humans [134]. Protein kinase A also phosphorylates intracellular Ca^{2+} handling. In addition, PKA phosphorylates troponin I, thereby decreases the Ca^{2+} sensitivity of the troponin complex. The effect is to reduce the sensitivity of the contractile machinery to intracellular Ca^{2+} , but more importantly to facilitate the release of Ca^{2+} from the myofilaments which quickens the relaxation. PKA also phosphorylates phospholamban, releasing SERCA2 inhibition. Therefore, Ca^{2+} uptake into the SR is accelerated and this too speeds up the relaxation. Activation of SERCA2a results in an increase in the Ca^{2+} content of the SR and if “ Ca^{2+} overload” occurs this is expected to increase the spontaneous releases of Ca^{2+} from the SR.

2.2.2.3 Sample preparation

To measure myocyte Ca^{2+} cycling, isolated cardiomyocytes loaded with Fura-2 were pipetted into a small measurement chamber containing perfusion buffer. For each measurement, approximately 2 to 3 drops of the cell suspension were carefully transferred to the microscope bath with a Pasteur pipette. At this bath stage, the cardiomyocytes were continuously rinsed with fresh buffer warmed to 37 °C. Into the bath, the fresh buffer was pumped and removed using a roller pump (Ismatec Reglo Digital Peristaltic Pump; 4-Channels, Cole-Parmer GmbH, Wertheim, Germany). In the buffer solution feed, a heater (micro- Temperature Controller (mTCII, IonOptix, Milton, MA, USA) was used to control the buffer temperature and kept it constant at the set value. Inflow and outflow each took place at constant pressure and constant flow rate (1 ml/min).

Further, cells were first recorded in perfusion buffer for 10 to 15 mins and then were switched to Isoproterenol solution for β -adrenergic measurements. Cells were exchanged after 10 mins, by sucking off the previous ones using a roller pump and again were switched to perfusion buffer for baseline measurement.

The following perfusion buffers were used:

- for basal stimulation: perfusion buffer, see Table 1;
- for β -adrenergic stimulation: isoproterenol hydrochloride (Sigma-Aldrich, Steinheim, Germany) dissolved in perfusion buffer (10^{-7} M).

2.2.2.4 Instrument setup

Right and left electrodes (MyoPacer EP Field Stimulator, IonOptix, Milton, MA, USA) were located on the sides of the cardiomyocyte bath. After electrical stimulation was activated with 10 V at 0.5 Hz, the cardiomyocytes contracted in time. The contraction of the cells was observed under the microscope (Myocyte Fluorescence Microscope, MoticAE31 & Olympus Uapo/340 Objective, IonOptix, Milton, MA, USA).

After the activation of electrical stimulation, a suitable cell was selected under the microscope based on its surface characteristics and cell shape which includes elongated cylindrical cells and

striations. Fine adjustment of the microscope camera (MyoCam-S™, IonOptix, Milton, MA, USA) was performed with the help of a monitor so that the selected cardiomyocyte properly filled the measurement area and then the measurement was started. Cytosolic Ca^{2+} concentrations and sarcomere shortening were recorded in parallel by keeping the electrical stimulation activated. The measurement of sarcomere function is described in chapter 2.2.3.

2.2.2.5 Measurement of cytosolic Ca^{2+} concentrations

The change in cytosolic Ca^{2+} concentration was detected by Fura-2 fluorescence (HyperSwitch Myocyte System, IonOptix, Corporation, Milton, MA, USA). When Fura-2 is bound to Ca^{2+} the emitted fluorescence at 510 nm is greatest when excited at a wavelength of 340 nm. Unbound Fura-2 shows the strongest fluorescence at 510 nm at an excitation wavelength of 380 nm (Figure 2.5). This ratiometric measurement minimizes the influence of photobleaching, inequalities in the loading of cardiomyocytes with Fura-2, and differences in cell thicknesses on the measured values.

During the measurement, the excitation wavelengths 340 nm and 380 nm were alternated at a frequency of 500 Hz. Thus, F1 at 340 nm and F0 at 380 nm was recorded 250 times per second and the ratio F_1 / F_0 was calculated thus ensuring a high temporal resolution of the Ca^{2+} kinetics measurements. With the activation of electrical stimulation, voltage-dependent L-type Ca^{2+} channels of the ventricular cardiomyocyte are stimulated, depolarization of the sarcolemma occurs, and Ca^{2+} flows into the cell, resulting in the stimulation of the RyR2 and opening for a few milliseconds [1] [9]. As a result, Ca^{2+} is released into the cytosol from the SR where it binds to Fura-2. A steep increase in F_1 / F_0 occurs in the Ca^{2+} transient (Figure 2.6). This rise represents the rate at which Ca^{2+} is released from the SR via the RyR2. Its amplitude is dependent on the amount of Ca^{2+} released.

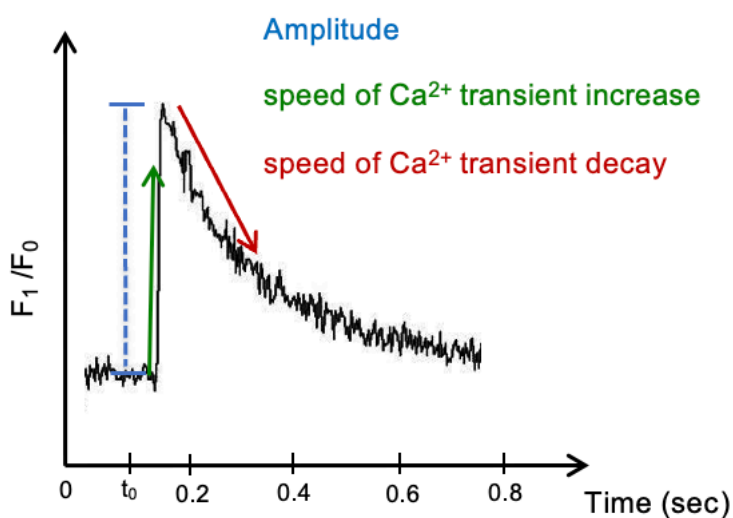


Figure 2.6: Representative Ca^{2+} transient. t_0 = time of electrical stimulation

Diastole is initiated after the rapid Ca^{2+} increase in the cytosol, and cytosolic Ca^{2+} is pumped back into the SR via SERCA2a. A small fraction leaves the cell via the sodium/calcium exchanger (NCX), the plasma membrane calcium ATPase (PMCA), and the mitochondrial uniporter. The concentration of cytosolic Ca^{2+} decreases, and now unbound Fura-2 is increasingly present. The decrease of $F1/F0$ in the Ca^{2+} transient determines the rate of Ca^{2+} from the cytosol into the SR via SERCA2a. The measurement of the isolated cardiomyocytes should last at most 15 minutes from the onset of electrical stimulation. Thereafter, the cardiomyocytes were aspirated from the bath and fresh resuspended cardiomyocytes were pipetted into the measurement chamber.

2.2.2.6 Measurement of Ca^{2+} transients of cardiomyocytes treated with plasma dialysates

Ethical approval for the collection and use of the human specimens was granted by the Ethics Committee of the University Hospital Essen (Az.20-9250-BO and Az.18-8279-BO). Ca^{2+} cycling in cardiomyocytes was analyzed after treatment with plasma dialysates of human blood samples from 10 healthy volunteers (Figure 2.7 A). These volunteers were subjected to RIC by 3 cycles of 5 min forearm ischemia and reperfusion (blood pressure cuff inflation/deflation). Venous blood samples were taken before ("Pre") and 30 min after ("Post") the RIC protocol. Frozen serum samples were provided by Prof. Petra Kleinbongard, Institute of Pathophysiology, University Hospital Essen, who guided the human studies. The day before the experiment, samples were thawed and plasma-dialysates were prepared (12-14 kDa dialysis tubing; dialysis over night at 4°C against sample buffer in a 1:5 volume ratio). Isolated mouse cardiomyocytes (C57BL/6) were exposed to the dialysates for 30 min. Next, the myocytes were incubated into hypoxia buffer and the buffer was overlayed with a layer of mineral oil for 50 min at room temp followed by reoxygenation of 5 min. Finally, they were loaded with the fluorescent Ca^{2+} indicator Fura-2 and paced (0.5 Hz) to measure cytosolic Ca^{2+} and sarcomere length during contractile cycles (Figure 2.7 B).

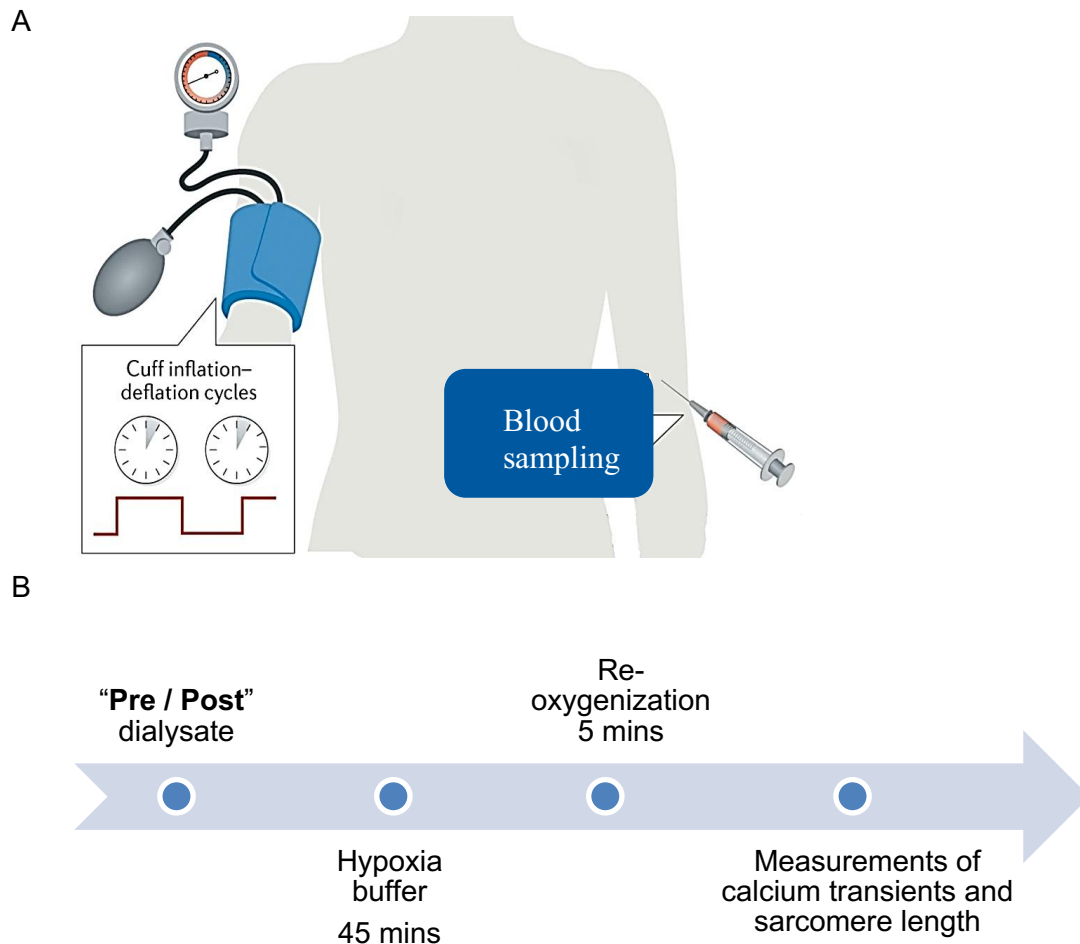


Figure 2.7: Illustration of treatment of cardiomyocytes with plasma dialysates. A: Representative blood sampling before and after RIC modified after Heusch [135]. B: Schematic showing the sequence of the experimental steps.

2.2.3 Measurement of sarcomere length

As already described in the measurement of the myocyte Ca^{2+} cycle (chapter 2.2.2), during each electrical stimulation, the IonOptix instrument (HyperSwitch Myocyte System, IonOptix, Milton, MA, USA) measures the sarcomere function and Ca^{2+} cycle simultaneously. The changes in cytosolic Ca^{2+} concentration is detected via fluorescence recordings. The contractile amplitude as well as the contraction and relaxation of the sarcomeres were analyzed via video recordings (MyoCam-S™, IonOptix Corporation, Milton, MA, USA). Initially, it is important to align the striation pattern in a vertical way within the field of view to get a proper sarcomere length measurement. A small section of the sarcomeres must be selected on the screen known as the region of interest (ROI) where sarcomere length is measured (Figure 2.8). Ideally, this is an area that should be defined, where the striped pattern of the sarcomeres is clearly visible. The ROI is the square enclosed by the magenta box in the video display and can be repositioned and resized at each cell. The selection of the ROI depends on the height and length of the ROI.

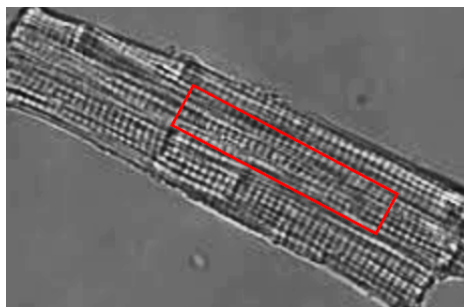


Figure 2.8: Selection of the user-defined region of interest of a cardiomyocyte for the measurement of Ca^{2+} transients and sarcomere function.

The approach used by the software is to estimate the frequency of the striation pattern located in the ROI, i.e., how many sarcomeres can be found per μm (Figure 2.8). It measures the distances between the stripes, acquiring 1000 data points per second. A fast Fourier transform (FFT) is calculated. The average sarcomere spacing is represented by the peak within the power spectrum, measured in real-time. When the basal resting phase ends and electrical stimulation occurs, the shortening of the contractile amplitude starts at time t_0 (Figure 2.9). It becomes maximal at the curve minimum. The rate at which the minimum of the function is reached after stimulation is determined by contraction velocity. On the other hand, the relaxation velocity measures the speed of the sarcomere relengthening before the electrical stimulation is regained.

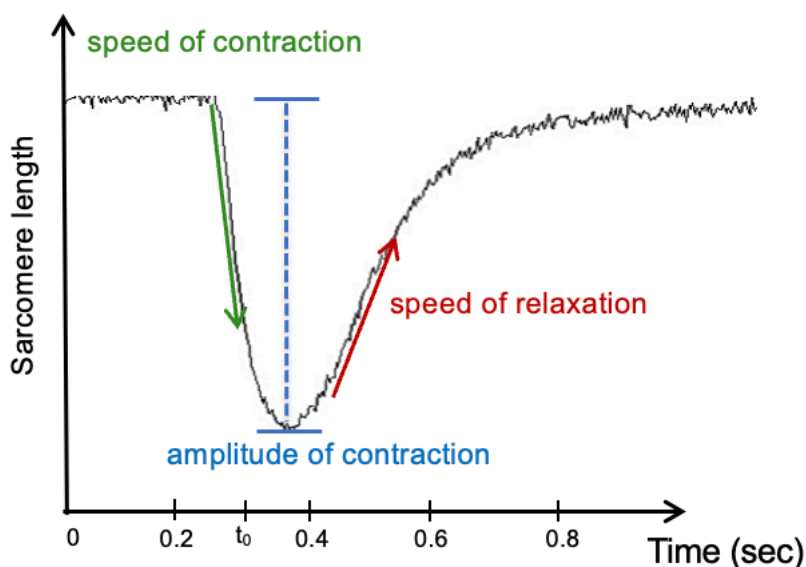


Figure 2.9: Representative sarcomere function. t_0 = time at which the electrical stimulation takes place.

2.2.4 Evaluation of Ca^{2+} transients and sarcomere function

The calculation of Ca^{2+} transients and the sarcomere functions recorded from each cardiomyocyte in parallel were evaluated to determine whether they were suitable for further evaluation. Selection criteria were: The amplitude of the sarcomere function and Ca^{2+} transient should be greater than $0.03 \mu\text{m}$ and the slope of the Ca^{2+} transient should be of maximum transition without side maxima. A cell should contract by electrical stimulation, not by spontaneous contraction and a clear stripe pattern should be recognizable to evaluate the sarcomere function of a cardiomyocyte. At least

ten sarcomere functions and Ca^{2+} transients were selected from each measured cardiomyocyte for further analysis.

Ion Wizard software (version 6.4, IonOptix, Milton, MA, USA) was used to evaluate the Ca^{2+} transients and sarcomere functions. The 10 transients or sarcomere functions of a cardiomyocyte were added up and averaged. From this averaged transient or averaged sarcomere function, parameters were then calculated, e.g., amplitude, rise, and decline of Ca^{2+} concentration. These characteristic parameters represent the arithmetic mean value from 10 cardiomyocytes with 10 transients averaged per myocyte for each mouse heart.

2.2.4.1 Determination of the speed of Ca^{2+} increase in the cytosol

The speed of Ca^{2+} released from the SR into the cytosol can be determined from the increase of the Ca^{2+} transient which increases almost linearly after electrical stimulation. Thus, the speed of Ca^{2+} increase (V_{Increase}) was calculated using the time $t_{p75\%}$ (time to 75% of the peak height) after which the amplitude increased by 75% (Figure 2.10).

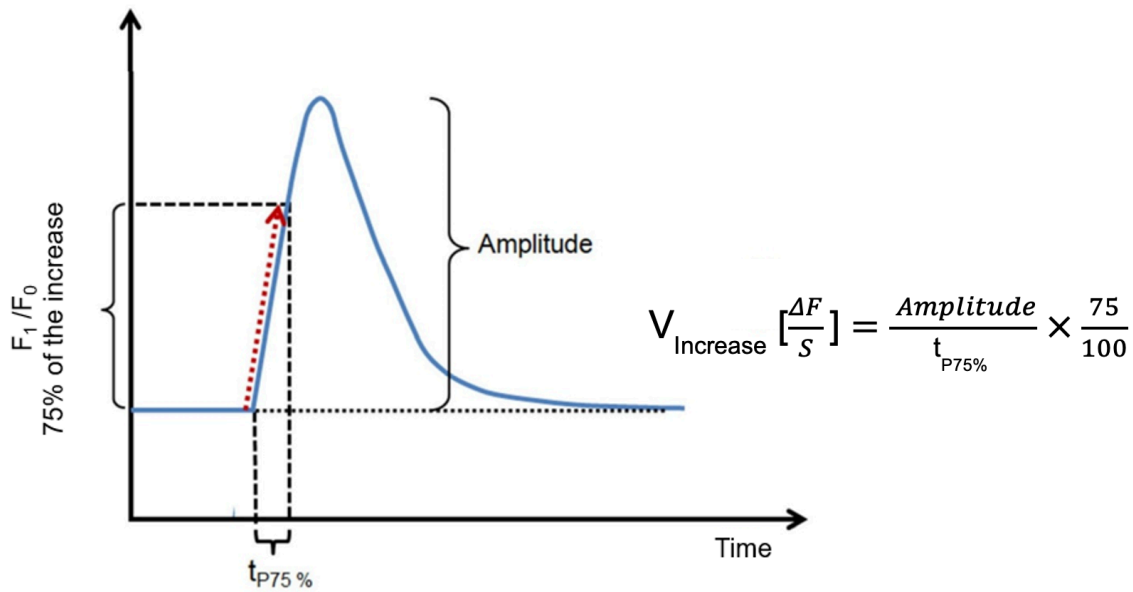


Figure 2.10: Determination of the speed of Ca^{2+} increase

2.2.4.2 Determination of the speed of Ca^{2+} decrease from the cytosol

After passing through the maximum, the rate at which Ca^{2+} is eliminated from the cytosol and reabsorbed into the SR can be seen from the drop in the Ca^{2+} transient. The Ca^{2+} transient drops almost linearly once it has reached the maximum. Only towards the end of Ca^{2+} transient decay, its speed significantly decelerates. The time $t_{b175\%}$ (time to 75% of the baseline) at which 75% of the maximum amplitude had dropped, was evaluated to determine the speed of the Ca^{2+} decrease (V_{Decrease}) (Figure 2.11).

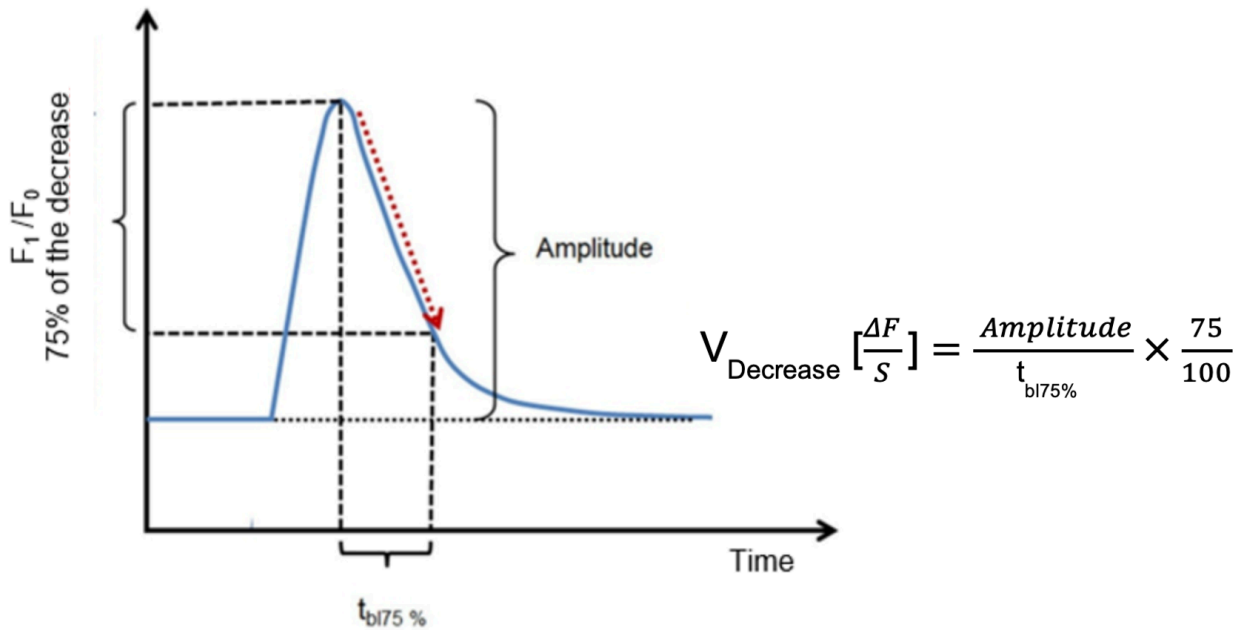


Figure 2.11: Determination of the speed of Ca^{2+} decrease

2.2.4.3 Determination of the contraction velocity of the sarcomeres

The sarcomeres contract almost linearly immediately after stimulation. Therefore, the time $t_{k75\%}$ (time to 75% of the contraction) was evaluated to determine the contraction speed ($V_{\text{Contraction}}$), after which the contraction has reached 75% of its maximum (Figure 2.12).

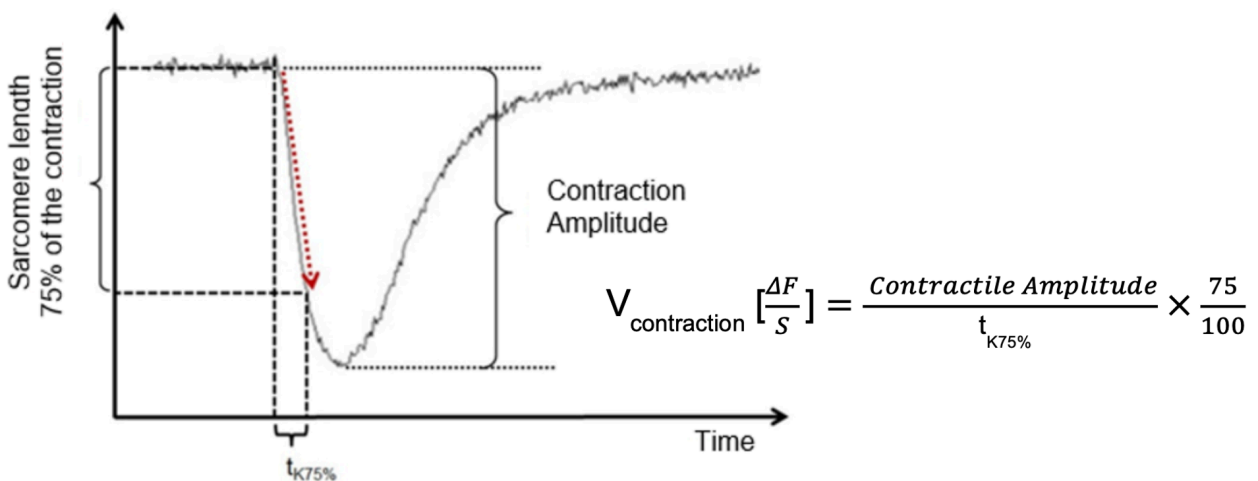


Figure 2.12: Determination of the contraction velocity from the sarcomere function

2.2.4.4 Determination of the relaxation speed of sarcomeres

After the sarcomere function has passed through the minimum, it increases again almost linearly in the first phase. The time $t_{r75\%}$ (time to 75% of the relaxation) was therefore evaluated to determine the relaxation speed ($V_{\text{Relaxation}}$), after which the sarcomere function had risen again to 75% (Figure 2.13).

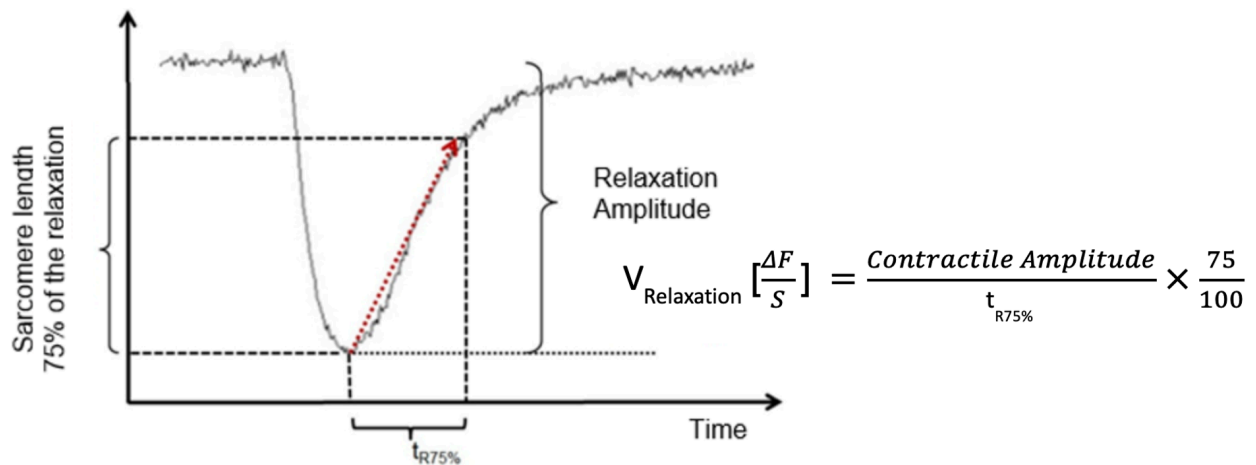


Figure 2.13: Determination of the relaxation velocity from the sarcomere function

2.3 Protein analysis

2.3.1 Work steps

Western blot is a method which is used to detect specific protein molecules from among a mixture of proteins by transferring it to a carrier membrane and subsequently a protein of choice can be quantitatively evaluated. The preparation steps are described in the following subchapters.

2.3.2 Production of the heart lysates

The heart was removed by killing the mice via cervical dislocation and the atria were discarded. Similarly, the heart infarcted apex was separated from the noninfarcted tissue. The middle portion between the infarcted area and the nonischemic tissue was generously eliminated to ensure that the remote tissue is free from the infarcted tissue and tissue of the marginal zones of infarction. The remote tissue samples were briefly placed in 0.9% NaCl solution to rinse out blood. Then immediately, they were frozen in liquid nitrogen and stored at -80°C .

To prepare the heart lysates, the frozen heart tissues were each placed in 1 mL of preparation buffer and cooled on ice. An Ultra Turrax IKA® T10 basic (IKA® Works, Inc., Wilmington USA) was used to homogenize the heart tissue samples. Each tissue sample was homogenized with ice for 10 seconds under cooling in three consecutive intervals, waiting 10 seconds between each interval. The cardiac lysates were then aliquoted, and Laemmli buffer (Table 2) was added in a 1:2 ratio to some of the aliquots.

Table 2: Buffers used in protein analysis (preparation of heart lysates)

Buffer	Composition	
Preparation buffer	10 mM	Trishydromethylaminomethane (Tris) (50 mM), pH 8.0
	0.5 mM	Ethylene glycol-bis (β -aminoethyl ether)-N,N,N',N'-Tetra-Acetic acid (EGTA)
	0.5 %	Titron-X 100
	0.1 %	Deoxycholic acid Titron-X 100
	0.1 %	Sodium dodecyl sulphate (SDS)
	140 mM	Sodium chloride (NaCl)
Laemmli buffer	1.5 mg	Bromophenol blue
	0,6 g	Sodium dodecyl sulfate (SDS)
	3ml	Glycerol
	3.9 ml	Trishydromethylaminomethane (Tris) (50 mM), pH 6.8
	10 ml	DH2 O (Millipore water)

2.3.3 Quantitative detection of the amount of protein using the BCA method

The bicinchoninic acid assay (BCA assay) is an assay, which is used to determine the total concentration of protein in a solution (0.5 $\mu\text{g/mL}$ to 1.5 mg/mL). The total protein concentration is indicated by a color change of the sample solution from green to purple in proportion to protein concentration, which can then be measured using colorimetric techniques. The protein concentration present in a solution can be quantified by measuring the absorption spectra and comparing it with protein solutions of known concentration.

For protein concentration determination in the heart lysates, they were diluted 1:5 with distilled water and mixed 25 μL + 200 μL with a reagent consisting of Pierce™ BCA Protein Assay Reagent B and Pierce™ BCA Protein Assay Reagent A (Thermo Scientific, Rockford, USA) (composition 1:50). Bovine serum albumin (BSA) dilution series served as the standard. The evaluation of protein levels was done photometrically at a wavelength of 562 nm using the Synergy™ Mx Microplate reader (BioTek Instruments, Inc., Winooski, VT, USA).

2.3.4 Polyacrylamide gel electrophoresis (SDS-PAGE)

Polyacrylamide gel electrophoresis (SDS-PAGE) is the most used method that ensures the dissociation of the proteins into their individual polypeptide subunits in accordance with their size. An anionic detergent SDS (Sodium Dodecyl Sulfate) is used in combination with a reducing agent followed by heating to break ionic and disulfide bonds of the proteins before they are loaded on the gel. When the denatured proteins bind to SDS, they become negatively charged. According to the size of the polypeptide, SDS-polypeptide complexes travel through polyacrylamide gels when an electric current is applied between the electrodes. This is because the amount of SDS bound is independent of its sequence and is proportional to the protein's molecular weight. For this purpose, two types of polyacrylamide gels were used: 1. A stacking gel that concentrates all proteins in one band and 2. a separating gel that allows to separate the proteins subsequently based on their molecular weight (Table 3). After polymerization is complete (around 30-40 min), the stacking gel is layered directly on to the surface of the separating gel which is prepared using 2-5% of acrylamide and separating gel is prepared using 5-15% acrylamide.

The same amount of protein should be loaded in a pre-determined order to each gel pocket. In addition, a marker (Prestained Protein Molecular Weight Marker, Fermentas, Thermo Fisher Scientific, Waltham, MA, USA) was applied to estimate the molecular weight of the polypeptide chain(s). At an electrical voltage of 80 V (PowerPac™ Basic Power Supply, Bio Rad Laboratories GmbH, Munich, Germany), the proteins were separated for approximately 20 minutes until the dye front has moved into the separating gel. Thereafter, the voltage was increased to 150 V for one hour.

Table 3: Buffers and gels used in protein analysis (gel electrophoresis)

Buffer	Composition	
10 x running buffer	250 mM	Trishydromethylaminomethane (Tris)
	1.9 mM	Glycine
	1 %	Sodium dodecyl sulfate (SDS)
1 x lysis buffer	1 %	Sodium dodecyl sulfate (SDS)
	1 mM	Phenylmethylsulfonyl fluoride (PMSF)
	10 mM	Trishydromethylaminomethane (Tris), pH 7.4
Separating gel (15 %)	2.13 ml	DdH ₂ O (Millipore water)
	1.97 ml	Separating gel buffer

	3.79 ml	Acrylamide/ Bis-acrylamide (30 %)
	3.9 µl	N, N, N', N'-tetramethylethylenediamine (TEMED)
	51.1 µl	Ammonium persulfate (APS) (100mg/ml)
Separating gel buffer	1.5 M	Trishydromethylaminomethane (Tris)
	0.4 %	Sodium dodecyl sulfate (SDS)
		pH 8.8
Collection gel	2.06 ml	DdH ₂ O (Millipore water)
	825 µl	Collection gel buffer
	412.5 µl	Acrylamide/ Bis-acrylamide
	3.3 µl	N, N, N', N'-tetramethylethylenediamine (TEMED)
	33 µl	Ammonium persulphate (APS)
Collecting gel buffer	0.5 M	Trishydromethylaminomethane (Tris)
	0.4 %	Sodium dodecyl sulfate (SDS)
		pH 6.8

2.3.5 Western blot

The transfer stack was constructed in the form of a layered structure. Gel and transfer membrane (Immobilon® -P Transfer Membrane, Millipore, Merck KGaA, Darmstadt, Germany) were arranged on top of each other and sandwiched between three layers of Whatman® Chromatography Paper (Whatman® 3 mm Chr Chromatography Paper, GE Healthcare Life Sciences, Buckinghamshire, UK). Prior to placement of the membrane on the gel, it was activated with 100% methanol for 30 seconds and then rinsed with Western blot buffer.

The stack was terminated on both sides with a blotting sponge. The transfer stack was then placed in the blot chamber with the membrane opposite to the anode (+) and the gel opposite to the cathode (-). Once the voltage is applied, the electric field is directed perpendicular to the membrane and gel. The chamber was filled with Western blot buffer. Protein transfer was performed at a constant voltage of 100 V for 1 hour. After the transfer, unspecific binding sites on the membrane were blocked using 0.5% block milk (see Table 4) and the SNAP i.d.® 2.0 Protein Detection System (Merck KGaA, Darmstadt, Germany). Membranes were incubated with one of the primary antibodies in a chilled glass Petri dish at 4 °C on a shaker overnight. Primary antibodies were dissolved in 5% block milk. The next day, the primary antibody was withdrawn

from the Petri dish and frozen at -20°C. The primary antibodies were reused up to five times. Membranes were then washed four times with 30 ml of TBST buffer, each in the SNAP i.d.® 2.0 Protein Detection System. Then, the corresponding secondary antibody was attached to the membrane for 10 minutes followed by four more washes with TBST buffer and finally, the membrane was placed in a Petri dish filled with ECL reagent (Immobilon™ forte, Millipore Corporation, Billerica, MA, USA). Secondary antibodies were dissolved in 0.5% block milk.

Table 4: Buffers and solutions used in protein analysis (Western blot)

Buffer	Composition	
Block milk		Milk powder in TBST buffer (0.5 %; 5 %)
10 x TBS	100 mM	Trishydromethylaminomethane hydrochloride (Tris / HCl)
	1.5 mM	Sodium chloride (NaCl), pH 7.4
1 x TBST	1 x	TBS
	0.1%	Tween 20
	1000 ml	DdH ₂ O (Millipore water)
Western blot buffer 10x	15.15 g	Trishydromethylaminomethane (Tris)
	56.25 g	Glycine
	500 ml	Methanol (10 %)
	500 ml	DdH ₂ O (Millipore water)

2.3.6 Western Blot Imaging

The images of Western blots were taken by using UVP ChemStudio imaging system (UVP ChemStudio™, Analytik Jena, USA). In this gel and blot imagers, no film is required for imaging. A clear visual of faint bands and finer details of images are possible with an integrated 13.3-inch, wide touch-screen computer. Large and visible icons on the VisionWorks touch Software, enhances the accessibility for improved and efficient workflow. For quick selection of various gel and blot applications, image capture and enhancement are automated with application-based icons.

2.4 Statistics

The software program i.e., used for analysis is ion wizard 6.4 which performs a standard analysis of data with contractility and Ca^{2+} transients. The software integrates the presentation of fluorescence traces and images analog voltages and cell length data. It analyses raw data by performing ratio, ion, or linear calibration calculations. Statistical analyses were executed using the software GraphPad Prism 9.4.0 (Graph- Pad Software, Inc., La Jolla-San Diego, CA, USA). Two groups were compared by unpaired, two-sided Student's t-test. 2-way ANOVA was used to compare data sets of more than 2 groups followed by correction of P-values using Tukey's multiple comparisons test. $P < 0.05$ was considered as statistically significant. Data were presented as mean \pm standard error (SEM) from N independent experiments.

3 Results

3.1 Diabetes mellitus type II

People who have type II diabetes mellitus (T2DM) are at increased risk of acute myocardial infarction, and mortality in diabetic patients is higher immediately after MI compared with non-diabetics after MI [136]. Therefore, it is important to better understand the mechanisms of maladaptation of the diabetic heart occurring during this early period. The remote myocardium compensates for the loss of function of the ischemic myocardium. This work investigated the size and velocity of intracellular Ca^{2+} cycling in remote myocardium 10 days after I/R during the proliferative phase of infarct healing when ventricular remodeling of cardiac tissue occurs. It pursued the hypothesis that T2DM impairs electromechanical coupling and sarcomeric function and thereby impedes important early adaptive ventricular remodeling of the remote myocardium.

Leptin receptor-deficient db/db mice exhibiting typical characteristics of T2DM from 9 to 10 weeks of age were used as a model organism (for more details, see chapter 1.7.2) because at this age, weight, and blood glucose levels were already significantly elevated, but cardiac function was still intact. The db/db mice do not yet develop heart failure at this age, but they are insulin resistant [137]. To analyze the comorbidity of MI and T2DM, both groups, i.e., db/db mice and db/+ mice, were subjected to 1 hour of ischemia followed by 10 days reperfusion (for performance, see chapter 2.1.2). Subsequently, it was investigated whether - and, if so, why - the size and velocity of intracellular Ca^{2+} fluxes as well as sarcomere function change in isolated remote cardiomyocytes comparing mice with (db/db) and without (db/+) the diabetic metabolic state.

3.1.1 Size and velocity of intracellular Ca^{2+} cycle

Measurement of Ca^{2+} kinetics and Ca^{2+} amount (chapter 2.2.2.5) was performed on remote cardiomyocytes isolated from 9 homozygous (db/db) hearts and 10 heterozygous (db/+) hearts. The Ca^{2+} transients were determined and evaluated according to the procedure described in chapter 2.2.4.

3.1.1.1 Peak Height (amplitude) of Ca^{2+} Transients

Figure 3.1 shows the peak height (amplitude) of the measured Ca^{2+} transients. For each heart, 10 cells were measured and the amplitude of 10 Ca^{2+} transients was averaged. The amplitude is proportional to the amount of Ca^{2+} released from the SR into the cytosol after electrical stimulus at time t_0 . At 10 days after I/R, the amount of Ca^{2+} released from the SR into the cytosol after each electrical stimulation in db/db cardiomyocytes was only $73 \pm 3\%$ of that in db/+; $P = 0.15$). Upon isoproterenol stimulation, there was an increase in the peak height by $86 \pm 15\%$ ($P < 0.0001$) in

db/+ and by $53 \pm 7\%$ ($P = 0.03$) in db/db groups. After stimulation with the β -adrenoceptor agonist isoproterenol (10^{-7} M), the peak height, reflecting the amount of Ca^{2+} released into the cytosol, in remote cardiomyocytes of db/db was only $58 \pm 3\%$ of the size in remote cardiomyocytes from the non-diabetic db/+ mice ($P < 0.0001$) (Figure 3.1). Therefore, PKA stimulation did not normalize the amount of Ca^{2+} released after electrical stimulation but even enhanced the impairment of cytosolic Ca^{2+} increase in the db/db mouse model of diabetes mellitus type 2.

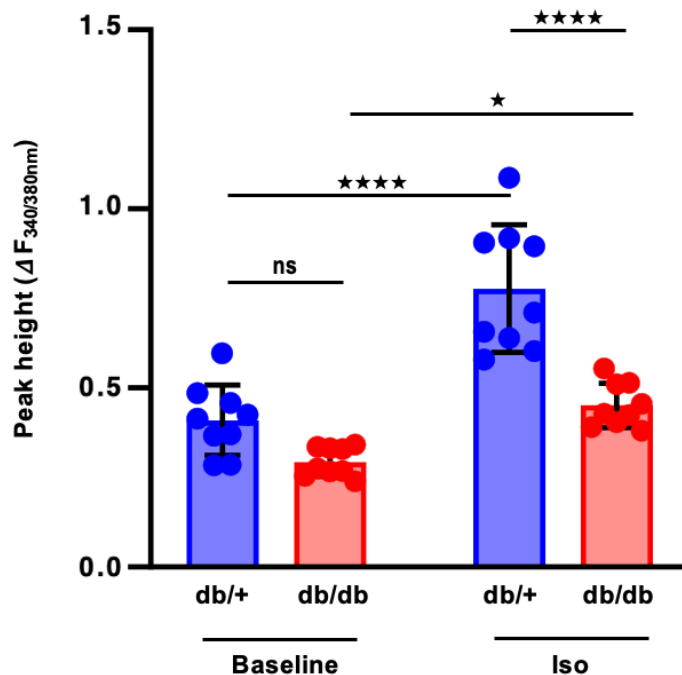


Figure 3.1: Amplitude of Ca^{2+} transients at baseline and after β -adrenergic stimulation of remote cardiomyocytes from db/db and db/+ mice 10 days after ischemia and reperfusion injury (I/R). The bar graphs show mean values of the amplitudes of Ca^{2+} transients \pm SEM. Remote cardiomyocytes from $N = 10$ db/+ (non-diabetic) and $N = 9$ db/db (diabetic) hearts. * $P < 0.05$; **** $P < 0.0001$; $\Delta F_{340/380\text{nm}}$ = change of fluorescence intensity induced by 340nm over 380nm excitation; iso = isoproterenol; ns = not significant.

With the reduced amount of Ca^{2+} released from the SR into the cytosol, the question was addressed whether the speed of SR Ca^{2+} release is also altered in cardiomyocytes with diabetic metabolic state.

3.1.1.2 Speed of Ca^{2+} increase

Like amplitude, the rate of Ca^{2+} increase in the cytosol also showed a trend decrease in db/db and was only $63 \pm 2\%$ of the speed in db/+ ($P = 0.57$) in remote cardiomyocytes at baseline. After stimulation of cardiomyocytes with isoproterenol, the rate of Ca^{2+} increase was significantly enhanced in db/+ by $196 \pm 33\%$ ($P < 0.0001$) and by $140 \pm 11\%$ ($P = 0.004$) in db/db. This increase was more pronounced in db/+ remote cardiomyocytes, so that the speed of Ca^{2+} transient increase in db/db now was only $48 \pm 2\%$ ($P < 0.0001$) compared to db/+ remote cardiomyocytes (Figure 3.2).

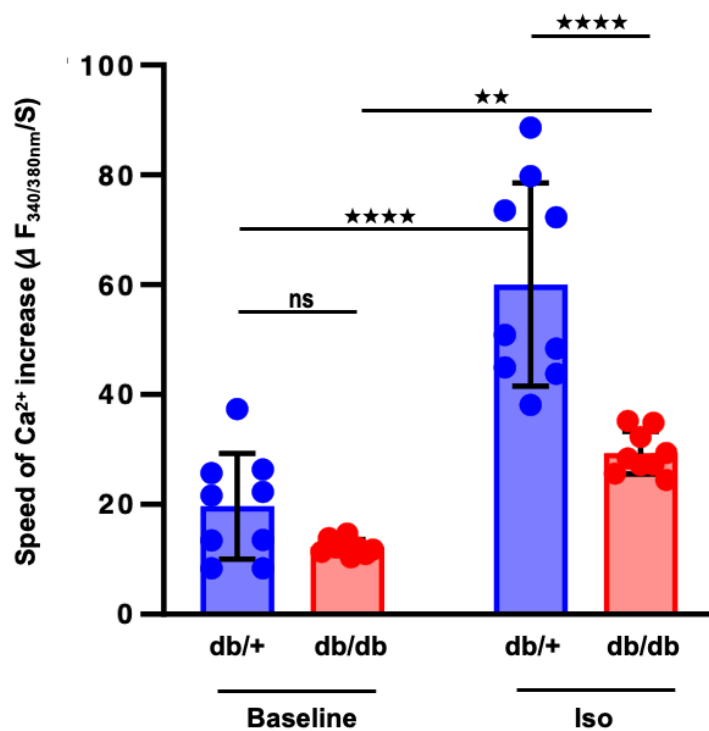


Figure 3.2: Speed of Ca^{2+} increase at baseline and after β -adrenergic stimulation of remote cardiomyocytes from db/db and db/+ mice 10 days after I/R. The bar graphs show mean values of Ca^{2+} velocity \pm SEM. Remote cardiomyocytes from a total of N = 10 db/+ (non-diabetic) and N = 9 db/db (diabetic) hearts per group. ** $P < 0.01$; **** $P < 0.0001$; Ca^{2+} = free calcium; $\Delta F_{340/380nm/s}$ = change of fluorescence intensity induced by 340nm over 380nm excitation per second; iso = isoproterenol; ns = not significant.

3.1.1.3 Speed of Ca^{2+} decrease

During diastole, approximately 92% of cytosolic Ca^{2+} in mouse cardiomyocytes is pumped back into the SR via SERCA2a and 7% is eliminated from the cell via the NCX [11]. 10 days after I/R, the rate of Ca^{2+} decrease in remote db/db cardiomyocytes was only $56 \pm 7\%$ of the rate in remote db/+ cardiomyocytes ($P = 0.52$). The speed of cytosolic Ca^{2+} elimination showed an increase by $162 \pm 42\%$ ($P < 0.0001$) in db/+ and by $150 \pm 9\%$ ($P = 0.02$) in db/db groups after isoproterenol stimulation, so that the rate of Ca^{2+} reuptake into the SR after stimulation with isoproterenol in remote db/db cardiomyocytes was still only $60 \pm 2\%$ of the rate in remote db/+ cardiomyocytes ($P < 0.01$; Figure 3.3).

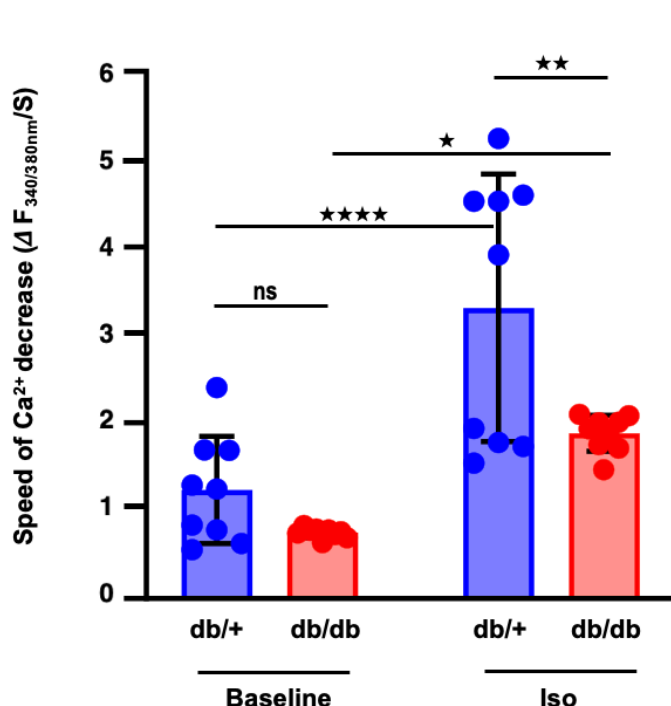


Figure 3.3: Speed of Ca^{2+} decrease at baseline and after β -adrenergic stimulation of cardiomyocytes from db/db and db/+ hearts 10 days after I/R. The bar graph shows mean values of Ca^{2+} velocity \pm SEM. Remote cardiomyocytes from a total of N = 10 db/+ (non-diabetic) hearts N = 9 db/db (diabetic) per group. * $P < 0.05$; ** $P < 0.01$; **** $P < 0.0001$; Ca^{2+} = free calcium; $\Delta F_{340/380nm/s}$ = change of fluorescence intensity induced by 340nm over 380nm excitation per second;; ns = not significant.

Taken together, a strong trend towards slowed velocity of the intracellular Ca^{2+} cycle and a reduced SR Ca^{2+} release were observed in remote db/db compared with db/+ remote cardiomyocytes 10 days after one hour of LAD occlusion. Upon β -adrenergic stimulation, this difference between mice with and without diabetic metabolic state became highly significant. The amplitude was smaller, and cytosolic Ca^{2+} release and Ca^{2+} reuptake into the SR were slowed.

3.1.2 Sarcomere function

Ca^{2+} mediates sarcomere function thus, we wanted to check the functional consequences of altered Ca^{2+} cycling. The measurement of sarcomere function (2.2.3) was performed in parallel with the measurement of myocyte Ca^{2+} kinetics in isolated remote cardiomyocytes 10 days after I/R. The evaluation of the sarcomere function was performed according to the procedure outlined in chapter 2.2.4. The cells analyzed or evaluated were selected according to the following criteria: Sarcomere function of a cardiomyocyte was measured if a clear stripe pattern was evident, and the cardiomyocyte could be electrically stimulated (0.5 Hz), i.e., the contractile amplitude of the sarcomere function had to be greater than 0.03 μm . Isoproterenol was applied in the same manner as for measurements of Ca^{2+} cycling (see 3.1.1) to evaluate the effects of β -adrenergic stimulation on sarcomere contraction and relaxation of remote cardiomyocytes with and without diabetic metabolic state (method see 2.2.3).

Raw values were obtained for each cell as the mean of at least 10 contractile cycles. Nine (db/db) hearts with diabetic metabolic state and ten (db/+) hearts without diabetic metabolic state at the age of 8 to 9 weeks were evaluated.

3.1.2.1 Contractile Amplitude

After 1 hour of ischemia and after 10 days of reperfusion, the contractile amplitude of sarcomeres in remote cardiomyocytes was smaller by trend in db/db compared to db/+ ($0.21 \pm 0.01 \mu\text{m}$ versus $0.18 \pm 0.01 \mu\text{m}$; $p=0.43$; Figure 3.4). Upon isoproterenol stimulation, the increase in the contractile amplitude was $16 \pm 9\%$ ($P = 0.46$) in db/+ and $27 \pm 10\%$ ($P = 0.22$) in db/db groups. After β -adrenergic stimulation, contractile amplitudes of db/db and db/+ sarcomeres were virtually identical ($P = 0.78$; Figure 3.4).

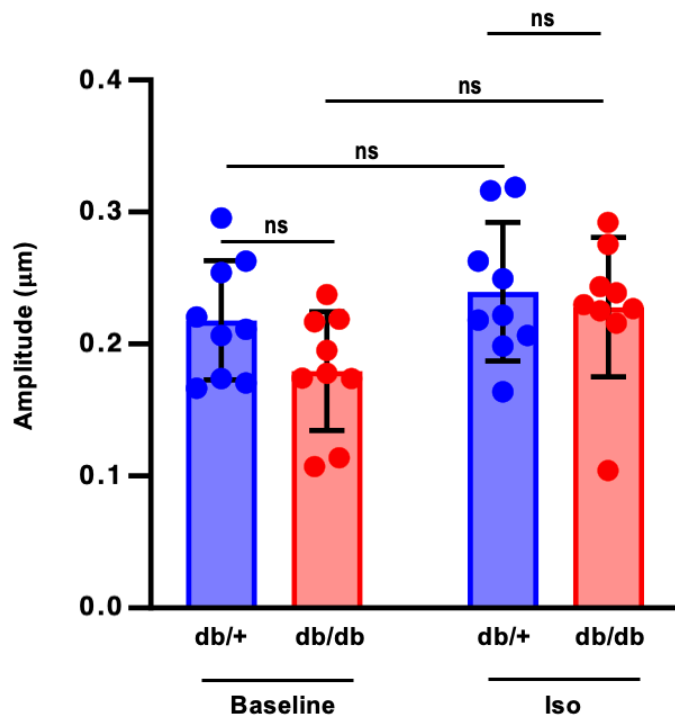


Figure 3.4: Contractile amplitude at baseline and after β -adrenergic stimulation of sarcomeres from remote cardiomyocytes of db/db and db/+ mice 10 days after I/R. The bar graph shows mean values of contractile amplitude \pm SEM. Remote cardiomyocytes from a total of $N = 10$ db/+ hearts and $N = 9$ db/db hearts. iso = isoproterenol; ns = not significant.

3.1.2.2 Speed of contraction

The contraction velocity was lower by trend in db/db remote cardiomyocytes compared to db/+ at baseline ($2.0 \pm 0.1 \mu\text{m/s}$ versus $2.4 \pm 0.2 \mu\text{m/s}$ $P = 0.56$). After stimulation of cardiomyocytes with isoproterenol, the speed of contraction was significantly enhanced in db/+ by $55 \pm 12\%$ ($P = 0.002$) and $75 \pm 15\%$ ($P = 0.001$) in db/db; Figure 3.5).

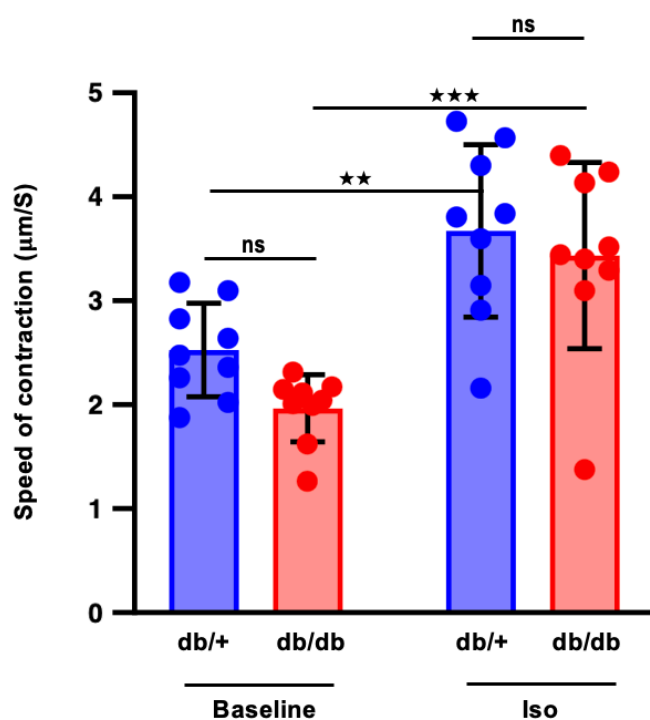


Figure 3.5: Contraction velocity at baseline and after β -adrenergic stimulation of sarcomeres from remote cardiomyocytes of db/db and db/+ mice 10 days after I/R. The bar graph shows mean values of contraction velocity \pm SEM. Remote cardiomyocytes from a total of N = 10 db/+ hearts and N = 9 db/db hearts. ** $P < 0.01$; *** $P < 0.001$; iso = isoproterenol; ns = not significant.

3.1.2.3 Speed of relaxation

As with contraction velocity, the velocity of sarcomere relaxation velocity in remote cardiomyocytes 10 days after I/R was lower by a small trend in db/db compared with db/+ remote cardiomyocytes under basal conditions (0.65 ± 0.04 $\mu\text{m/s}$ versus 0.70 ± 0.05 $\mu\text{m/s}$ $P = 0.92$). The speed of relaxation was increased by $47 \pm 10\%$ ($P = 0.004$) in db/+ and $47 \pm 11\%$ ($P = 0.01$) in db/db after isoproterenol stimulation resulting in similar relaxation velocities in both groups ($P = 0.81$; Figure 3.6).

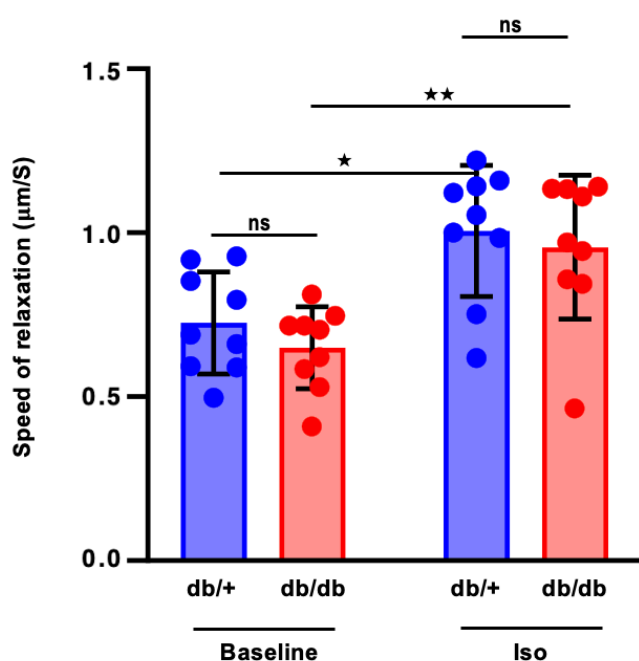


Figure 3.6: Relaxation velocity at baseline and after β -adrenergic stimulation of sarcomeres from remote cardiomyocytes of db/db and db/+ mice 10 days after I/R. The bar graph shows mean values of relaxation velocity \pm SEM. Remote cardiomyocytes from a total of N = 10 db/+ hearts and N = 9 db/db hearts. * $P < 0.05$; ** $P < 0.01$; iso = isoproterenol; ns = not significant.

Overall, measurements of sarcomere lengths in intact isolated primary cells 10 days after I/R showed that Ca^{2+} kinetics were slowed in remote cardiomyocytes of db/db hearts compared with db/+. β -adrenergic stimulation did not normalize the slowed Ca^{2+} circulation in db/db cardiomyocytes; in fact, the differences between both groups reached significance upon isoproterenol treatment of cells.

Little dysfunction of cardiomyocyte sarcomeres was noted in db/db compared with db/+ remote cardiomyocytes 10 days after I/R. The difference was less than expected with regards to the observe Ca^{2+} defects in db/db remote myocardium, and it did not reach significance between both genotypes for any of the investigated parameters.

3.1.3 Expression of Ca^{2+} regulatory proteins in the remote myocardium

In the experiments described in 2.3, Western blot analyses were performed under the supervision of Dr. rer. nat. Florian Funk (from the workgroup of Prof. Dr. J.P. Schmitt). Potential causes for impaired myocyte Ca^{2+} cycling include changes of expression, interaction, and activity of Ca^{2+} regulatory proteins. To investigate the expression levels Western blot was performed (Figure 3.7- Figure 3.9). Unlike human myocytes, where at least 25% of diastolic Ca^{2+} removal from the cytosol is accomplished by NCX, the sarcolemmal Ca^{2+} ATPase (PMCA) and the mitochondrial Ca^{2+} uniporter (MCU), the sarcoplasmic reticulum (SR) accounts for ~93% of cytosolic Ca^{2+} changes during each cardiac cycle in small rodents. Therefore, the focus was on the expression analyses of the Ca^{2+} regulatory proteins of the SR. The determined protein expression was normalized to calsequestrin (CASQ), a stably expressed myocyte-specific protein. Phosphorylation was normalized to the total amounts of the respective protein (for RyR2, PLN, TnI). For equal loading of the gel, protein amounts were determined by the BCA method (see chapter 2.3.3).

Because β -adrenergic agonists increase the function of Ca^{2+} regulators through PKA-dependent phosphorylation, the phosphorylation state of these phosphorylation sites was determined in this work. Phospholamban is a main regulator of cardiac contractility and inhibits SERCA2a activity by lowering its affinity for Ca^{2+} in its dephosphorylated state. Upon phosphorylation of PLN, which is mediated through β -adrenergic stimulation, and enhanced cyclic AMP-dependent protein kinase A activity, the inhibitory effect of phospholamban on the function of SERCA is relieved. This leads to increased initial rates of SR Ca^{2+} uptake, accelerated relaxation, and enhanced SR Ca^{2+} load, which is available for release through the ryanodine receptor resulting in enhanced contraction. Therefore, PLN, SERCA2A, and RyR2 at Ser(2808) were first examined. Since it is known that PLN is predominantly present as a pentamer, but only the PLN monomer inhibits SERCA2A by direct interaction, the focus was on PLN monomer expression and the pentamer to monomer ratios. Expression analysis of SERCA2a (Figure 3.7), and PLN monomers (Figure 3.8) showed no differences between db/db and db/+ hearts, neither without I/R injury, nor in remote myocardium 10 days after I/R. Of note, there was a trend towards higher expression of PLN monomers due to

a shift in the pentamer-to-monomer ratio 10 days after I/R. However, the blot analyses for RyR2 at Ser(2808) showed a reduction 10 days after I/R but this could not be quantified for phosphorylation site of Ser(2808). Furthermore, we examined the expression of S100A1 that interacts with and can modify SERCA2a and PLN function. The expression of S100A1 did not differ between db/+ and db/db at baseline and also not 10 days after I/R ($P=0.05$; Figure 3.9). Thus, it can be concluded that impaired Ca^{2+} cycling in myocytes of the RM 10 days after I/R does not seem to be caused by altered expression of the central SR Ca^{2+} regulatory proteins.

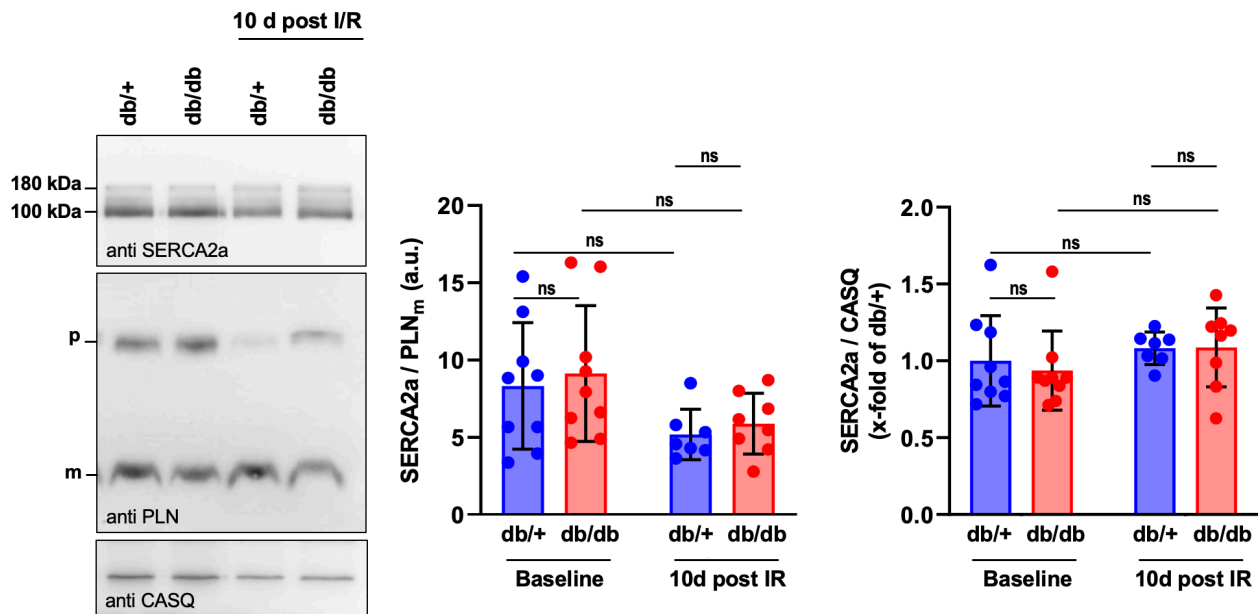


Figure 3.7: Western blot analyses of the sarco-/endoplasmic Ca^{2+} ATPase 2A (SERCA2A). Representative gel images and bar graphs showing mean protein expression \pm SEM in hearts without I/R (baseline) and in the remote myocardium 10 days after I/R; P -values were calculated by 2-way ANOVA. CASQ = Calsequestrin; PLN = phospholamban; I/R = ischemia/reperfusion; ns = not significant.

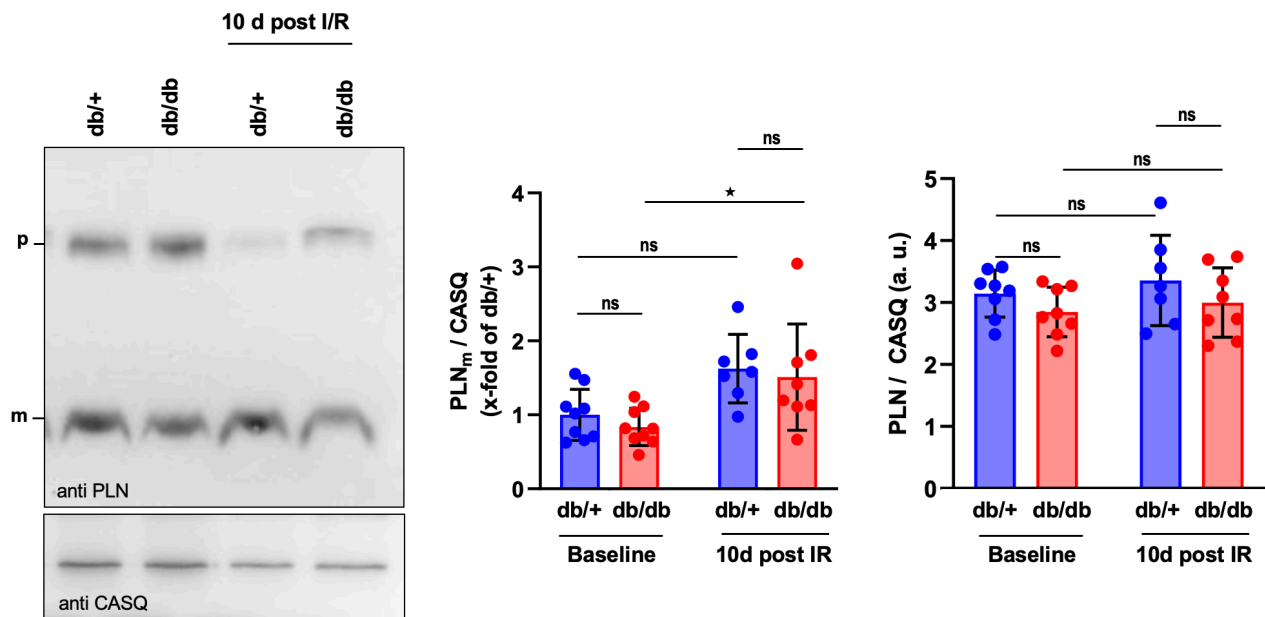


Figure 3.8: Western blot analyses of phospholamban (PLN). Representative gel images and bar graphs showing mean protein expression ± SEM in hearts without I/R (baseline) and in the remote myocardium 10 days after I/R; P -values were calculated by 2-way ANOVA. * $P < 0.05$; CASQ = Calsequestrin; I/R = ischemia/reperfusion; ns = not significant.

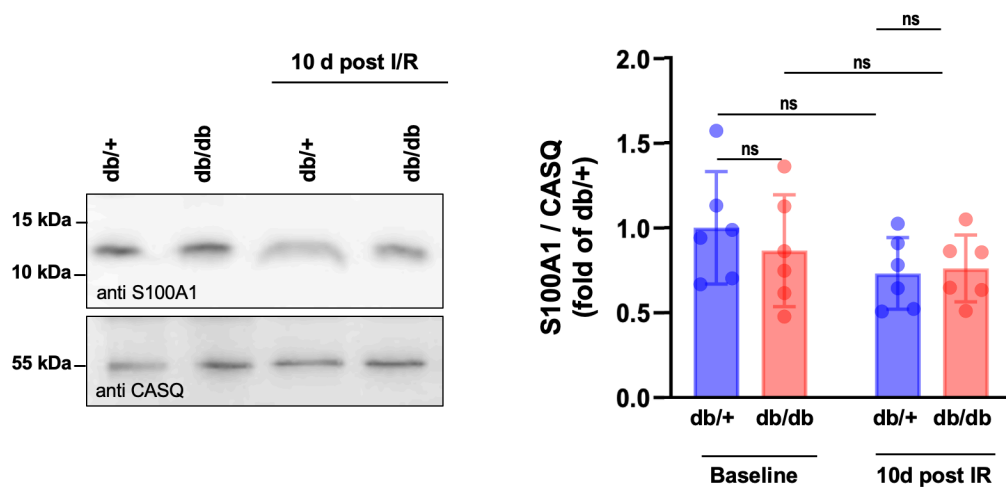


Figure 3.9: Protein expression of S100A1 10 days after I/R. Representative Western blot analyses and bar graphs showing mean protein expression ± SEM in hearts without I/R (baseline) and in the remote myocardium 10 days after I/R; P -values were calculated by 2-way ANOVA. CASQ = Calsequestrin; I/R = ischemia/reperfusion; ns = not significant.

3.1.4 Activity measurement of regulators of myocytic Ca^{2+} cycle

In addition to the protein expression of Ca^{2+} regulators, their phosphorylation status and thus their activity was measured. We first examined the phosphorylation status of PLN monomers that had been found significantly decreased in phosphorylation at the PKA-dependent phosphorylation site Ser16 in remote myocardium 24 hours after I/R [138]. In addition, the CaMKII-dependent phosphorylation site of PLN at Thr17 was examined. The kinetics of SR Ca^{2+} cycling largely

depend on the phosphorylation status of PLN. PLN phosphorylation was assessed using regular SDS gels and anti-phospho-PLN(Ser16) and anti-phospho-PLN(Thr17) antibodies (Figure 3.10; Figure 3.11).

For S16, we found more unphosphorylated PLN monomers, the PLN species that inhibits SERCA2a, in RM 10 days after I/R in both db/db and db/+ hearts compared to hearts without I/R ($P < 0.001$; Figure 3.10). While S16 phosphorylation was slightly reduced in db/db at baseline ($P < 0.05$), no differences in PLN phosphorylation between db/db and db/+ were observed in the RM, neither for S16 nor for T17. In contrast to S16, Western blot analyses using phospho-specific antibodies demonstrated increased phosphorylation of PLN at Thr17 in the RM 10 days after I/R compared to non-infarcted myocardium for both db/+ and db/db hearts ($P < 0.0001$; Figure 3.11).

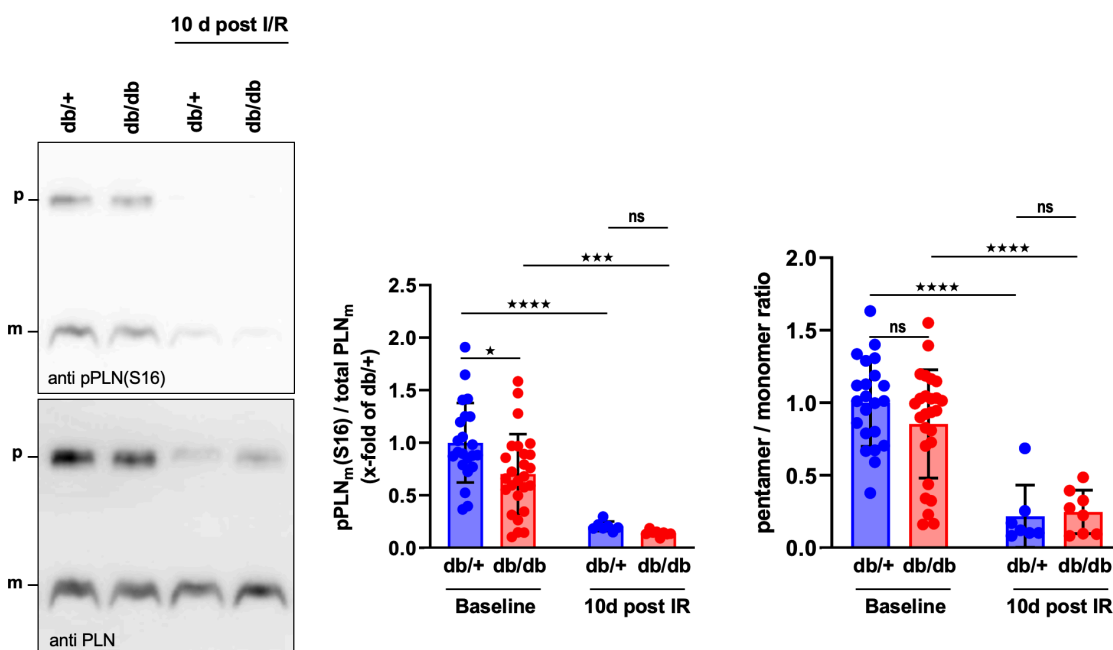


Figure 3.10: Phosphorylation of PLN monomers at Ser16 and pentamer-to-monomer ratios of PLN. Representative Western blot analyses and bar graphs showing mean values \pm SEM in hearts without I/R (baseline) and in the remote myocardium 10 days after I/R from $N = 7-8$ hearts per group. P -values were calculated by 2-way ANOVA. *** $P < 0.001$; **** $P < 0.0001$; PLN = phospholamban; pPLN (Ser16) = phospho-phospholamban (serine16); I/R = ischemia/reperfusion; ns = not significant.

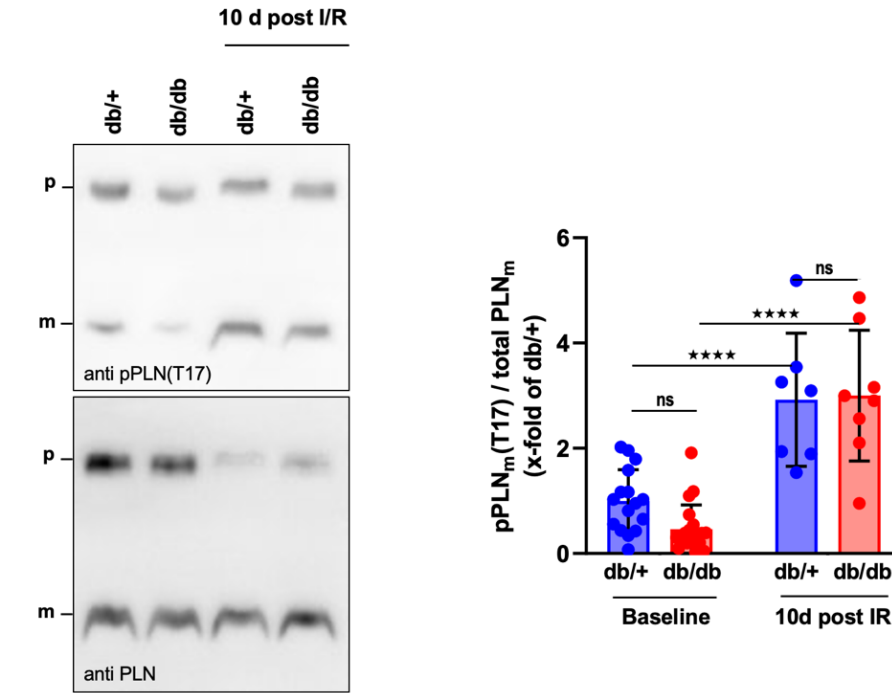


Figure 3.11: Phosphorylation of PLN monomers at Thr17. Representative Western blot analyses and bar graphs showing mean values \pm SEM in hearts without I/R (baseline) and in the remote myocardium 10 days after I/R from N = 7-8 hearts per group. * P-values were calculated by 2-way ANOVA. ****P < 0.0001; PLN = phospholamban; pPLN (Thr17) = phospho-phospholamban (Thr17); I/R = ischemia/reperfusion; ns = not significant.

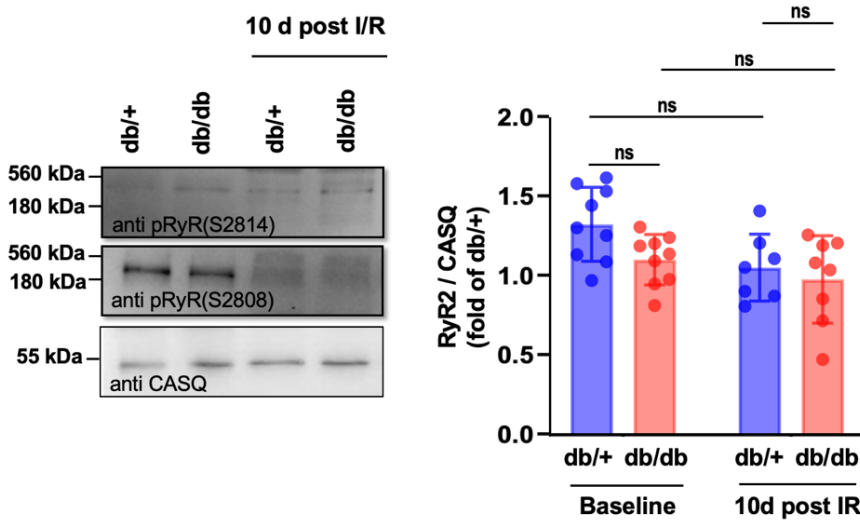


Figure 3.12: Western blot analyses of ryanodine receptor 2 (RyR2). Representative gel images and bar graphs showing mean protein expression \pm SEM in hearts without I/R (baseline) and in the remote myocardium 10 days after I/R; P-values were calculated by 2-way ANOVA. *** P < 0.001; CASQ = Calsequestrin; I/R = ischemia/reperfusion; ns = not significant.

Cardiac troponin I (cTnI) is phosphorylated via PKA at its phosphorylation site serine23/24. It is not a direct Ca^{2+} regulator, but because of its function as a Ca^{2+} sensitizer on myofilaments and the disparity between Ca^{2+} cycling and sarcomere function in isolated remote db/db cardiomyocytes 10 days after I/R, the phosphorylation state of cTnI at S23/24 was investigated and normalized to total cTnI. However, phosphorylation of cTnI at S23/24 was unchanged in db/+ and db/db hearts in the remote myocardium 10 days after I/R and also in control myocardium without I/R (Figure 3.13).

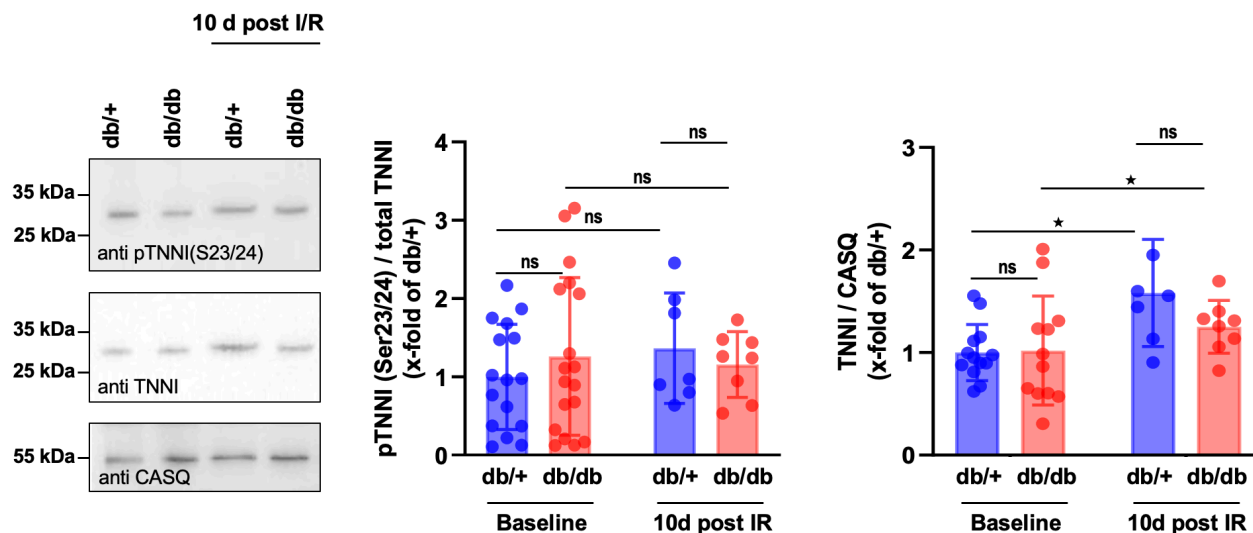


Figure 3.13: Expression and phosphorylation of cTnI at Ser23/24. Representative Western blot analyses and bar graphs showing mean values \pm SEM in hearts without I/R (baseline) and in the remote myocardium 10 days after I/R from a total of N = 7-8 hearts. * $P < 0.05$; cTnI = cardiac troponin I; pTnI (Ser23/24) = phospho troponin I (Serin23/24); Ser23/24 = Serin23/24; I/R = ischemia/reperfusion; ns = not significant.

3.2 Diet-induced obesity (DIO)

It is known that T2DM evolves over years going through various stages. Thus, we wanted to study if early-stage T2DM (pre-diabetes) as modeled by DIO impacts cardiomyocyte Ca^{2+} cycling since previous studies have shown that db/db mice already at baseline showed impaired Ca^{2+} cycling that additively contributes to depression of Ca^{2+} cycling and sarcomere function in the RM after I/R [138]. Therefore, this study was designed to determine the interaction between pre-diabetes / early-stage diabetes and cardiac contractile and intracellular Ca^{2+} properties. The Ca^{2+} kinetics and sarcomere function in the DIO mouse model in comparison with control mice were investigated.

Male C57BL/6 mice were distributed into two groups: control (C, N = 8; standard diet) and obese (DIO, N = 9; high-fat diet), which were fed for 9 weeks with a diabetogenic diet, whereas the control group received regular chow. Over the feeding period, and on a weekly basis, the group on diabetogenic diet gained more weight due to higher caloric intake than the control group. DIO mice started to show increased weight gain compared to controls within 6 weeks on diet and their weight was >30% higher at the end of the feeding period ($P < 0.001$). At this time point, basal blood glucose levels were not different between groups. To determine glucose tolerance, blood glucose of mice was measured before and after application of glucose (20% glucose i.p.) over a period of two hours. While blood glucose returned to basal levels within 60 min in controls it remained elevated in DIO mice indicating impaired glucose tolerance (Figure 3.14 below).

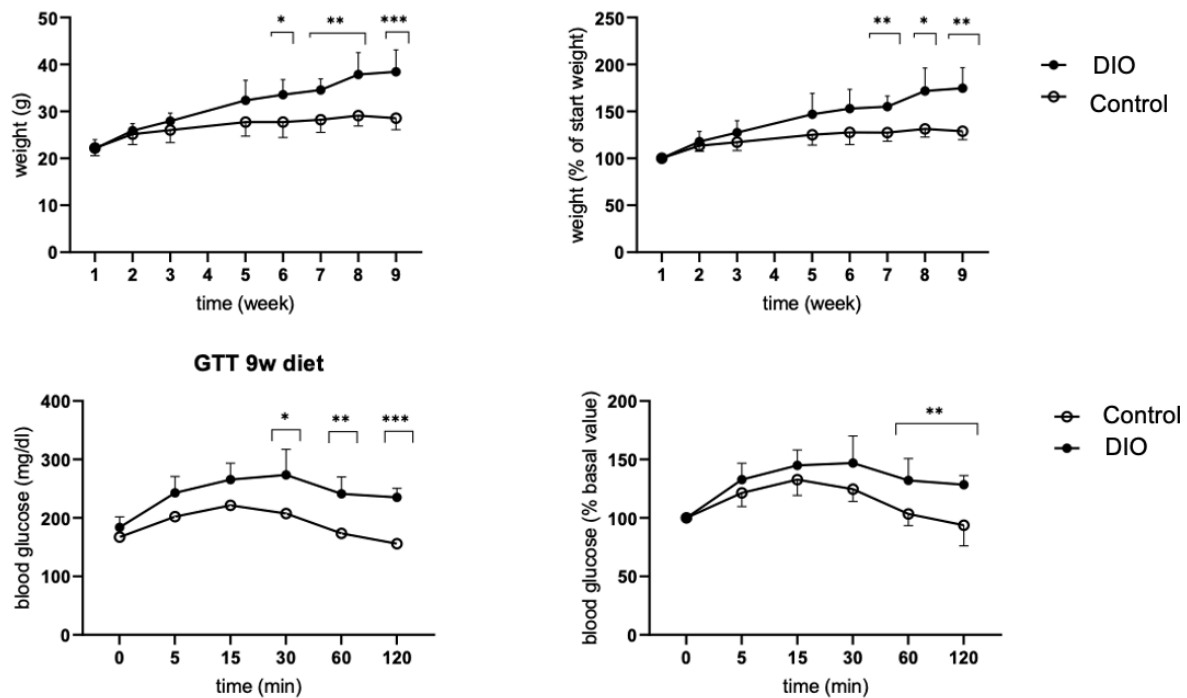


Figure 3.14: Metabolic parameters in Diet Induced Obese (DIO) mice. Male C57BL/6 mice were distributed into two groups: control (N = 8; standard diet) and DIO (N = 9; high-fat diet), fed for 9 weeks. The graphs show over the feeding period, and on a weekly basis, that DIO mice gained more weight and after 9 weeks demonstrated higher glucose levels compared to the control group upon glucose tolerance testing (GTT) by intraperitoneal injection of a glucose bolus at timepoint 0 and subsequent measurements of blood glucose. * $P < 0.05$, ** $P < 0.01$, *** $P < 0.001$. These results were provided by Katja Wegener, Institute of Translational Pharmacology of the HHU. Data are displayed as mean \pm SD.

3.2.1 Size and velocity of intracellular Ca^{2+} cycle

Measurement of Ca^{2+} kinetics and Ca^{2+} amount (chapter 2.2.2.5) was performed on ventricular cardiomyocytes isolated from 9 DIO mice and 8 control mice. The Ca^{2+} transients were determined and evaluated according to the procedure described in chapter 2.2.4.

3.2.1.1 Peak Height (amplitude) of Ca^{2+} Transients

Figure 3.15 shows the amplitude of the measured Ca^{2+} transients. As in db/db mice, for each heart 10 cells were measured and the amplitude of 10 Ca^{2+} transients was averaged. The amount of Ca^{2+} released from the SR into the cytosol after each electrical stimulation showed a small increase by $14 \pm 2\%$ in cardiomyocytes from DIO mice compared with controls ($P < 0.05$). Upon isoproterenol stimulation, there was an increase in the peak height by $48 \pm 9\%$ ($P = 0.001$) in control and by $23 \pm 5\%$ ($P = 0.002$) in DIO groups. After stimulation with isoproterenol (10^{-7} M), the amount of Ca^{2+} released into the cytosol showed no difference between the two groups ($P = 0.70$).

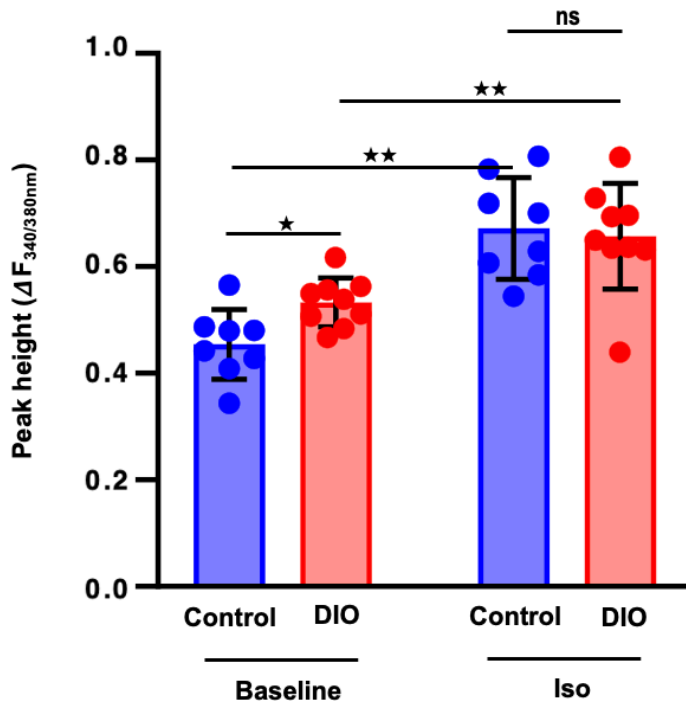


Figure 3.15: Amplitude of Ca^{2+} transients at baseline and after β -adrenergic stimulation of cardiomyocytes from DIO and control mice. The bar graphs show mean values of the amplitude of Ca^{2+} transients \pm SEM. Isolated cardiomyocytes from N = 9 hearts with diet induced obesity and N = 8 control hearts were measured at baseline and after stimulation with isoproterenol. * $P < 0.05$; ** $P < 0.01$; iso = isoproterenol; DIO = diet-induced obesity; $\Delta F_{340/380nm}$ = change of fluorescence intensity induced by 340nm over 380nm excitation; ns = not significant.

3.2.1.2 Speed of Ca^{2+} increase

The rate of Ca^{2+} increase in the cytosol was higher by $16 \pm 3\%$ in the DIO group compared to controls at baseline ($P = 0.03$). After stimulation of cardiomyocytes with isoproterenol, the rate of Ca^{2+} increase was significantly enhanced in controls by $83 \pm 8\%$ ($P < 0.0001$) and by $49 \pm 12\%$ ($P = 0.003$) in DIO. Like for the amplitude, there was no difference between both groups when stimulated with isoproterenol ($P = 0.61$; Figure 3.16).

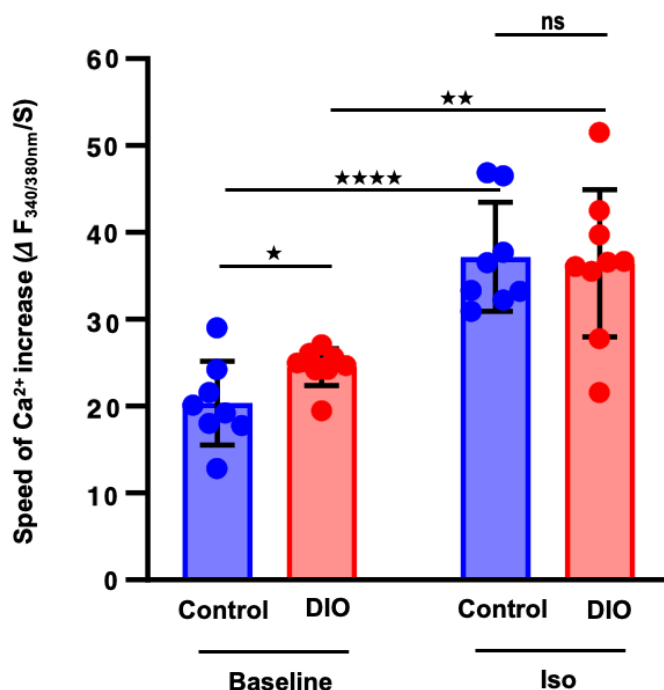


Figure 3.16: Speed of Ca^{2+} increase at baseline and after β -adrenergic stimulation of cardiomyocytes from DIO and control mice. The bar graphs show mean values of the rate of Ca^{2+} increase \pm SEM. Isolated cardiomyocytes from N = 9 hearts with diet induced obesity and N = 8 control hearts were measured at baseline and after stimulation with isoproterenol. * $P < 0.05$; ** $P < 0.01$; **** $P < 0.0001$; iso = isoproterenol; DIO = diet induced obesity; $\Delta F_{340/380nm}/s$ = change of fluorescence intensity induced by 340nm over 380nm excitation per second; ns = not significant.

3.2.1.3 Speed of Ca^{2+} decrease

The rate of Ca^{2+} decrease was higher by strong trend in ventricular cardiomyocytes isolated from DIO mice compared to controls at baseline ($15 \pm 3\%$; $P = 0.06$). The speed of cytosolic Ca^{2+} elimination showed an increase by $66 \pm 9\%$ ($P = 0.0002$) in controls and by $45 \pm 10\%$ ($P = 0.002$) in the DIO group after isoproterenol stimulation. The rate of Ca^{2+} decrease was unchanged in cardiomyocytes from DIO mice compared to controls after β -adrenergic stimulation ($P = 0.90$; Figure 3.17).

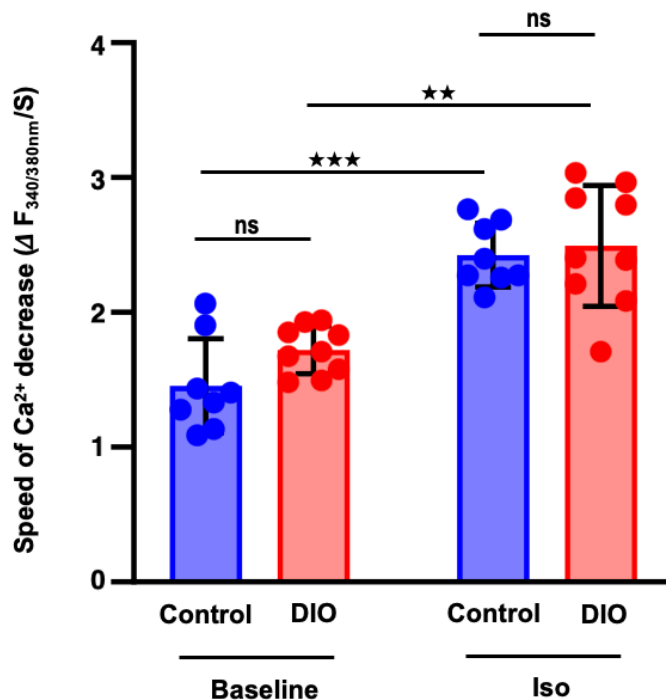


Figure 3.17: Speed of Ca^{2+} decrease at baseline and after β -adrenergic stimulation of cardiomyocytes from DIO and control mice. The bar graphs show mean values of Ca^{2+} velocity \pm SEM. Cardiomyocytes from $N = 9$ DIO hearts and $N = 8$ control hearts were measured. $**P < 0.01$; $***P < 0.001$; iso = isoproterenol; DIO = diet induced obesity; $\Delta F_{340/380\text{nm}}/\text{s}$ = change of fluorescence intensity induced by 340nm over 380nm excitation per second; ns = not significant.

In conclusion, cardiomyocyte Ca^{2+} cycling was slightly enhanced in DIO mice compared to controls on a regular diet under basal conditions. This finding contrasts previous observations in db/db mice. The measured differences between DIO and controls fully vanished upon stimulation of cells with isoproterenol.

3.2.2 Sarcomere function

The measurement of sarcomere function (2.2.3) was performed in parallel with the measurement of myocyte Ca^{2+} kinetics in isolated cardiomyocytes. The evaluation of the sarcomere function was performed according to the procedure outlined in chapter 2.2.4. The cells analyzed again were selected according to the following criteria: Sarcomere function of a cardiomyocyte was measured if a clear stripe pattern was evident, and the cardiomyocyte could be electrically stimulated (0.5 Hz). The contractile amplitude of the sarcomere function had to be greater than $0.03 \mu\text{m}$. Raw values were obtained for each cell as the mean of at least 10 contractile cycles. Nine mice of the DIO group and eight control mice were evaluated.

3.2.2.1 Contractile Amplitude

When contractile amplitude of sarcomeres was analyzed, a trend increases by $19 \pm 4\%$ in the DIO group was observed at baseline ($P = 0.07$). Upon isoproterenol stimulation, there was a trend increase in the contractile amplitude by $22 \pm 18\%$ ($P = 0.26$) in control and a significant increase by $21 \pm 7\%$ ($P = 0.013$) in DIO groups. After β -adrenergic stimulation, the contractile amplitude was higher in the DIO group by $18 \pm 10\%$ ($P = 0.12$; Figure 3.18).

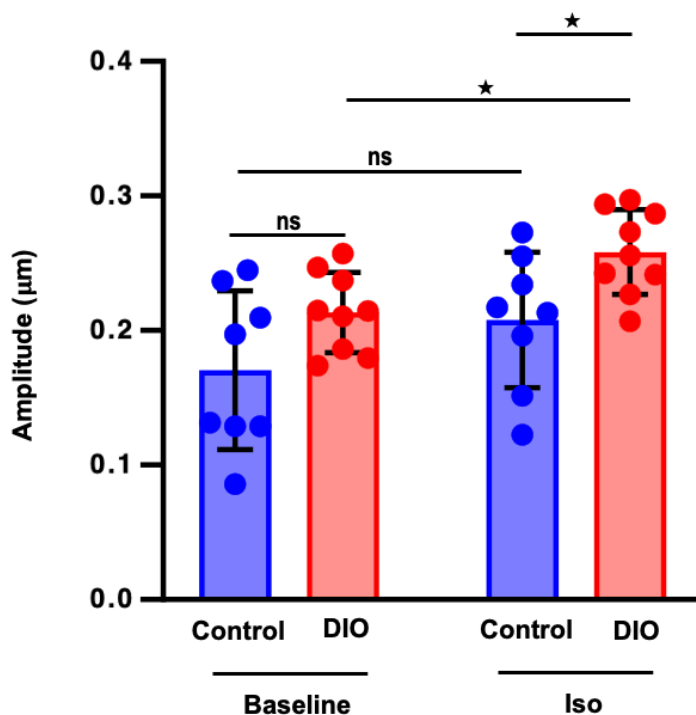


Figure 3.18: Contractile amplitude of sarcomeres at baseline and after β -adrenergic stimulation of cardiomyocytes from DIO mice compared with control cardiomyocytes. The bar graph shows mean values of contractile amplitude \pm SEM. Cardiomyocytes from N = 9 DIO mice and N = 8 controls; iso = isoproterenol; DIO = diet induced obesity, * $P < 0.05$; ns = not significant.

3.2.2.2 Speed of contraction

The contraction velocity of sarcomeres was higher in DIO mice by $26 \pm 4\%$ at baseline ($P = 0.013$). After stimulation of cardiomyocytes with isoproterenol, the speed of contraction was significantly enhanced in control by $51 \pm 21\%$ ($P = 0.045$) and by $37 \pm 11\%$ ($P = 0.010$) in DIO. After stimulation with β -adrenergic receptors, the speed of sarcomere contraction was $15 \pm 8\%$ higher on average in cardiomyocytes of DIO mice, however, the difference did not reach significance ($P = 0.15$; Figure 3.19).

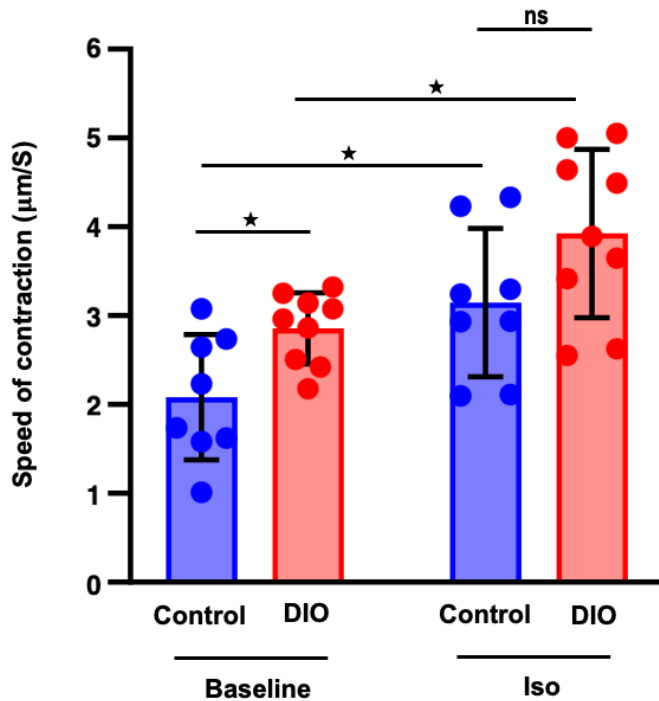


Figure 3.19: Contraction velocity of sarcomeres at baseline and after β -adrenergic stimulation of cardiomyocytes from DIO mice compared with controls. The bar graph shows mean values of contraction velocity \pm SEM. Cardiomyocytes from a total of N = 9 DIO mice and N = 8 controls; * P < 0.05; iso = isoproterenol; DIO = diet induced obesity; ns = not significant.

3.2.2.3 Speed of relaxation

As with contraction velocity, there was an increase by $23 \pm 5\%$ in sarcomere relaxation velocity of cardiomyocytes from DIO mice at baseline ($P = 0.024$). The speed of relaxation showed an increase by $44 \pm 21\%$ ($P = 0.08$) in control and by $31 \pm 8\%$ ($P = 0.04$) in DIO groups after isoproterenol stimulation. The relaxation velocity was higher by trend in DIO mice ($14 \pm 7\%$) after stimulation of cardiomyocytes with isoproterenol ($P = 0.19$).

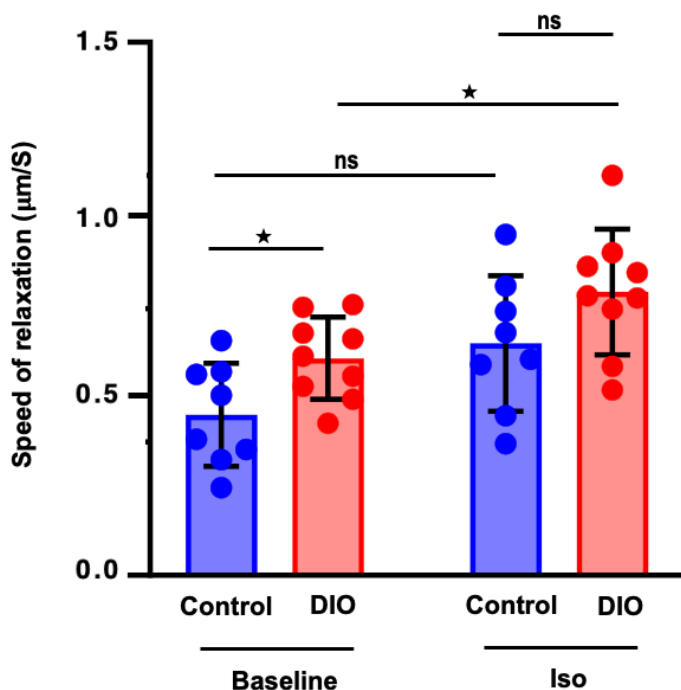


Figure 3.20: Relaxation velocity of sarcomeres at baseline and after β -adrenergic stimulation of cardiomyocytes from DIO mice compared with controls. The bar graph shows mean values of relaxation velocity \pm SEM. Cardiomyocytes from a total of N = 9 DIO mice and N = 8 controls; iso = isoproterenol; DIO = diet induced obesity, * P < 0.05; ns = not significant.

3.3 RIC dialysates

The second part of this thesis work addressed the clinically urgent question of how cardiomyocytes may be protected from ischemic damage during I/R, as in myocardial infarction. Various animal and human studies have shown that short periods of ischemia in peripheral organs (remote ischemic conditioning, RIC) before I/R of the heart could induce the humoral and neuronal transfer of protective factors that reduce infarct size and improve the contractile function of the heart [139]. We hypothesized that one or more of these humoral factors induced by RIC affects cardiomyocyte Ca^{2+} homeostasis because calcium mediates muscle contraction.

To test this hypothesis, we performed three sets of experimental approaches using blood samples that were taken before and after RIC by repetitive cycles of forearm ischemia/reperfusion (see 2.2.2.6) on 12 healthy human probands. Subsequently, mouse cardiomyocytes were treated with plasma dialysates of these blood samples and subjected to 50min of hypoxia before reoxygenation and measurements of myocyte Ca^{2+} cycling. In the first set, we evaluated whether the plasma dialysates before and after RIC influence myocyte Ca^{2+} kinetics and sarcomere function of cardiomyocytes (without hypoxia). Next, we determined the effects of hypoxia and reoxygenation on Ca^{2+} cycling and sarcomere function of untreated cardiomyocytes. Finally, we investigated the influence of the plasma dialysates before and after RIC on Ca^{2+} kinetics and sarcomere function of isolated cardiomyocytes that were subjected to hypoxia and reoxygenation.

3.3.1 Effects of plasma dialysates without hypoxia on myocyte Ca^{2+} cycling

3.3.1.1 Peak Height (amplitude) of Ca^{2+} transients

Figure 3.21 shows the peak height (amplitude) of the measured Ca^{2+} transients. Each data point represents the average value of 10 measured cardiomyocytes, and for each cell the data from 10 Ca^{2+} transients were averaged. For each heart, 10 cells were measured and the amplitude of 10 Ca^{2+} transients was averaged. Ca^{2+} transients of cardiomyocytes were higher compared to respective controls by $15 \pm 5\%$ if treated with RIC dialysates in 10 out of 10 sample pairs ($P = 0.023$; Figure 3.21A). After stimulation with the β -adrenoceptor agonist isoproterenol (10^{-7} M), the amount of Ca^{2+} released into the cytosol was significantly higher by $13 \pm 5\%$ ($P = 0.007$) when cells had been pre-treated with RIC dialysates (Figure 3.21B).

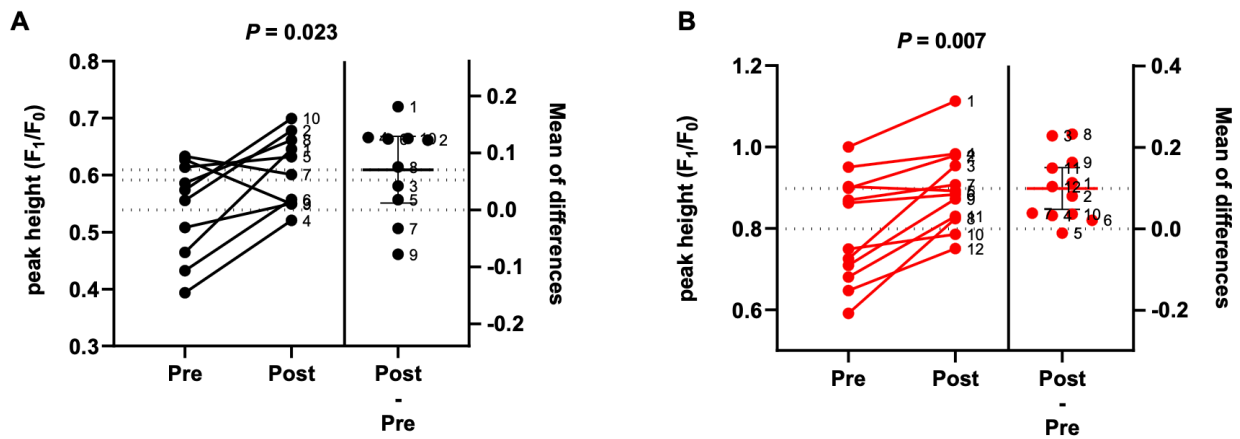


Figure 3.21: Height of Ca^{2+} transients at baseline and after β -adrenergic stimulation of cardiomyocytes incubated with dialysates of blood samples taken before (pre) and after (post) RIC. The solid lines indicate measurements using plasma pre and post RIC from the same proband. Ca^{2+} transients of paced cardiomyocytes (0.5 Hz) were recorded under basal conditions (black, A) and after stimulation of cells with the beta-adrenergic agonist isoproterenol (10^{-7} M; red, B). Each data point represents the mean value from 10 myocytes with 10 transients averaged per myocyte; P-values were calculated by paired t-test. The scatter plots to the right indicate the difference (post minus pre) for the sample pairs of every individual; mean \pm SEM.

3.3.1.2 Speed of Ca^{2+} increase

Like amplitude, RIC dialysates also enhanced the kinetics of Ca^{2+} liberation, but only by trend due to wide variation of results ($55 \pm 28\%$ ($P = 0.12$; Figure 3.22A). Beta-adrenergic stimulation resulted in greater maximum speeds of Ca^{2+} liberation that was consistently faster in all sample pairs when cells had been pre-treated with RIC dialysates ($19 \pm 7\%$; $P = 0.004$; Figure 3.22B).

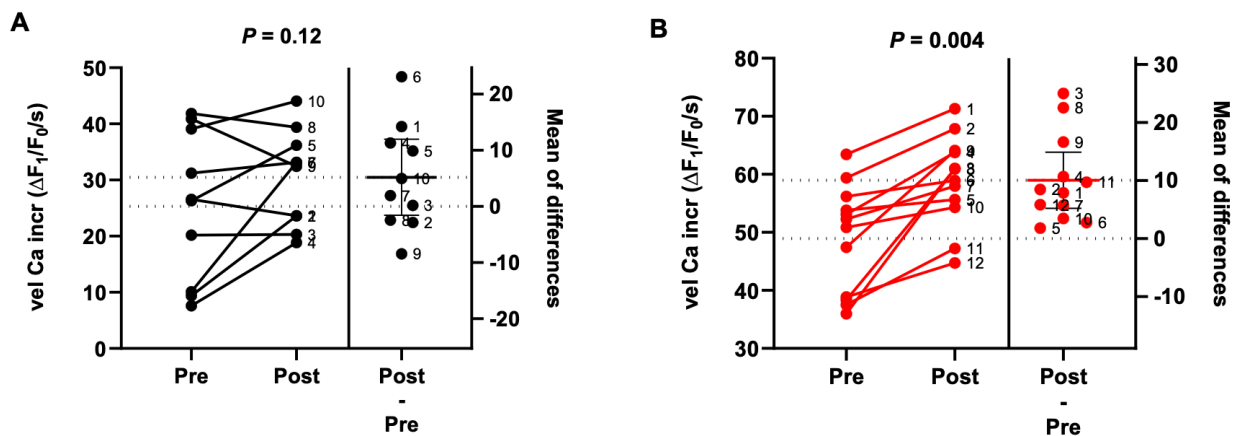


Figure 3.22: Speed of Ca^{2+} increase at baseline and after β -adrenergic stimulation of cardiomyocytes incubated with dialysates of blood samples taken before (pre) and after (post) RIC. The solid lines indicate measurements using plasma pre and post RIC from the same proband. Ca^{2+} transients of paced cardiomyocytes (0.5 Hz) were recorded under basal conditions (black, A) and after stimulation of cells with the beta-adrenergic agonist isoproterenol (10^{-7} M; red, B) to further activate the Ca^{2+} regulatory proteins. Each data point represents the mean value from 10 myocytes with 10 transients averaged per myocyte; P-values were calculated by paired t-test. The scatter plots to the right indicate the difference (post minus pre) for the sample pairs of every individual; mean \pm SEM. Vel Ca incr = velocity of calcium increase.

3.3.1.3 Speed of Ca^{2+} decrease

The rate of Ca^{2+} decrease showed an increase with RIC dialysates by $22 \pm 6\%$ ($P = 0.004$; Figure 3.23A). The rate of Ca^{2+} elimination after stimulation with isoproterenol was $21 \pm 8\%$ faster ($P = 0.015$; Figure 3.23B), when cells had been pre-treated with RIC dialysates.

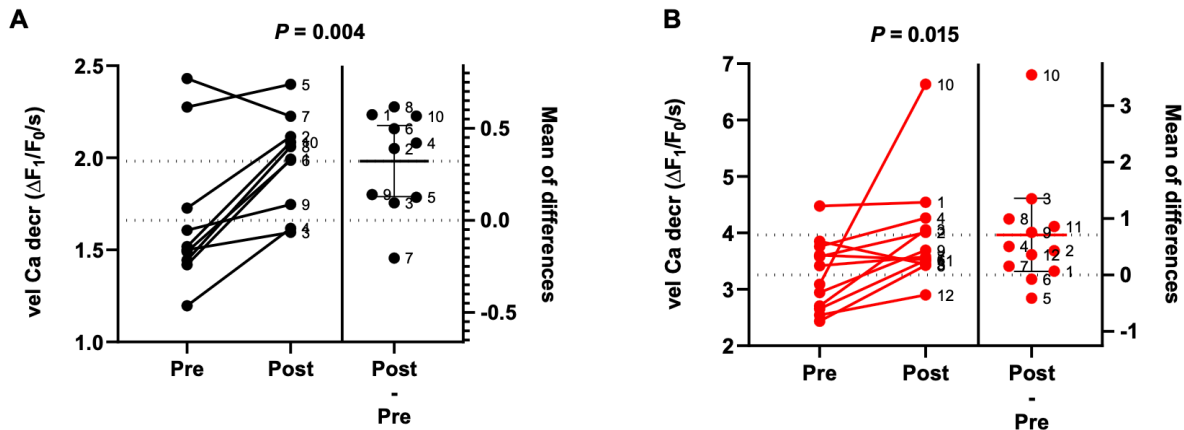


Figure 3.23: Speed of Ca^{2+} decrease at baseline and after β -adrenergic stimulation of cardiomyocytes incubated with dialysates of blood samples taken before (pre) and after (post) RIC. The solid lines indicate measurements using plasma pre and post RIC from the same proband. Ca^{2+} transients of paced cardiomyocytes (0.5 Hz) were recorded under basal conditions (black, A) and after stimulation of cells with the beta-adrenergic agonist isoproterenol (10^{-7} M; red, B) to further activate the Ca^{2+} regulatory proteins. Each data point represents the mean value from 10 myocytes with 10 transients averaged per myocyte; P-values were calculated by paired t-test. The scatter plots to the right indicate the difference (post minus pre) for the sample pairs of every individual; mean \pm SEM. Vel Ca decr = velocity of calcium decrease.

Taken together, the data demonstrate that RIC dialysates enhanced the peak height of Ca^{2+} transients and the kinetics of Ca^{2+} liberation and elimination in isolated mouse cardiomyocytes.

3.3.2 Effects of plasma dialysates from humans before and after RIC on myocyte sarcomere function of cardiomyocytes without hypoxia

3.3.2.1 Contractile Amplitude

When contractile amplitude was analyzed, RIC also increased the amplitude, however, the data varied substantially and the increase did not reach significance ($P = 0.13$; Figure 3.24A). The same applied after isoproterenol stimulation of RIC-treated cells ($P = 0.29$; Figure 3.24B).

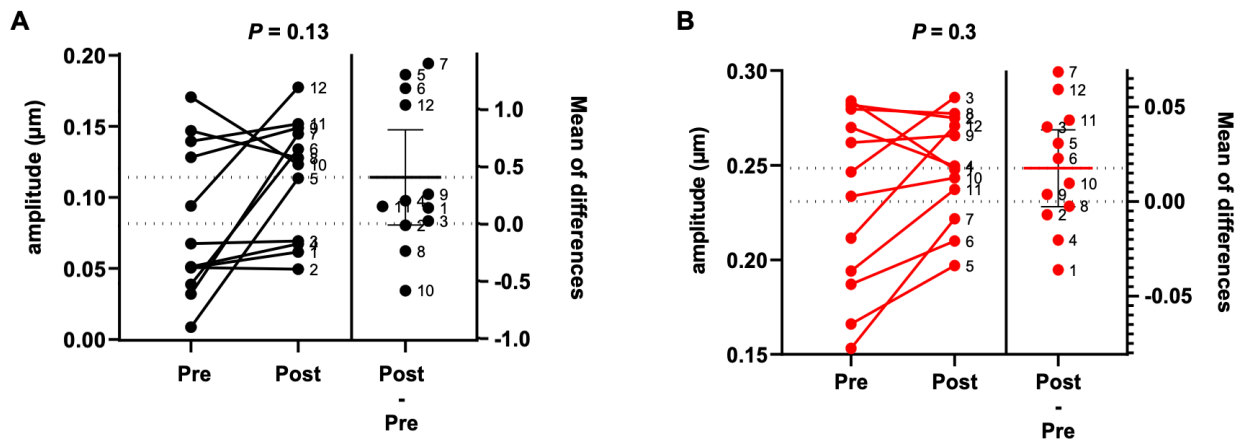


Figure 3.24: Contractile amplitude at baseline and after β -adrenergic stimulation of cardiomyocytes incubated with dialysates of blood samples taken before (pre) and after (post) RIC. The solid lines indicate measurements using plasma pre and post RIC from the same proband. Sarcomere contraction and relaxation of paced cardiomyocytes (0.5 Hz) were assessed at baseline (black, A) and after stimulation of myocytes with 10^{-7} M isoproterenol (red, B). Each data point represents the mean value from 10 myocytes with 10 transients averaged per myocyte; P-values were calculated by paired t-test. The scatter plots to the right indicate the difference (post minus pre) for the sample pairs of every individual; mean \pm SEM.

3.3.2.2 Speed of contraction

The velocity of sarcomere contraction showed a small trend increase if cells were treated with dialysates of RIC plasma ($P = 0.5$; Figure 3.25A). After isoproterenol stimulation there was also no significant difference between cells treated with dialysates taken before or after RIC ($P = 0.7$; Figure 3.25B).

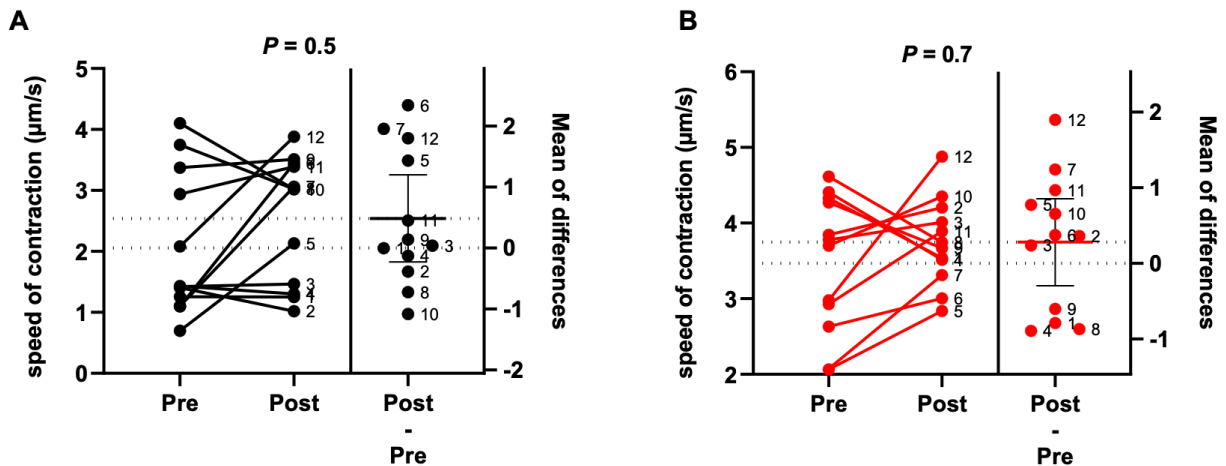


Figure 3.25: Contraction velocity at baseline and after β -adrenergic stimulation of cardiomyocytes incubated with dialysates of blood samples taken before (pre) and after (post) RIC. The solid lines indicate measurements using plasma pre and post RIC from the same proband. Sarcomere contraction and relaxation of paced cardiomyocytes (0.5 Hz) were assessed at baseline (black, A) and after stimulation of myocytes with 10^{-7} M isoproterenol (red, B). Each data point represents the mean value from 10 myocytes with 10 transients averaged per myocyte; P-values were calculated by paired t-test. The scatter plots to the right indicate the difference (post minus pre) for the sample pairs of every individual; mean \pm SEM.

3.3.2.3 Speed of relaxation

As with contraction velocity, the velocity of sarcomere relaxation was also only enhanced by trend in the RIC group before as well as after isoproterenol stimulation of cardiomyocytes ($P = 0.28$ and 0.38 ; Figure 3.26).

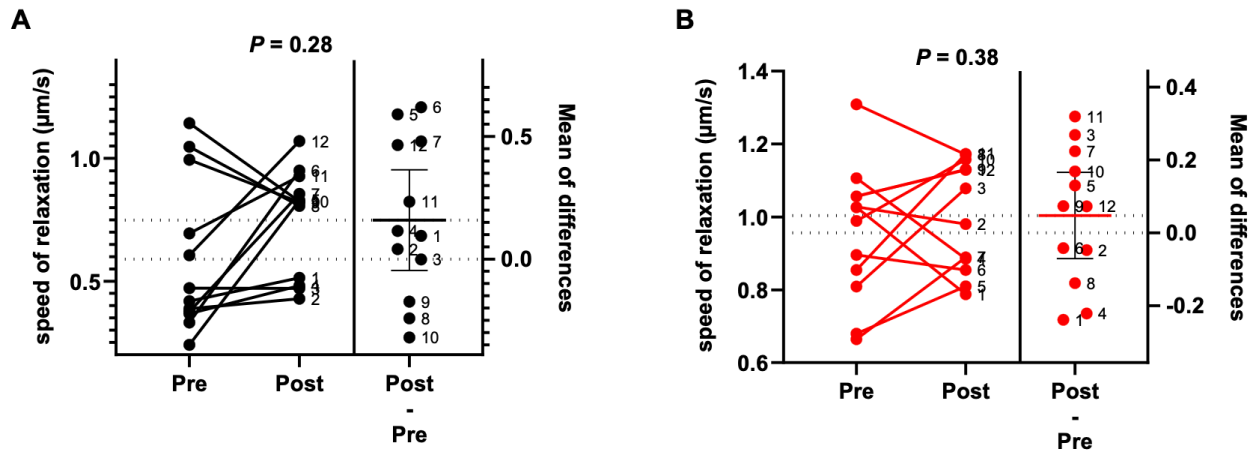


Figure 3.26: Relaxation velocity at baseline and after β -adrenergic stimulation of cardiomyocytes incubated with dialysates of blood samples taken before (pre) and after (post) RIC. The solid lines indicate measurements using plasma pre and post RIC from the same proband. Sarcomere contraction and relaxation of paced cardiomyocytes (0.5 Hz) were assessed at baseline (black, A) and after stimulation of myocytes with 10^{-7} M isoproterenol (red, B). Each data point represents the mean value from 10 myocytes with 10 transients averaged per myocyte; P-values were calculated by paired t-test. The scatter plots to the right indicate the difference (post minus pre) for the sample pairs of every individual; mean \pm SEM.

In summary, RIC increased the amplitude and the velocities of sarcomere contraction and relaxation of cardiomyocytes only by a weak trend, both under basal conditions and after β -sympathomimetic isoproterenol stimulation.

3.3.3 Effects of hypoxia on cardiomyocyte Ca^{2+} cycling

Next, we studied to define hypoxia-induced effects on cardiomyocyte calcium cycling. Isolated cardiomyocytes of 10 mice were exposed to hypoxia for 50 min, followed by 3 min of reoxygenation and measurements of cellular Ca^{2+} cycling compared to non-hypoxic control cells from the same cell preparation.

3.3.3.1 Peak Height (amplitude) of Ca^{2+} transients

Figure 3.27 shows the peak height (amplitude) of the measured Ca^{2+} transients. For each heart, 10 cells were measured and the amplitude of 10 Ca^{2+} transients was averaged per cell. Ca^{2+} transient peak height was significantly decreased in all sample pairs by an average of $38 \pm 2\%$ in cardiomyocytes that underwent hypoxia/reoxygenation ($P < 0.0001$; Figure 3.27A). Upon isoproterenol stimulation, Ca^{2+} amplitudes were lower in cells that underwent hypoxia/reoxygenation by $25 \pm 7\%$ ($P = 0.009$; Figure 3.27B).

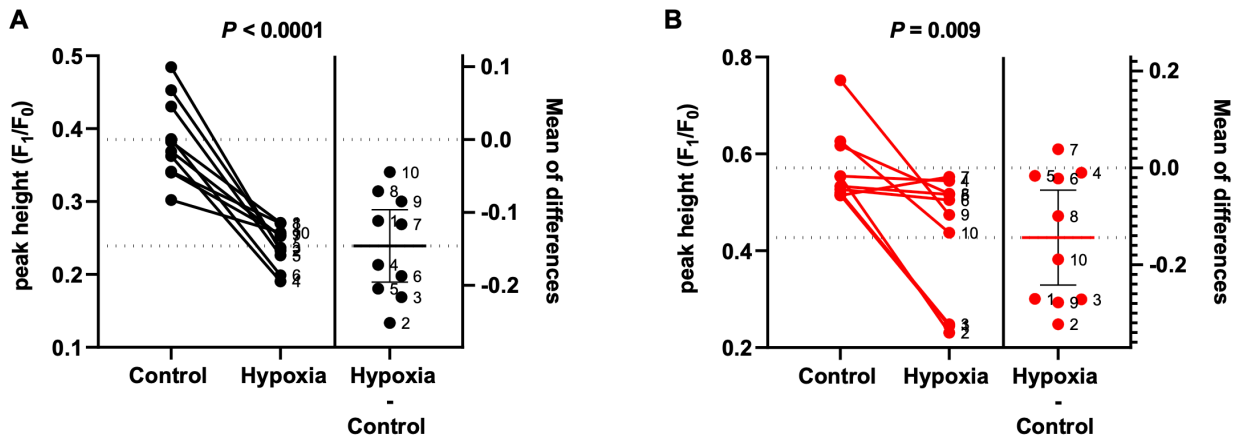


Figure 3.27: Height of Ca^{2+} transients at baseline and after β -adrenergic stimulation of cardiomyocytes after hypoxia and reoxygenation. The solid lines indicate measurements using cells from the same mouse heart. Ca^{2+} transients of paced cardiomyocytes (0.5 Hz) with and without hypoxia and reoxygenation were recorded under basal conditions (black, A) and after stimulation of cells with the beta-adrenergic agonist isoproterenol (10^{-7} M; red, B). Each data point represents the mean value from 10 myocytes with 10 transients averaged per myocyte; P-values were calculated by paired t-test. The scatter plots to the right indicate the difference for the same cell preparation with minus without hypoxia; mean \pm SEM.

3.3.3.2 Speed of Ca^{2+} increase

Like amplitude, the rate of Ca^{2+} increase in the cytosol also showed a decrease by $44 \pm 1\%$ ($P = 0.0002$; Figure 3.28A) in hypoxic cells at baseline. After stimulation of cardiomyocytes with isoproterenol, the rate of Ca^{2+} increase was reduced in hypoxic cells by $38 \pm 6\%$ ($P = 0.001$; Figure 3.28B).

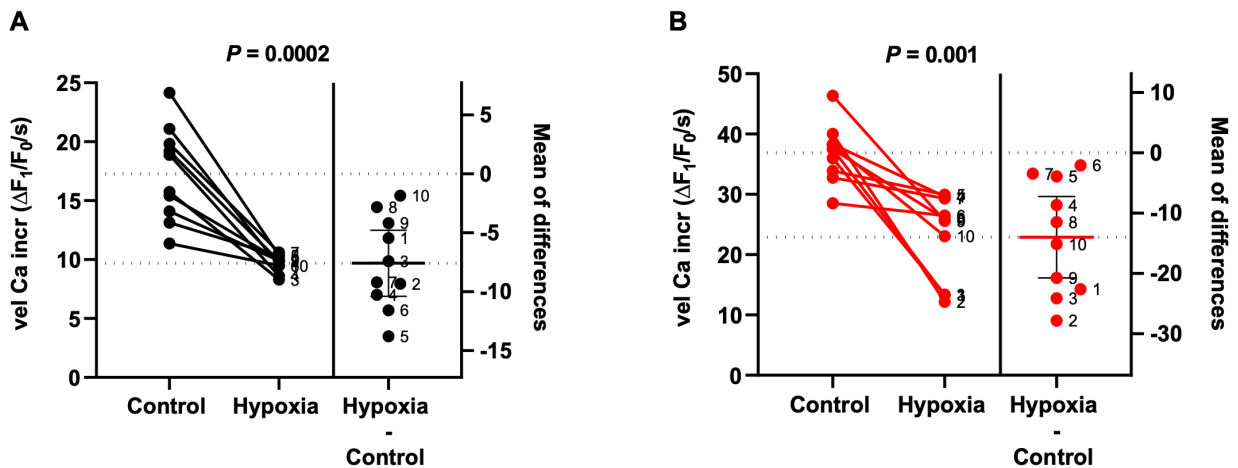


Figure 3.28: Velocity of Ca^{2+} increase at baseline and after β -adrenergic stimulation of cardiomyocytes after hypoxia and reoxygenation. The solid lines indicate measurements using cells from the same mouse heart. Ca^{2+} transients of paced cardiomyocytes (0.5 Hz) with and without hypoxia and reoxygenation were recorded under basal conditions (black, A) and after stimulation of cells with the beta-adrenergic agonist isoproterenol (10^{-7} M; red, B). Each data point represents the mean value from 10 myocytes with 10 transients averaged per myocyte; P-values were calculated by paired t-test. Vel cal incr = velocity calcium increase. The scatter plots to the right indicate the difference for the same cell preparation with minus without hypoxia; mean \pm SEM.

3.3.3.3 Speed of Ca^{2+} decrease

Similarly, the rate of Ca^{2+} elimination was significantly reduced in cells after hypoxia/reoxygenation by $30 \pm 2\%$ ($P < 0.01$; Figure 3.29A) at baseline. After isoproterenol stimulation of cells, the change in the speed of cytosolic Ca^{2+} elimination varied substantially between sample pairs, on average there was a decrease by $14 \pm 9\%$ in hypoxic cells, but it did not reach significance ($P = 0.29$; Figure 3.29B).

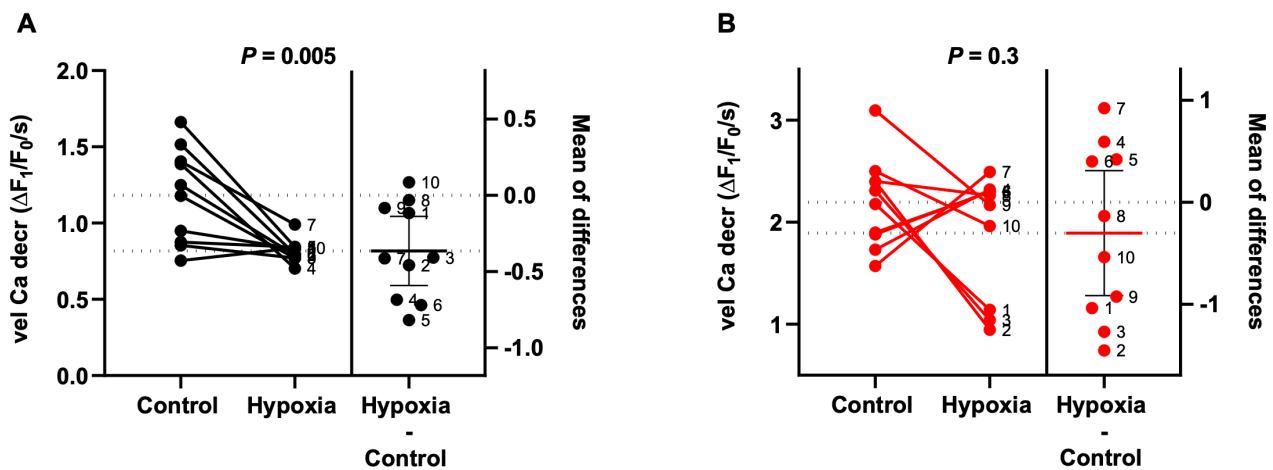


Figure 3.29: Velocity of Ca^{2+} decrease at baseline and after β -adrenergic stimulation of cardiomyocytes after hypoxia and reoxygenation. The solid lines indicate measurements using cells from the same mouse heart. Ca^{2+} transients of paced cardiomyocytes (0.5 Hz) with and without hypoxia and reoxygenation were recorded under basal conditions (black, A) and after stimulation of cells with the beta-adrenergic agonist isoproterenol (10^{-7} M; red, B). Each data point represents the mean value from 10 myocytes with 10 transients averaged per myocyte; P-values were calculated by paired t-test. Vel cal decr = velocity calcium decrease. The scatter plots to the right indicate the difference for the same cell preparation with minus without hypoxia; mean \pm SEM.

Overall, the data indicate depressed Ca^{2+} cycling in cardiomyocytes that underwent hypoxia/reoxygenation, both at baseline and after isoproterenol stimulation of cells. Isoproterenol (10^{-7} M) enhanced Ca^{2+} cycling parameters to a similar degree above baseline values in both groups.

3.3.4 Effects of hypoxia on sarcomere function

To determine how the changes in Ca^{2+} cycling translate into altered mechanical function of cardiomyocytes, parallel measurements of sarcomere contraction and relaxation were performed in isolated mouse cardiomyocytes with and without hypoxia plus reoxygenation.

3.3.4.1 Contractile Amplitude

The amplitude of sarcomere contraction surprisingly did not change in cells after hypoxia ($10 \pm 6\%$ increase, $P = 0.3$; Figure 3.30 A). The contractile amplitude showed a trend decrease by $13 \pm 6\%$ in cell after hypoxia upon β -adrenergic stimulation ($P = 0.08$; Figure 3.30B).

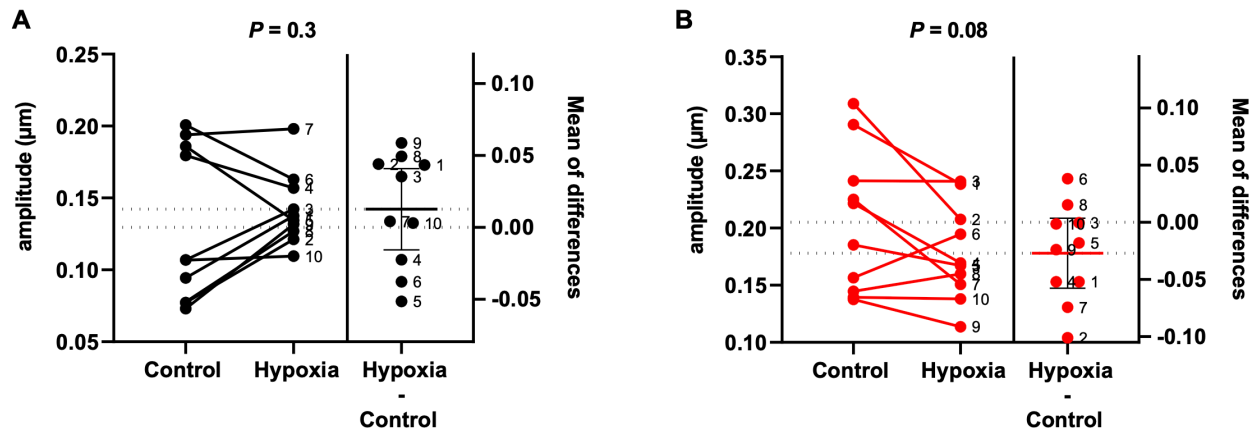


Figure 3.30: Contractile amplitude at baseline and after β -adrenergic stimulation of cardiomyocytes after hypoxia and reoxygenation. The solid lines indicate measurements using cells from the same mouse heart. The amplitude of sarcomere contraction in paced cardiomyocytes (0.5 Hz) with and without hypoxia and reoxygenation were assessed at baseline (black, A) and after stimulation of myocytes with 10^{-7} M isoproterenol (red, B). Each data point represents the mean value from 10 myocytes with 10 transients averaged per myocyte; P-values were calculated by paired t-test. The scatter plots to the right indicate the difference for the same cell preparation with minus without hypoxia; mean \pm SEM.

3.3.4.2 Speed of contraction

At baseline, the velocity of sarcomere contraction surprisingly increased by $32 \pm 10\%$ in cells after hypoxia ($P = 0.009$; Figure 3.31A). No difference between groups was observed after stimulation of β -adrenergic receptors ($6 \pm 11\%$ decrease in hypoxic cells; $P = 0.6$; Figure 3.31B).

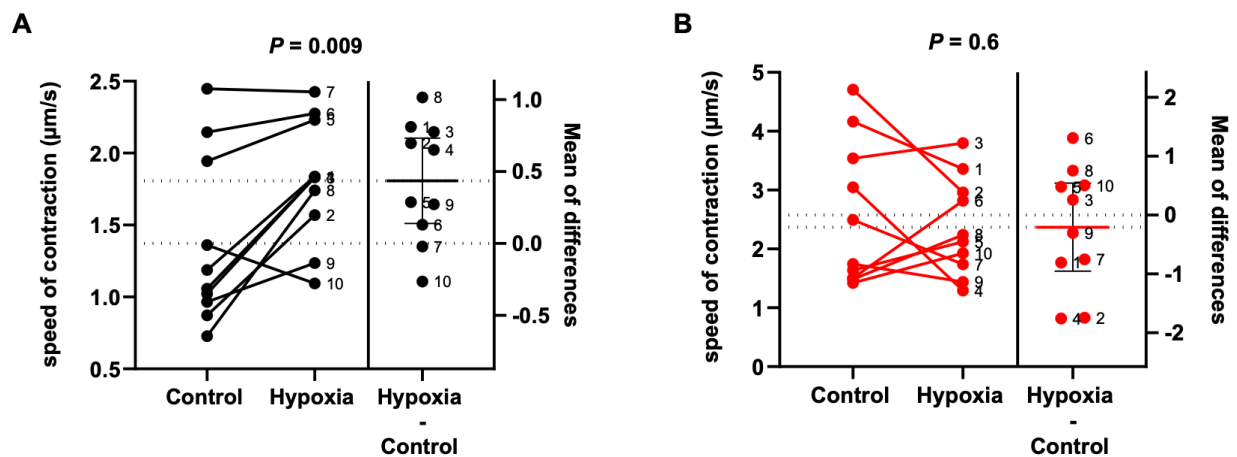


Figure 3.31: Contraction velocity at baseline and after β -adrenergic stimulation of cardiomyocytes after hypoxia and reoxygenation. The solid lines indicate measurements using cells from the same mouse heart. The speed of sarcomere contraction in paced cardiomyocytes (0.5 Hz) with and without hypoxia and reoxygenation were assessed at baseline (black, A) and after stimulation of myocytes with 10^{-7} M isoproterenol (red, B). Each data point represents the mean value from 10 myocytes with 10 transients averaged per myocyte; P-values were calculated by paired t-test. The scatter plots to the right indicate the difference for the same cell preparation with minus without hypoxia; mean \pm SEM.

3.3.4.3 Speed of relaxation

As with contraction velocity, the velocity of sarcomere relaxation was significantly enhanced by $29 \pm 10\%$ in myocytes exposed to hypoxia ($P = 0.02$; Figure 3.32A). After stimulation of β -adrenergic receptors the difference between groups vanished completely ($P = 0.5$; Figure 3.32B).

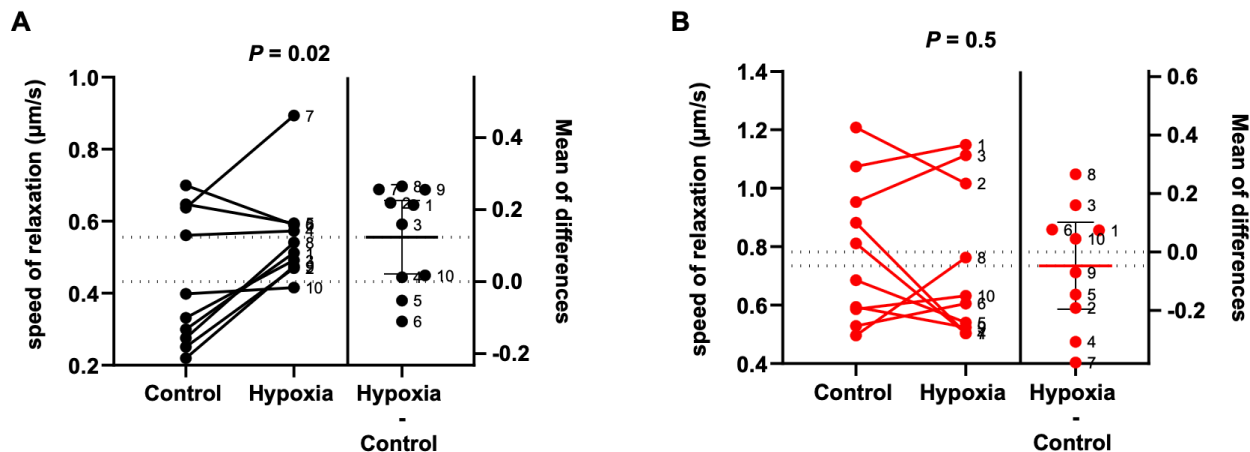


Figure 3.32: Relaxation velocity at baseline and after β -adrenergic stimulation of cardiomyocytes after hypoxia and reoxygenation. The solid lines indicate measurements using cells from the same mouse heart. The speed of sarcomere relaxation in paced cardiomyocytes (0.5 Hz) with and without hypoxia and reoxygenation were assessed at baseline (black, A) and after stimulation of myocytes with 10^{-7} M isoproterenol (red; B). Each data point represents the mean value from 10 myocytes with 10 transients averaged per myocyte; P-values were calculated by paired t-test. The scatter plots to the right indicate the difference for the same cell preparation with minus without hypoxia; mean \pm SEM.

Taken together, the amplitude of sarcomere contraction as well as the velocities of sarcomere contraction and relaxation surprisingly were not significantly reduced after hypoxia. A trend reduction was observed only after β -adrenergic stimulation of cells.

3.3.5 Effects of plasma dialysates from humans before and after RIC on myocyte Ca^{2+} cycling after transient hypoxia

3.3.5.1 Peak Height (amplitude) of Ca^{2+} transients

Figure 3.33 shows the peak height (amplitude) of the measured Ca^{2+} transients. For each heart, 10 cells were measured and the amplitude of 10 Ca^{2+} transients was averaged. The amount of Ca^{2+} released from the SR into the cytosol after each electrical stimulation showed a pronounced increase by $39 \pm 7\%$ ($P < 0.001$; Figure 3.33A) in the cells incubated with RIC dialysates followed by hypoxia and reoxygenation. Upon isoproterenol stimulation, there was an increase in the peak height by $31 \pm 7\%$ ($P < 0.01$; Figure 3.33B).

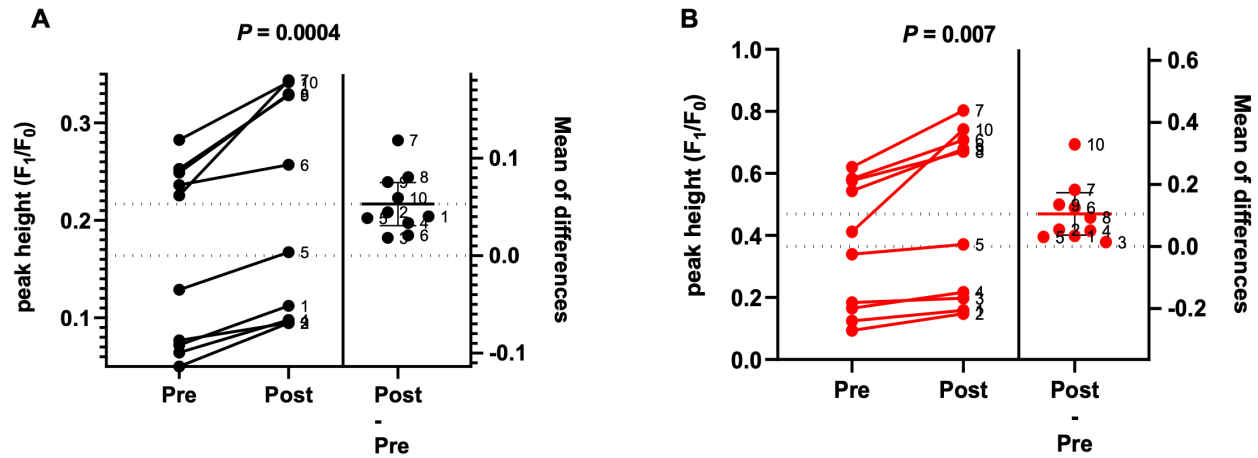


Figure 3.33: Height of Ca^{2+} transients. Isolated mouse cardiomyocytes were incubated with dialysates of human plasma taken from 10 healthy individuals (1-10) before (pre) and after (post) RIC followed by 50min hypoxia and 5 min reoxygenation. The solid lines indicate measurements using plasma pre and post RIC from the same proband. Ca^{2+} transients of paced cardiomyocytes (0.5 Hz) were recorded under basal conditions (black, A) and after stimulation of cells with the beta-adrenergic agonist isoproterenol (10^{-7} M; red, B). Each data point represents the mean value from 10 myocytes with 10 transients averaged per myocyte; P-values were calculated by paired t-test. The scatter plots to the right indicate the difference (post minus pre) for the sample pairs of every individual; mean \pm SEM.

3.3.5.2 Speed of Ca^{2+} increase

Like amplitude, the rate of Ca^{2+} increase in the cytosol also showed an increase in all 10 sample pairs in cardiomyocytes treated with RIC dialysates before hypoxia and reoxygenation ($41 \pm 7\%$ ($P < 0.001$; Figure 3.34A). After stimulation of cardiomyocytes with isoproterenol, the rate of Ca^{2+} increase was faster in all sample pairs ($32 \pm 7\%$ ($P < 0.01$; Figure 3.34B).

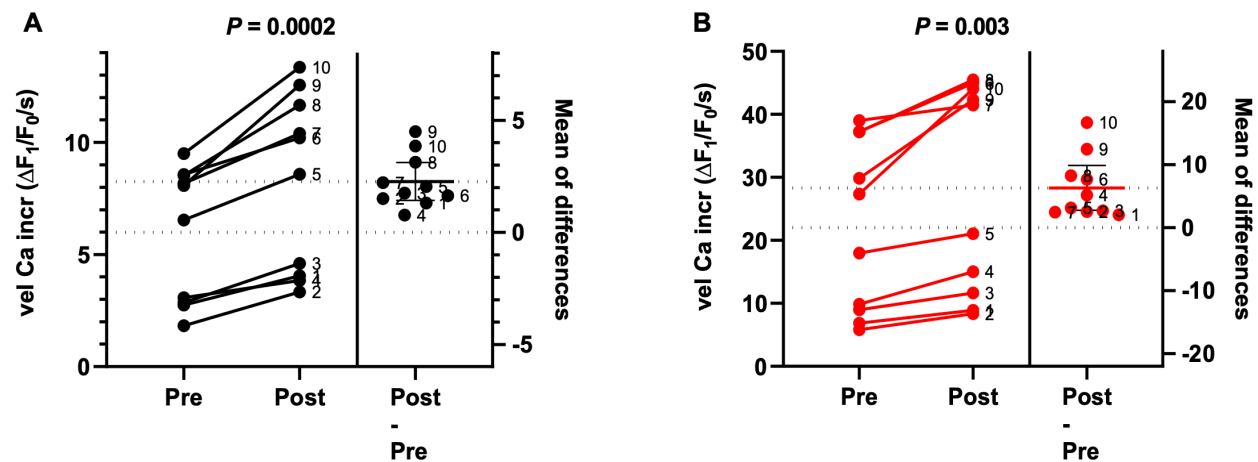


Figure 3.34: Velocity of Ca^{2+} increase at baseline and after β -adrenergic stimulation of cardiomyocytes incubated with dialysates of blood samples taken before (pre) and after (post) RIC. Isolated mouse cardiomyocytes were incubated with dialysates of human plasma taken from 10 healthy individuals (1-10) before (pre) and after (post) RIC followed by 50min hypoxia and 5 min reoxygenation. The solid lines indicate measurements using plasma pre and post RIC from the same proband. Ca^{2+} transients of paced cardiomyocytes (0.5 Hz) were recorded under basal conditions (black, A) and after stimulation of cells with the beta-adrenergic agonist isoproterenol (10^{-7} M; red, B). Each data point represents the mean value from 10 myocytes with 10 transients averaged per myocyte; P-values were calculated by paired t-test. vel ca incr = velocity calcium increase. The scatter plots to the right indicate the difference (post minus pre) for the sample pairs of every individual; mean \pm SEM.

3.3.5.3 Speed of Ca^{2+} decrease

The rate of cytosolic Ca^{2+} decrease was also faster in cells that were conditioned with RIC dialysates ($50 \pm 10\%$, $P < 0.01$; Figure 3.35A). The same applied after isoproterenol stimulation of cardiomyocytes, albeit the difference was smaller ($22 \pm 6\%$ increase, $P < 0.05$; Figure 3.35B).

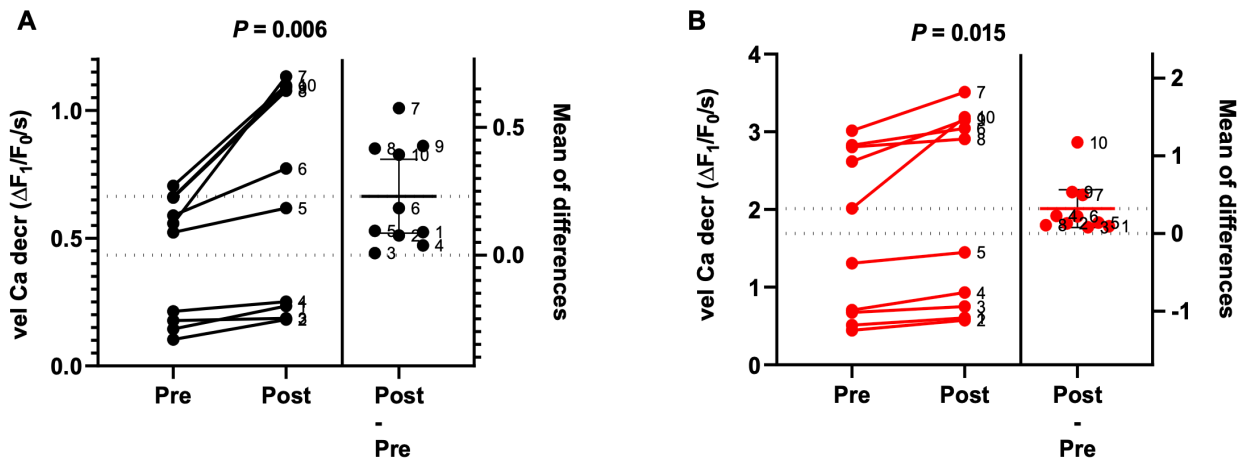


Figure 3.35: Velocity of Ca^{2+} decrease of cardiomyocytes incubated with dialysates of blood samples taken before (pre) and after (post) RIC. Isolated mouse cardiomyocytes were incubated with dialysates of human plasma taken from 10 healthy individuals (1-10) before (pre) and after (post) RIC followed by 50min hypoxia and 5 min reoxygenation. The solid lines indicate measurements using plasma pre and post RIC from the same proband. Ca^{2+} transients of paced cardiomyocytes (0.5 Hz) were recorded under basal conditions (black, A) and after stimulation of cells with the beta-adrenergic agonist isoproterenol (10^{-7} M; red, B). Each data point represents the mean value from 10 myocytes with 10 transients averaged per myocyte; P-values were calculated by paired t-test. vel Ca decr = velocity of calcium decrease. The scatter plots to the right indicate the difference (post minus pre) for the sample pairs of every individual; mean \pm SEM.

Taken together, Ca^{2+} transients of cardiomyocytes followed by hypoxia and reoxygenation were higher compared to respective controls in 10 out of 10 sample pairs if incubated with RIC dialysates. RIC dialysates also enhanced the speed of Ca^{2+} rise and Ca^{2+} decrease. Isoproterenol (10^{-7} M) enhanced myocyte Ca^{2+} cycling in all groups. However, RIC-induced differences were still observed, albeit to a lesser extent as without isoproterenol.

3.3.6 Effects of plasma dialysates on myocyte sarcomere function of cardiomyocytes after transient hypoxia

3.3.6.1 Contractile Amplitude

When the amplitude of sarcomere contraction was analyzed, myocytes after RIC showed a small trend increase compared to controls by $23 \pm 14\%$ ($P = 0.2$; Figure 3.36A) at baseline. Upon isoproterenol stimulation, contractile amplitudes were virtually identical in both groups ($3 \pm 10\%$ higher in RIC-treated cells, $P = 0.8$; Figure 3.36B).

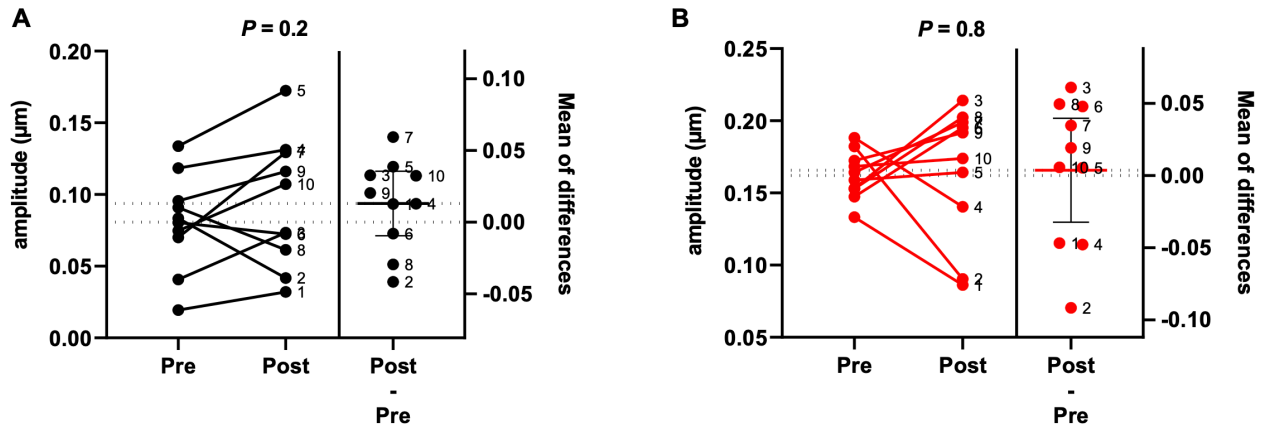


Figure 3.36: Contractile amplitude of cardiomyocytes incubated with dialysates of blood samples taken before (pre) and after (post) RIC. Isolated mouse cardiomyocytes were incubated with dialysates of human plasma taken from 10 healthy individuals (1-10) before (pre) and after (post) RIC followed by 50min hypoxia and 5 min reoxygenation. The solid lines indicate measurements using plasma pre and post RIC from the same proband. Sarcomere contraction and relaxation of paced cardiomyocytes (0.5 Hz) were assessed at baseline (black, A) and after stimulation of myocytes with 10^{-7} M isoproterenol (red, B). Each data point represents the mean value from 10 myocytes with 10 transients averaged per myocyte; P-values were calculated by paired t-test. The scatter plots to the right indicate the difference (post minus pre) for the sample pairs of every individual; mean \pm SEM.

3.3.6.2 Speed of contraction

The velocity of sarcomere contraction showed a trend increase in myocytes after incubation with RIC dialysates by $23 \pm 15\%$ at baseline ($P = 0.2$; Figure 3.37A). After stimulation of cardiomyocytes with isoproterenol, the speed of contraction was unchanged by RIC treatment ($P = 0.9$; Figure 3.37B).

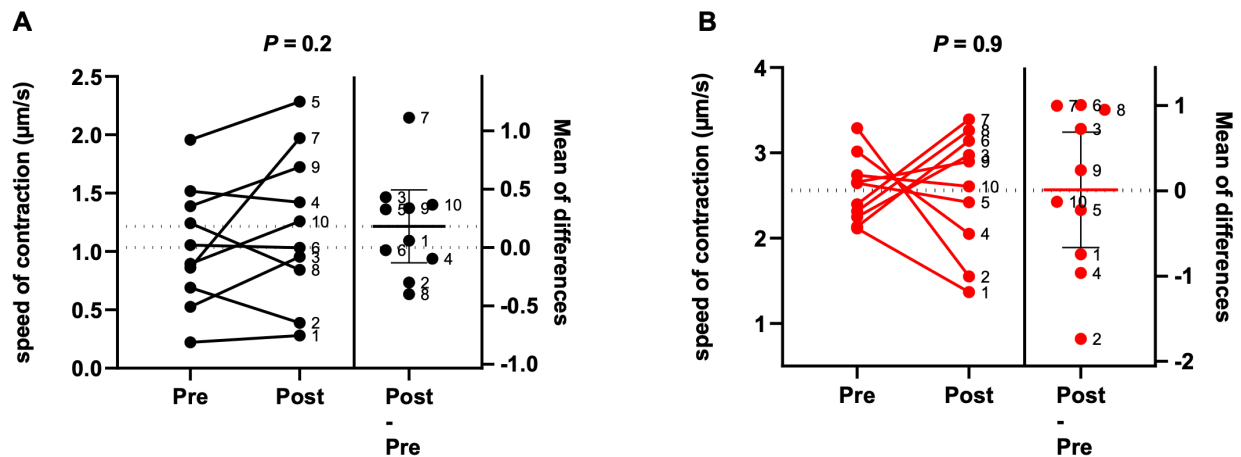


Figure 3.37: Contraction velocity of cardiomyocytes incubated with dialysates of blood samples taken before (pre) and after (post) RIC. Isolated mouse cardiomyocytes were incubated with dialysates of human plasma taken from 10 healthy individuals (1-10) before (pre) and after (post) RIC followed by 50min hypoxia and 5 min reoxygenation. The solid lines indicate measurements using plasma pre and post RIC from the same proband. Sarcomere contraction and relaxation of paced cardiomyocytes (0.5 Hz) were assessed at baseline (black, A) and after stimulation of myocytes with 10^{-7} M isoproterenol (red, B). Each data point represents the mean value from 10 myocytes with 10 transients averaged per myocyte; P-values were calculated by paired t-test. The scatter plots to the right indicate the difference (post minus pre) for the sample pairs of every individual; mean \pm SEM.

3.3.6.3 Speed of relaxation

As with contraction velocity, there was a trend increase by $32 \pm 21\%$ in the velocity of the sarcomere relaxation in cells incubated with RIC dialysates ($P = 0.3$; Figure 3.38A). No increase, but even a trend decrease was observed after isoproterenol stimulation (decrease by $4 \pm 13\%$, $P = 0.55$; Figure 3.38B).

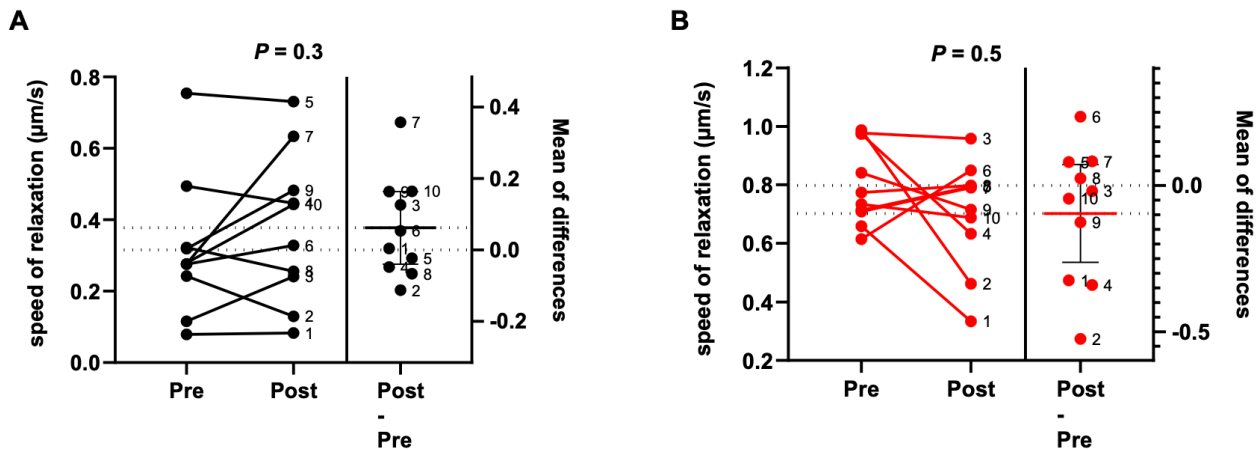


Figure 3.38: Relaxation velocity of cardiomyocytes incubated with dialysates of blood samples taken before (pre) and after (post) RIC. Isolated mouse cardiomyocytes were incubated with dialysates of human plasma taken from 10 healthy individuals (1-10) before (pre) and after (post) RIC followed by 50min hypoxia and 5 min reoxygenation. The scatter plots to the right indicate the difference (post minus pre) for the sample pairs of every individual; mean \pm SEM. Sarcomere contraction and relaxation of paced cardiomyocytes (0.5 Hz) were assessed at baseline (black, A) and after stimulation of myocytes with 10^{-7} M isoproterenol (red, B). Each data point represents the mean value from 10 myocytes with 10 transients averaged per myocyte; P-values were calculated by paired t-test. The scatter plots to the right indicate the difference (post minus pre) for the sample pairs of every individual; mean \pm SEM.

The data indicate that, unlike Ca^{2+} cycling, RIC dialysates did not significantly alter the amplitude of sarcomere contraction in this experimental setting. It also did not alter the kinetics of sarcomere contraction and relaxation, neither under basal conditions nor after β -sympathomimetic stimulation with isoproterenol.

4 Discussion

4.1 Diabetes mellitus type II

40% of MI patients die within the first 24 hours after the acute event. [140]. In diabetic patients mortality is still higher even if myocardial reperfusion is attained by angioplasty, and in-hospital death due to reinfarction has occurred in 13.1% of patients versus 8.5% in non-diabetics at 30 days [141].

Although the infarcted areas of the myocardium are well studied, little is known so far about the changes in the non-ischemic areas of the heart, the remote myocardium, after MI. Detailed knowledge of the conditions for contraction and relaxation of the remote myocardium in the early phase of infarction is of great clinical interest, however, because these parts of the heart must compensate for the loss of function of the infarcted myocardium to ensure adequate cardiac output.

The remote myocardium was analyzed 10 days after I/R and it was investigated whether and, if so, what changes occurred. Studies at this time point are of interest because cardiac remodeling has begun after MI [75]. A healing process occurs in the ischemic myocardium. Dead cardiomyocytes are replaced by collagen.

Intracellular Ca^{2+} kinetics and sarcomere function were investigated in remote cardiomyocytes with diabetic metabolic state 10 days after I/R to reveal potential additive effects on Ca^{2+} homeostasis of cardiomyocytes.

4.1.1 Slowed intracellular Ca^{2+} kinetics in *remote* cardiomyocytes of db/db mice 10 days after I/R

In the present work, the influence of diabetes mellitus type II on the Ca^{2+} cycle and on the sarcomere function of the remote myocardium 10 days after I/R was investigated. Therefore, the intracellular Ca^{2+} kinetics were measured in the mouse model of diabetes type II with the influence of I/R. For this purpose, db/db mouse hearts with diabetic metabolic state and their db/+ littermates were used as described in chapter 1.7.2. The amount of Ca^{2+} released from the SR into the cytosol with each electrical stimulus, represented by the amplitude of the Ca^{2+} transient, was decreased by trend 10 days after I/R in nonischemic db/db cardiomyocytes compared with remote cardiomyocytes from the non-diabetic db/+ mice. The difference reached significance upon stimulation of myocytes with isoproterenol. Isoproterenol is a β -sympathomimetic substance that stimulates the Gs protein-coupled receptor leading to stimulation of PKA-mediated Ca^{2+} -regulatory proteins. This way, slowed Ca^{2+} kinetics often is restored to normal if the underlying defect is

based on the altered activity of Ca^{2+} -regulators. Moreover, the rate of Ca^{2+} increase in the cytosol and that of cytosolic Ca^{2+} decrease was slowed in remote db/db cardiomyocytes (3.1.1). These data show that the already slowed Ca^{2+} kinetics in remote myocardium of non-diabetic organisms are further reduced after MI if a diabetic metabolic state is present. This could possibly contribute to the clinical observation that diabetic patients die more frequently after MI than patients without a history of diabetes [142].

Previous data from our group demonstrated that 24 hours after I/R Ca^{2+} kinetics were slowed in remote cardiomyocytes from db/db mice with diabetic metabolism compared with remote cardiomyocytes from normoglycemic db/+ mice [138]. Also, slowed Ca^{2+} kinetics were demonstrated 24 hours after I/R in remote cardiomyocytes of non-diabetic mice [63]. In contrast to the current study, in both previous studies Ca^{2+} kinetics could be largely improved by β -adrenergic stimulation. Thus, the expression and/or regulation of Ca^{2+} -regulatory proteins seem to be different in remote cardiomyocytes 24 hours and 10 days after I/R. A possible role for the reduced response to isoproterenol in the current study could play decreased β -adrenergic receptor density due to the [143] well-known phenomenon of increased sympathetic tone in diabetic patients [144]. Possibly, increased sympathetic tone in concert with I/R injury leads to sympathetic overdrive and desensitization and downregulation of β -adrenergic receptors within 10 days after I/R.

Previous work described depressed Ca^{2+} homeostasis of naïve db/db cardiomyocytes without I/R injury [140]. Belke et al. also described contractile dysfunction of db/db hearts [89]. In other diabetes models for both type I and type II diabetes mellitus, it has also been shown that intracellular Ca^{2+} circulation is impaired and contractile dysfunction is present [89] [145]. This was manifested by the fact that the rate of cytosolic Ca^{2+} increase and cytosolic Ca^{2+} decrease was slowed and cytosolic Ca^{2+} concentration was decreased. At this point, it should be mentioned that db/db mice develop diabetic cardiomyopathy at advanced ages (> 14 weeks) [146]. Therefore, only animals aged 10 to 12 weeks were used in the present work, when hyperglycemia and insulin resistance have already developed but heart failure is not yet present.

Furthermore, it remains an open question what causes the greater impairment of Ca^{2+} homeostasis of db/db hearts by I/R. To understand the causes of impairment of the contractile apparatus of diabetic hearts, several studies have been performed using different diabetes mellitus models. Using diabetes mellitus induced by streptozotocin (STZ) injections to damage the insulin-producing pancreatic cells and subsequent high-fat and high-sugar diet, Bai et al. showed that the hearts of treated mice had increased protein kinase C- α and PLN expression and decreased SERCA2a and RyR2 expression [147]. A diabetogenic diet in combination with low-dose STZ is experimentally used to produce an animal model of T2DM. The increased presence of PLN, which inhibits SERCA2a in the unphosphorylated state, would lead to decreased

SERCA2a activity, thereby offering an explanation for the decreased uptake of Ca^{2+} into the SR and ultimately the slowed Ca^{2+} kinetics of db/db mice.

Therapeutic approaches tested in the past to improve intracellular Ca^{2+} currents in the failing heart have been studied, for example, in PLN-deficient mice [148]. PLN inhibits SERCA2a by interaction and thereby determines its activity. Cross et al. demonstrated that PLN-deficient mice had improved cardiac contractile function after I/R but were also more sensitive to ischemic injury [148]. In further studies, an antibody against PLN was used to avoid a complete absence of the SERCA2a regulator PLN [149]. This prevented the interaction between PLN and SERCA2a. Indeed, this improved myocyte Ca^{2+} circulation and sarcomere contractility. Unfortunately, neither long-term studies in animals nor clinical studies are known to date to allow conclusions to be drawn about a possible therapeutic benefit in the setting of I/R.

It is known that during ischemia in the ischemic myocardium, anaerobic ATP production is prevented by prolonged oxygen deprivation and increasing acidosis. The resulting ATP deficiency prevents Na^+ ions that influx across the cell membrane from being actively transported out of the cell. The increased cytosolic Na^+ concentration activates the $\text{Na}^+/\text{Ca}^{2+}$ exchanger (NCX) in the opposite direction, so that Na^+ ions leave the cardiomyocyte, with Ca^{2+} flowing in return. During reperfusion, the ischemic myocardium is reoxygenated. ATP-dependent processes are restarted. Ca^{2+} oscillations are the result, which can lead to irreversible damage to the cardiomyocyte.

Activation of NCX in the reverse direction was one of the main causes of cytosolic Ca^{2+} accumulation [150] [151]. Therefore, at the beginning of reperfusion, an inhibitor was used to block the activity of NCX. The use of the NCX inhibitor Cariporide was tested in phase 2 and 3 of a large clinical trial [125]. Three different doses (20 mg, 80 mg, 120 mg) were administered. At 20 mg and 80 mg Cariporide showed no effect. At 120 mg, patients in one subgroup had a 10% lower risk of mortality. Cariporide also showed reduced necrosis in ischemic myocardium. However, when overall mortality was considered, there was no difference between placebo and cariporide use. Inhibition of NCX after MI seems to have little effect on the accumulation of cytosolic Ca^{2+} . Also, it appears unlikely that altered NCX activity could contribute significantly to the disturbed Ca^{2+} regulation 10 days after I/R, observed in the present study, because it would not explain impaired SR Ca^{2+} uptake that was observed here (Fig. 3.3). In fact, impaired SR Ca^{2+} uptake was identified as the main cause of db/db cardiomyocyte Ca^{2+} dysregulation in previous work [140].

Ca^{2+} is released from the SR into the cytosol via the RyR2 after each stimulus, and Ca^{2+} concentration in the luminal SR is the driving force for this SR Ca^{2+} release [152]. Therefore, it is likely that the reduced filling of the SR with Ca^{2+} by SERCA2a is responsible in full or in part for the reduced and slowed cytosolic Ca^{2+} increase. It is known that in the resting state, without being stimulated, the RyR2 releases small amounts of Ca^{2+} into the cytosol. However, physiologically, these spontaneous Ca^{2+} sparks usually are too small that contraction of the sarcomeres would

occur. At the same time, a constant Ca^{2+} loss from the SR in remote myocardium could also be partly responsible for the fact that less Ca^{2+} is released from the SR upon stimulation.

4.1.2 Preserved sarcomere function in remote cardiomyocytes of db/db mice 10 days after I/R

While Ca^{2+} kinetics 10 days after I/R (chapter 3.1.1) were impaired, sarcomere function in remote cardiomyocytes of db/db mice was not significantly different from non-diabetic mice at 10 to 12 weeks of age. The contractile amplitude as well as the contraction and relaxation velocity were similar in remote cardiomyocytes from mice with and without a diabetic metabolic state despite depressed Ca^{2+} cycling. The previous findings from our group showed that at 24 hours after I/R, sarcomere function was altered in remote db/db cardiomyocytes. Contractile amplitude was decreased, and relaxation velocity was slowed in db/db versus db/+ remote cardiomyocytes. In remote cardiomyocytes, impaired sarcomere function was also observed after 1 hour of ischemia and 24 hours of reperfusion in non-diabetic mice. Contractile dysfunction further exacerbated in db/db hearts. Underlying causes were identified as impaired SR Ca^{2+} filling, which was no longer compensated by increased Ca^{2+} sensitivity of myofilaments, as observed in db/db hearts before I/R injury [140]. Thus, the mismatch between depressed Ca^{2+} cycling and maintained sarcomere function of db/db remote cardiomyocytes 10 days after I/R seems to involve the restoration of increased myofilament Ca^{2+} sensitivity as in non-infarcted db/db hearts. However, the exact mechanism causing preserved sarcomere function remains to be identified.

There is evidence that adaptive changes such as altered protein phosphorylation, increase myocyte stiffness have occurred in the sarcomeres 10 days after MI to counteract the myocardial loss of function. The findings in db/db animals are consistent with human studies, as diabetic patients have a poorer cardiac function and higher mortality than non-diabetic patients after MI [142]. Mortality is over 50% in diabetic patients after MI [153]. According to the results presented in this work, changes in the non-ischemic remote myocardium may play an important role.

4.1.3 Unchanged protein expression of regulators of the myocyte Ca^{2+} cycle

To clarify the causes for the impairment of myocyte Ca^{2+} homeostasis 10 days after I/R, the protein expression of the Ca^{2+} regulating proteins was examined in the remote myocardium [158]. Cardiac lysates were examined by Western-blot analysis (chapter 2.3.5) by quantifying the band strength of the protein applied in each case. At the protein level, no altered expressions of the major Ca^{2+} regulators were found in db/db hearts compared to age-matched non-diabetic db/+ mice 10 days after I/R. SERCA2a expression, PLN monomer, RyR2, and S100A1 expression were all unchanged. Thus, no evidence was found that decreased expression of the investigated Ca^{2+} regulators could be the cause of the slowed intracellular Ca^{2+} cycle.

Similarly, the expression of SERCA2a, PLN monomer, RyR2, and S100A1 was also unchanged in the remote myocardium of db/db compared to db/+ mice 24 hours after I/R [138]. At the protein level, no altered expressions of the major Ca^{2+} regulators were found. RyR2 expression, SERCA2a expression, and PLN monomer expression as well as the SERCA2a/PLN monomer ratio were all unchanged. In the literature, expression changes of Ca^{2+} regulators are only described at later time points, in non-diabetic hearts and after non-reperfused MI. Omura et al. demonstrated in rats by mRNA analysis that SERCA gene expression was reduced in the remote myocardium three weeks after MI [154]. Later, after two and four months, SERCA expression was further reduced in the failing heart. The difference of these data from our findings would be sufficiently explained by the different models used, but the later time point of the analyses may also suggest that protein changes may not occur within the first 10 days after ischemia. Furthermore, the considerable variance of expression between samples in our analyses may have obscured potential changes. Finally, all named Ca^{2+} regulatory proteins are highly expressed in cardiomyocytes so that even a substantial gain or loss of protein may not result in a significant percent change of the respective Ca^{2+} regulatory protein.

4.1.4 Unchanged activity of regulators of the Ca^{2+} cycle

Decreased PLN phosphorylation at the PKA-dependent phosphorylation site Ser16 was observed in remote myocardium of db/db mice after 1 hour of ischemia and 24 hours of reperfusion [138]. PLN monomers interact with and inhibit SERCA2a. If the PLN monomer is present unphosphorylated, this inhibition is more pronounced, and less cytosolic Ca^{2+} is transported back into the SR. Thus, the finding of reduced PLN phosphorylation explained impaired Ca^{2+} cycling 24 hours after I/R and prompted us to also investigate this phosphorylation site in the present work 10 days after I/R. However, unchanged PLN phosphorylation at the PKA-dependent phosphorylation site Ser16 was observed in remote myocardium. Thus, this does not explain the slowed intracellular Ca^{2+} cycle and decreased cytosolic Ca^{2+} concentration after I/R in remote myocardium of db/db hearts and constitutes a clear difference to the situation 24 hours after I/R. Consistent with the finding of unchanged PLN phosphorylation and different from the 24 hour time point, β -adrenergic stimulation that would increase Ser16-phosphorylation of PLN did not normalize Ca^{2+} kinetics and transient amplitudes in the remote myocardium but even increased the difference compared with the db/+ myocardium in the present study.

Of note, we found a significant about 3-fold increase of Thr17 phosphorylation, the second phosphorylation site of PLN, in the remote myocardium 10 days after I/R. Thr17 is phosphorylated by Ca^{2+} -calmodulin-dependent protein kinase II, CaMKII, with CaMKII δ as the leading subtype in the heart. Although myocardial infarction is well known to activate this enzyme [155], it seems remarkable to find a 3-fold increase even in the non-ischemic remote myocardium. However, since Thr17 phosphorylation was identical in db/db and db/+ remote myocardium, this phosphorylation

cannot serve as an explanation for the observed differences in myocyte Ca^{2+} cycling of both groups.

Previous work described higher Ca^{2+} sensitivity of db/db hearts, which allowed maintained cardiac contractile function despite impaired cardiomyocyte Ca^{2+} cycling [138]. Therefore, the present study also determined phosphorylation of cTnI, but found no change when normalized for cTnI expression. The same was found 24 hours after I/R suggesting that increased Ca^{2+} sensitivity as a compensatory mechanism to maintain sarcomere function is lost early after I/R injury and does not reconstitute within the first 10 days thereafter. Direct measurements of Ca^{2+} -activated force generation would help to further validate this assumption.

In summary, no differences between db/db and db/+ remote myocardium were detected for the phosphorylation site of PLN at Ser16 but there was increased phosphorylation of PLN at Thr17 in remote myocardium of both groups, diabetic and non-diabetic mice, 10 days after I/R and 24 hours after I/R.

4.2 Diet-induced obesity

We wanted to investigate and compare data with another established mouse model of diabetes, i.e. diet-induced obesity (DIO). Both mouse models, db/db mice and DIO mice, develop a diabetic phenotype due to obesity, a leading cause for the development of T2DM in humans. Disorders induced in mice on a high-fat diet resemble the human comorbidities caused by obesity, such as glucose intolerance, insulin resistance, increased blood pressure, dyslipidemia, hyperinsulinemia, and hyperleptinemia, which are found in obese patients with metabolic syndrome [156]–[158]. The C57BL/6J mouse has a genetic susceptibility to develop diabetes when fed with a high-fat diet. DIO mice were fed a high caloric diet over 9 weeks, whereas db/db mice receive regular chow and develop symptoms due to severe hyperphagia. The metabolic phenotype is similar in both models, however, as compared with DIO mice, db/db mice on average gain even more body weight and their symptoms progress to cardiomyopathy, peripheral neuropathy, and impairment of pancreatic β -cells when the animals are more than 12 weeks old.

Obesity is a condition that has reached epidemic levels in recent years, and its adverse effects have been widely studied in experimental animals. Obesity has been found to impair myocardial performance [159]. Nevertheless, the mechanisms underlying the involvement of Ca^{2+} handling on cardiac dysfunction in obesity models remain unknown. L-type Ca^{2+} channels and sarcoplasmic reticulum (SR) Ca^{2+} -ATPase (SERCA2a) may contribute to the cardiac dysfunction caused by obesity. Interestingly, limited information is available on the relationships between obesity and Ca^{2+} handling. Thus, this study was performed to investigate whether obesity promotes cardiac dysfunction due to changes of intracellular calcium homeostasis.

Many scientific literatures have shown that mice consuming diets containing high content of fat gained weight faster than those on diets containing minimal proportions of fat [160]. Although obese mice manifested a modest but remarkable increase in total body weight, they developed substantially more adipose tissue than control mice; the adiposity index, an important determinant of obesity, was elevated in obese mice relative to that in control mice. Adipose tissue *per se* is an endocrine organ that secretes cytokines such as IL-6 and TNF α ; thus, obesity could potentially be regarded as a chronic inflammatory disease [160]. The possible reason of obesity in these mice is related to the caloric content of this diet. Rather than simply an increased percentage of dietary fat, it has been suggested that energy density is the predisposing factor for weight gain in several animal studies.

High fat intake has been related to insulin resistance and cardiac pathology. Dietary induced myocardial signaling and morphological alterations have been described, but whether cardiomyocyte function is influenced by chronic high fat diet intake is yet to be elucidated. Therefore, the goal was to evaluate the effects of obesity on cardiac function and Ca²⁺ handling-associated myocardial proteins.

4.2.1 Changed myofilament Ca²⁺ kinetics in high-fat diet-induced obesity mouse cardiomyocytes

The two groups of body weight-matched C57BL/6 mice were placed on either a fat-enriched diet or a control diet. The major difference between the two diets was the fat content. Mice fed with fat-enriched diet (DIO) gained weight at a more rapid rate than controls and the weight gain became significant after 9 weeks of feeding (Fig. 3.14). This work determined the progressive consequences of a fat enriched diet on intracellular Ca²⁺ and cell contraction in ventricular myocytes from the C57BL/6J mouse. The characteristics of DIO mice fed compared to mice receiving control diet included increase in the rate of body weight gain, increased blood glucose and differences based on the time-dependent in the disposal of blood glucose.

Cardiomyocytes were isolated to analyze the Ca²⁺ cycling at baseline and after β -adrenergic stimulation by isoproterenol. The increase in the peak height of intracellular Ca²⁺ transients in DIO cardiomyocytes was contrary to what had been observed in db/db mice [142]. In db/db cardiomyocytes, calcium cycling was found depressed both in the size and the kinetics of Ca²⁺ transients. We conclude that the excess adipose tissue and hyperglycemia alone are not sufficient to impair intracellular Ca²⁺ handling of ventricular cardiomyocytes. Despite having similar fat mass and body weight, the onset of metabolic complications in DIO and db/db mice are different and could serve as possible explanations for the observed differences in cardiomyocyte Ca²⁺ cycling. Furthermore, both mouse models of diabetes show differences in glucose and insulin profiles, different energy metabolism and/or different lipid profiles and possibly resulting inflammatory responses.

4.2.2 Changed sarcomere function

Sarcomere shortening and relengthening was measured in paced ventricular cardiomyocytes at baseline and after β -adrenergic stimulation by isoproterenol. In parallel to the slightly higher peak height of Ca^{2+} transients in DIO cardiomyocytes (3.2.1), the contractile amplitude of sarcomere shortening showed an increase by trend in ventricular myocytes from DIO mice compared to controls, suggesting that alterations to myocytes shortening could be attributed to alterations in Ca^{2+} transport. This is different from db/db cardiomyocytes that showed regular sarcomere contraction and relaxation despite impaired Ca^{2+} kinetics [142]. This discrepancy was attributed to increased myofilament Ca^{2+} sensitivity found in db/db hearts under basal conditions. As opposed to these findings, increased myofilament Ca^{2+} sensitivity does not seem to be present in DIO hearts because sarcomere function matches well the size and the kinetics of myocyte Ca^{2+} transients. This is another difference between db/db and DIO mice that, apparently, cannot be attributed to hyperglycemia or adipositas alone, but rather result from additional metabolic differences between both mouse models of diabetes as detailed above.

Experimental studies of cardiac contractile function in animal models of diet-induced obesity revealed heterogeneous results. Rats on hypercaloric diet for 14 weeks showed regular cardiac function in vivo and in ventricular cardiomyocytes [161], [162]. On the other hand, other studies found mechanical dysfunction of isolated hearts and ventricular cardiomyocytes in rats and rabbits on high-fat diet [163], [164]. Thus the impact of diet-induced obesity on cardiac function will remain a matter of debate and seems to be dependent on the respective model organism and examination procedure. Based on the findings reported here in two different obese mouse models, adipositas alone - and also hyperglycemia - do not seem to cause dysfunction on the level of cardiomyocyte sarcomeres.

4.3 RIC dialysates

Even though immense progress has been made throughout the past 3 decades in the treatment of patients with acute myocardial infarction (MI), there is still a need for improvement [165], [166]. Although decreasing the incidence of acute MI and subsequent death remains unacceptably high, ischemia-related heart failure is becoming more frequent [167]. Myocardial ischemic conditioning is considered as an endogenous cardioprotective phenomenon that profoundly limits infarct size in experimental models. The classified definition of “conditioning” is the application of a series of alternating intervals of brief ischemia (hypoxia) and reperfusion (reoxygenation) applied in the setting of prolonged ischemia causing myocardial infarction. Cardioprotection, i.e. infarct size reduction as well as improved cardiac contractile function after I/R, was also observed if ischemia was applied to a limb before myocardial infarction suggesting that ischemic conditioning of hearts is mediated, at least in part, by humoral factors. The goal of this study was to evaluate the effects

of a humoral factor that is induced by ischemic preconditioning and confers cardioprotection from ischemia/reperfusion injury on cardiomyocyte Ca^{2+} homeostasis.

In theory, ischemic conditioning might either affect the signal transduction pathways within the heart or the inter-organ communication, i.e., the signal transduction from the remote organ or tissue to the heart. The observation that the transfer of blood samples after RIC to a isolated heart initiates cardioprotection supports the concept of blood-borne humoral factors as an important signalling step of the inter-organ communication [129]. Because of its non-invasive nature RIC seems to be an optimal therapeutic strategy to protect the heart from I/R injury in a safe and easy-applicable way. In the present study, we modeled the clinical situation in isolated cardiomyocytes by exposing isolated mouse cardiomyocytes to serum dialysates from probands with and without RIC. The experiments demonstrated that RIC dialysates alter myocyte Ca^{2+} handling independently of beta-adrenergic receptor stimulation and PKA-dependent phosphorylation of Ca^{2+} regulatory proteins. After transient hypoxia and reoxygenation, humoral factors released by RIC enhanced cardiomyocyte Ca^{2+} cycling, which may play a role in cardioprotection from hypoxic/ischemic damage.

4.3.1 Dialysates from blood samples post remote IPC enhance Ca^{2+} cycling and sarcomere contraction and relaxation in cardiomyocytes without hypoxia

Isolated mouse cardiomyocytes without hypoxia and reoxygenation were incubated with serum dialysates from 10 human probands. Samples were received from Prof. Petra Kleinbongard, Institute of Pathophysiology, University Hospital Essen. For each proband, sample pairs were obtained before and after RIC. Ca^{2+} transients of cardiomyocytes were higher compared to respective controls in all sample pairs. RIC dialysates also enhanced the speed of Ca^{2+} rise and the speed of Ca^{2+} decrease. In addition, after stimulation with β -adrenergic, the amount of Ca^{2+} released into the cytosol, the rate of Ca^{2+} increase and rate of Ca^{2+} decrease were also significantly increased. The sarcomere function measurement was also performed in parallel with the measurement of myocyte Ca^{2+} kinetics in isolated mouse cardiomyocytes. Like Ca^{2+} cycling, RIC also increased the contractile amplitude at baseline. The velocity of sarcomere contraction as well as the velocity of sarcomere relaxation were enhanced by trend. The β -sympathomimetic isoproterenol stimulation accelerated contraction and relaxation of all cells and the RIC-induced trend difference was still present. These data demonstrate that soluble factors that are present in the blood after RIC of healthy human probands seem to enhance Ca^{2+} cycling and increase sarcomere contraction in isolated mouse cardiomyocytes. Notably, these effects were observed in cells without previous subjection to ischemia and reoxygenation.

4.3.2 Hypoxia and reoxygenation impair cardiomyocyte Ca^{2+} cycling and sarcomere function

Ca^{2+} cycling in isolated mouse cardiomyocytes was depressed by hypoxia and reoxygenation injury in all experiments. The amplitude of the measured Ca^{2+} transients, representing the amount of Ca^{2+} released from the SR into the cytosol after each electrical stimulation, as well as the rates of cytosolic Ca^{2+} increase and Ca^{2+} elimination were significantly reduced. These alterations compared to untreated cells were still present after stimulation with isoproterenol (10^{-7} M) suggesting that the observed defects do not result from phosphorylation defects of Ca^{2+} regulatory proteins as described in remote myocardium early after ischemia and reperfusion [64].

The measurement of sarcomere function was performed in parallel with the measurement of myocyte Ca^{2+} kinetics in isolated mouse cardiomyocytes. Surprisingly, the amplitude as well as the velocities of sarcomere contraction and relaxation were not reduced in parallel with the observed changes in Ca^{2+} cycling and only showed a trend reduction upon β -adrenergic stress. Thus, the model used in this work appeared suitable to determine potential rescue effects of RIC dialysates to Ca^{2+} cycling induced by acute hypoxia and reoxygenation injury. The subtle effects of hypoxia observed for sarcomere function would explain why the experimental model used here did not reveal significant changes of sarcomere function after treatment of cells with RIC dialysates (see 4.3.3).

4.3.3 Dialysates from blood samples post remote RIC enhance Ca^{2+} cycling in cardiomyocytes after hypoxia

When isolated cardiomyocytes were incubated with plasma dialysates prior to hypoxia and reoxygenation, Ca^{2+} transients of cardiomyocytes were higher compared to respective controls in all sample pairs, indicating a more pronounced cytosolic Ca^{2+} increase. RIC dialysates also enhanced the speed of Ca^{2+} rise and the speed of Ca^{2+} decrease. Intriguingly, this increase of Ca^{2+} parameters was of comparable magnitude to that of their decrease due to 50 min hypoxia in untreated myocytes. Isoproterenol (10^{-7} M) stimulation also enhanced the myocyte Ca^{2+} cycling in all groups. RIC-induced differences were still present, but slightly reduced suggesting that RIC dialysates alter myocyte Ca^{2+} handling mainly, but not in fully, independent of β -adrenergic receptor stimulation and PKA-dependent phosphorylation of Ca^{2+} regulatory proteins.

Previous studies have shown that ischemic preconditioning has been related to reduced generation of oxygen free radicals and attenuated oxidant-related injury to endothelium and myocytes [168], [169]. *In vitro* studies using isolated cardiomyocytes and endothelial cells have reported that the generation of superoxide radicals and cytokines at reoxygenation was significantly attenuated by hypoxic preconditioning. These authors suggest that a transient low-level stimulation of oxygen radical generation by preconditioning may act as a signal that arouses

an anti-inflammatory type “cardiomyocyte and endothelial preconditioning,” which then depresses responsiveness of these cells to inflammatory mediators. Some cardio-depressive actions of ROS have been associated to the activation of signaling pathways that influence the phosphorylation, expression, or function of Ca^{2+} regulatory proteins (such as SERCA2a and RyR2), leading to changes in the magnitude of the calcium transient and an inadequate calcium-induced contractile response. ROS-induced structural modifications of the sarcomere due to direct oxidative modifications of myofilament proteins, myofilament protein phosphorylation by ROS-activated kinases, or myofilament protein cleavage by ROS-activated proteases that interfere with the transduction of Ca^{2+} -dependent contractile responses.

4.3.4 RIC dialysates did not enhance sarcomere function of cardiomyocytes after hypoxia in the used experimental model

Ca^{2+} transients of cardiomyocytes incubated with RIC dialysates followed by hypoxia and reoxygenation demonstrated wide variation of results, both for the amplitude and the kinetics of sarcomere contraction and relaxation. While RIC induced a trend increase without pharmacological stimulation of cells, the β -sympathomimetic isoproterenol accelerated contraction and relaxation, however, no differences between cells with and without RIC treatment were detectable. These results are consistent with the reduced changes observed with RIC for myocyte Ca^{2+} handling after isoproterenol stimulation. Furthermore, the measurements of myocytes with and without hypoxia (see 4.3.2) had revealed that the experimental setup used in the present work is suitable to detect RIC-induced changes of Ca^{2+} cycling in isolated cardiomyocytes, but it appeared to be less sensitive to detect changes of sarcomere function.

Previous work has demonstrated that RIC induces cardioprotection and reduces myocardial damage/infarct size in patients with acute myocardial infarction and those undergoing cardiovascular surgery. It is known at the subcellular level that RIC improves energy metabolism, preserves mitochondrial respiration, ATP production and Ca^{2+} homeostasis. Mechanisms for reversible myocardial contractile dysfunction involve a disruption in cardiomyocyte Ca^{2+} homeostasis which includes decreased responsiveness of the myofilaments to Ca^{2+} , intracellular Ca^{2+} overload, and disturbed excitation-contraction coupling due to SR dysfunction. Future studies will reveal the biochemical effects of RIC on Ca^{2+} regulatory proteins that accelerate intracellular Ca^{2+} transport and improve the contractile function of cardiomyocytes.

5 Outlook

The mechanisms that underlie diastolic dysfunction during diabetes are not well understood. A more established line of evidence points to a significant involvement of altered cardiomyocyte Ca^{2+} homeostasis in the development of T2DM-induced diastolic dysfunction. In mouse models of T2DM, decreased contractile function was related to increased cardiomyocyte Ca^{2+} efflux, reduced Ca^{2+} entry, decreased SR Ca^{2+} load and altered Ca^{2+} homeostasis. Based on the results obtained in this work, it was observed that T2DM exacerbates the depression of Ca^{2+} cycling in remote myocytes after I/R. Impaired myocyte Ca^{2+} homeostasis in db/db mice model of T2DM has previously been correlated with altered expression of myocyte Ca^{2+} handling proteins and consecutive changes in myocyte Ca^{2+} content and SR Ca^{2+} load. Cells were stimulated with isoproterenol to activate PKA, but unlike wild-type myocytes, PKA stimulation did not rescue the Ca^{2+} cycling phenotype. Isoproterenol also did not raise sarcomere function to the same level as in stimulated non-diabetic myocytes.

At 10 days after I/R, no restriction of sarcomere function could be detected in the remote myocardium. Whether this is also the case at later time points, for example, 28 days after I/R, could be of interest because by then another phase of post-infarct remodeling, the so-called maturation phase, has begun. Scarring occurs, and necrotic tissue is completely replaced by fibrous tissue. It is thought that in this late phase after MI, cardiac remodeling disrupts many signaling cascades, especially signal transduction of many protein kinases and protein phosphatases. This leads to hypertrophy and/or dilatation of the heart and, functionally, often to chronic heart failure. Thus, future studies should include a detailed and time-resolved characterization of oxidative stress-induced modification of sarcomeric proteins and their regulators and may also unravel the complex interplay of these modifications and their role in modulating cardiomyocyte function after I/R.

Obesity is often linked with changes in cardiac function; however, the mechanisms responsible for functional abnormalities have not yet been fully clarified. Considering the lack of information whether fat-enriched diet-induced obesity involved in myocardial Ca^{2+} handling, the results showed that obesity may lead to changes in myocardial Ca^{2+} kinetics. While a 9-week duration is longer than average prebiotic studies, extending the study period may help to determine whether the observed fold changes translate to functional improvements at the organ level. Furthermore, a longer study duration may be more representative of the chronic nature of obesity and thus provide a clearer understanding of whether diet-induced obesity mediates cardiac changes. Future research should also investigate the post-translational modifications, such as phosphorylation, which may be more indicative of cardiac function compared to protein abundance.

The present work evaluated the hypothesis that a humoral factor that is induced by RIC affects cardiomyocyte Ca^{2+} homeostasis, and it was shown that Ca^{2+} kinetics were enhanced. To follow up on the results of the present work, it would be interesting to see whether the potential effects of plasma from preconditioned humans improve Ca^{2+} kinetics also in myocytes isolated from diabetic mouse hearts. Another approach to take this project further could be to study the influence of myocardial (instead of remote) ischemic preconditioning on sarcomere function, and the ability of the preconditioned medium to alter cardiomyocyte Ca^{2+} homeostasis and contractility. This study will help to explain existing differences between the results of both experimental and clinical studies investigating the cardioprotective potential of RIC. More importantly, because the humoral factor(s) have the potential to initiate protection in the heart, the identification of the cardiac receptor is of great interest as a pharmacological target. Therefore, future studies should focus on the identification of the molecular structure of humoral factor(s) as well as the cardiac target structures.

6 Summary

Ischemia and reperfusion (I/R) impair myocardial contractile function not only in the infarct zone but also in non-infarcted regions, i.e., the remote myocardium (RM). We hypothesized that type 2 diabetes mellitus (T2DM) impairs electromechanical coupling and sarcomere function and thereby impedes important adaptive remodeling processes after I/R. The present study aimed to investigate (i) the sarcomere function and intracellular Ca^{2+} kinetics of a genetic mouse model of T2DM (db/db) 10 days after I/R, (ii) whether diet-induced obesity (DIO) plays a causal role in contractile dysfunction of cardiac myocytes and (iii) to test the hypothesis that the cardioprotective effects of remote ischemic preconditioning (RIC) by transient ischemia to one arm of healthy human probands involve alterations to myocyte Ca^{2+} homeostasis and/or cardiomyocyte contractile function on the sarcomere level.

Measurements of Ca^{2+} kinetics and sarcomere function in cardiomyocytes isolated from the remote myocardium of db/db mouse hearts 10 days after I/R revealed that myocyte Ca^{2+} transients are smaller, and Ca^{2+} kinetics are slowed, particularly after β -adrenergic stimulation of cells, compared to cells isolated from non-diabetic heterozygous db/+ control mice. However, sarcomere function was impaired only by trend. The additive effects of I/R and T2DM on myocyte Ca^{2+} homeostasis may contribute to the poor clinical outcome of patients with diabetes mellitus after myocardial infarction.

Diet-induced obesity has been described to impair myocardial performance. Thus, this study was performed to determine the interplay between DIO and intracellular Ca^{2+} properties and to compare the results from this model of pre-diabetes to the data obtained in db/db mice. Male C57BL/6 mice were fed a diabetogenic diet for 9 weeks. Unlike db/db mice, the intracellular Ca^{2+} kinetics and the amplitude of the Ca^{2+} transients were not depressed by the diabetogenic diet compared to control mice on regular chow. These findings show that neither obesity nor hyperglycemia alone are sufficient to impair myocyte Ca^{2+} transport.

RIC is known to reduce infarct size and to improve cardiac contractile function after I/R in animal models. In this study, mouse cardiomyocytes were incubated with serum dialysates obtained from human probands before and after RIC before cells were subjected to hypoxia and reoxygenation. Ca^{2+} transients were higher and intracellular Ca^{2+} kinetics was faster after RIC for all 10 sample pairs. For sarcomere length, there was a trend towards enhanced contraction and relaxation of cells. The results provide a good basis for evaluating the role of myocyte Ca^{2+} homeostasis for the positive inotropic effects induced by conditioned plasma. It can be concluded that humoral factors released by healthy human individuals upon RIC enhance cardiomyocyte Ca^{2+} cycling after transient hypoxia. These effects may play a critical role in RIC-induced protection of the heart from I/R injury.

7 Zusammenfassung

Ischämie und Reperfusion (I/R) beeinträchtigen die kontraktile Funktion des Myokards nicht nur in der Infarktzone, sondern auch in den nicht-infarzierten Regionen, dem sogenannten *remote* Myokard (RM). Wir stellten die Hypothese auf, dass Typ-2-Diabetes mellitus (T2DM) die elektromechanische Kopplung und die Funktion der Sarkomere beeinträchtigt und dadurch wichtige adaptive Prozesse im Myokard nach I/R verhindert. Ziel der vorliegenden Studie war es, (i) die Sarkomerfunktion und die intrazelluläre Ca^{2+} -Kinetik in einem genetischen Mausmodell für T2DM (db/db) 10 Tage nach I/R zu analysieren, (ii) zu untersuchen, ob eine diät-induzierte Adipositas (DIO) eine kausale Rolle für die kontraktile Dysfunktion von Herzmuskelzellen spielt, und (iii) die Hypothese zu testen, dass die kardioprotektiven Effekte der ischämischen Fernkonditionierung (RIC) durch transiente Ischämie an einem Arm gesunder Probanden mit Veränderungen der Sarkomerfunktion und/oder der Ca^{2+} -Homöostase der Myozyten einhergehen. Messungen der Ca^{2+} -Kinetik und der Sarkomerfunktion in Kardiomyozyten des *remote* Myokards von db/db-Mäusen 10 Tage nach I/R ergaben, dass die Ca^{2+} -Transienten kleiner und die Ca^{2+} -Kinetik langsamer waren als in Zellen aus nicht-diabetischen heterozygoten db/+ -Kontrolltieren, vor allem nach β -adrenerger Stimulation der Zellen. Die Sarkomerfunktion war dagegen nur tendenziell schlechter. Die additiven Effekte von I/R und T2DM auf die Ca^{2+} -Homöostase der Myozyten könnte zu dem schlechten klinischen Verlauf von Diabetikern nach Myokardinfarkt beitragen.

In der Literatur wurde beschrieben, dass DIO die Herzmuskelfunktion beeinträchtigt. In dieser Studie wurden daher die Wechselwirkungen zwischen DIO und dem intrazellulären Ca^{2+} -Transport untersucht und die Ergebnisse dieses Mausmodells für Prä-Diabetes mit den Daten der db/db-Mäuse verglichen. Männliche C57BL/6-Mäuse wurden 9 Wochen lang mit einer diabetogenen Diät gefüttert. Anders als bei db/db-Mäusen wurden die intrazelluläre Ca^{2+} -Kinetik und die Amplitude der Ca^{2+} -Transienten durch die diabetogene Ernährung im Vergleich zu Kontrollen mit normalem Futter nicht reduziert. Diese Ergebnisse zeigen, dass weder Adipositas noch Hyperglykämie alleine ausreichend sind, um den myozytären Ca^{2+} -Transport so wie im db/db-Modell für Typ-2-Diabetes zu beeinträchtigen.

In Tiermodellen verringert RIC die Infarktgröße und verbessert die kontraktile Funktion des Herzens nach I/R. In dieser Studie wurden Maus-Kardiomyozyten mit Serum-Dialysaten aus gesunden humanen Probanden vor und nach RIC inkubiert und anschließend transients Hypoxie ausgesetzt. In allen 10 Proben-Paaren waren die Ca^{2+} -Transienten höher und die intrazelluläre Ca^{2+} -Kinetik durch RIC beschleunigt. Die Sarkomerfunktion zeigte dagegen nur geringe Veränderungen. Die Ergebnisse bieten eine Grundlage für die Bewertung der Rolle der myozytären Ca^{2+} -Homöostase für die durch konditioniertes Plasma induzierten positiv inotropen Effekte. Diese Befunde zeigen, dass humorale Faktoren, die von gesunden Menschen bei RIC freigesetzt werden, spezieübergreifend den Ca^{2+} -Kreislauf der Kardiomyozyten nach transients Hypoxie beschleunigen können. Diese Effekte könnten eine wichtige Rolle beim RIC-induzierten Schutz des Herzens vor I/R-Schäden spielen.

8 Abbreviation

AAR	Area at risk
AC	Adenylate cyclase
Akt	Protein kinase B
AMI	Acute myocardial infarction
ATP	Adenosine triphosphate
β -AR	β -adrenergic receptor
Ca^{2+}	Calcium
CAD	Coronary artery disease
CaMKII	Calcium calmodulin-dependent protein kinase II
cAMP	Cyclic adenosine monophosphate
CHD	Coronary heart disease
CVD	Cardiovascular disease
db/db	Leptin receptor deficient homozygous mouse
db/+	Leptin receptor deficient heterozygous mouse
DIO	Diet induced obesity
ECC	Excitation contraction coupling
FFT	Fast Fourier transform
HFD	High fat diet
IHD	Ischemic heart disease
I/R	Ischemia/reperfusion
IS	Infarct size
LAD	Left anterior coronary artery
LV	Left ventricle
MI	Myocardial infarction
NCX	Sodium-Calcium Exchanger
Na^{2+}	Sodium
Nm	Nanometer
NO	Nitrogen monoxide
O_2	Oxygen
PLN	Phospholamban
PKA	Protein kinase A
PKC	Protein kinase C
PKG	Protein kinase G
PMCA	Sarcommal calcium ATPase
RIC	Remote ischemic conditioning
ROI	Region of interest
ROS	Reactive oxygen species
RyR	Ryanodine receptor
RV	Right ventricle
SERCA2a	Sarco/endoplasmic reticulum calcium ATPase 2a
Ser16	Serin16
SR	Sarcoplasmicreticulum

T1DM	Diabetes mellitus type I
T2DM	Diabetes mellitus type II
Thr17	Threonin17
Tm	Tropomyosin
TnC	Troponin C
TnI	Troponin L
TN Φ	Tumor necrosis factor
TnT	TroponinT

9 List of Figures

Figure 1.1: Schematic representation of the myocyte Ca^{2+} cycle in a ventricular cardiomyocyte..	1
Figure 1.2: PKA signaling pathways in cardiac myocytes.....	2
Figure 1.3: Release of Ca^{2+} from the SR into the cytosol via RyR2.....	6
Figure 1.4: Illustration of SERCA2a and PLN monomer.....	7
Figure 1.5: Representative sarcomere unit, schematic representation.....	9
Figure 1.6: Myofilaments during diastole and systole.....	10
Figure 1.7: The 10 most frequent causes of death in 2019 – WHO.....	12
Figure 1.8: Schematic division of the heart into remote area, peripheral area, and ischemic area.	13
Figure 1.9: The phases of healing in reperfused mouse infarcts (1-h coronary occlusion followed by reperfusion) [75].	19
Figure 1.10: Hypothesized role of Ca^{2+} in ischemic conditioning of cardiomyocytes.	26
Figure 1.11: Model of remote ischemic conditioning.....	27
Figure 2.1: Timeline of myocardial infarction performance.....	30
Figure 2.2: Illustration of the LAD ligation modified after Teramoto et al [130].	32
Figure 2.3: Section of a mouse electrocardiogram (ECG).	33
Figure 2.4: Cannulated heart.	33
Figure 2.5: Fluorescence excitation spectra of Fura-2 at different Ca^{2+} concentrations [133].	37
Figure 2.6: Representative Ca^{2+} transient.....	39
Figure 2.7: Illustration of treatment of cardiomyocytes with plasma dialysates	41
Figure 2.8: Selection of the user-defined region of interest of a cardiomyocyte for the measurement of Ca^{2+} transients and sarcomere function.....	42
Figure 2.9: Representative sarcomere function.....	42
Figure 2.10: Determination of the speed of Ca^{2+} increase.....	43
Figure 2.11: Determination of the speed of Ca^{2+} decrease.....	44
Figure 2.12: Determination of the contraction velocity from the sarcomere function	44
Figure 2.13: Determination of the relaxation velocity from the sarcomere function.....	45
Figure 3.1: Amplitude of Ca^{2+} transients at baseline and after β -adrenergic stimulation of remote cardiomyocytes from db/db and db/+ mice 10 days after ischemia and reperfusion injury (I/R). 52	52
Figure 3.2: Speed of Ca^{2+} increase at baseline and after β -adrenergic stimulation of remote cardiomyocytes from db/db and db/+ mice 10 days after I/R.....	53
Figure 3.3: Speed of Ca^{2+} decrease at baseline and after β -adrenergic stimulation of	54
Figure 3.4: Contractile amplitude at baseline and after β -adrenergic stimulation of sarcomeres from remote cardiomyocytes of db/db and db/+ mice 10 days after I/R.	55
Figure 3.5: Contraction velocity at baseline and after β -adrenergic stimulation of sarcomeres from remote cardiomyocytes of db/db and db/+ mice 10 days after I/R.	56
Figure 3.6: Relaxation velocity at baseline and after β -adrenergic stimulation of sarcomeres from remote cardiomyocytes of db/db and db/+ mice 10 days after I/R.....	56
Figure 3.7: Western blot analyses of the sarco-/endoplasmic Ca^{2+} ATPase 2A (SERCA2A).	58
Figure 3.8: Western blot analyses of phospholamban (PLN).	59
Figure 3.9: Protein expression of S100A1 10 days after I/R.....	59
Figure 3.10: Phosphorylation of PLN monomers at Ser16 and pentamer-to-monomer ratios of PLN.	60
Figure 3.11: Phosphorylation of PLN monomers at Thr17.....	61
Figure 3.12: Western blot analyses of ryanodine receptor 2 (RyR2).....	61
Figure 3.13: Expression and phosphorylation of cTnI at Ser23/24.....	62
Figure 3.14: Metabolic parameters in Diet Induced Obese (DIO) mice.....	63

Figure 3.15: Amplitude of Ca^{2+} transients at baseline and after β -adrenergic stimulation of cardiomyocytes from DIO and control mice.	64
Figure 3.16: Speed of Ca^{2+} increase at baseline and after β -adrenergic stimulation of cardiomyocytes from DIO and control mice.	64
Figure 3.17: Speed of Ca^{2+} decrease at baseline and after β -adrenergic stimulation of cardiomyocytes from DIO and control mice.	65
Figure 3.18: Contractile amplitude of sarcomeres at baseline and after β -adrenergic stimulation of cardiomyocytes from DIO mice compared with control cardiomyocytes.	66
Figure 3.19: Contraction velocity of sarcomeres at baseline and after β -adrenergic stimulation of cardiomyocytes from DIO mice compared with controls.	67
Figure 3.20: Relaxation velocity of sarcomeres at baseline and after β -adrenergic stimulation of cardiomyocytes from DIO mice compared with controls.	67
Figure 3.21: Height of Ca^{2+} transients at baseline and after β -adrenergic stimulation of cardiomyocytes incubated with dialysates of blood samples taken before (pre) and after (post) RIC.	69
Figure 3.22: Speed of Ca^{2+} increase at baseline and after β -adrenergic stimulation of cardiomyocytes incubated with dialysates of blood samples taken before (pre) and after (post) RIC.	69
Figure 3.23: Speed of Ca^{2+} decrease at baseline and after β -adrenergic stimulation of cardiomyocytes incubated with dialysates of blood samples taken before (pre) and after (post) RIC.	70
Figure 3.24: Contractile amplitude at baseline and after β -adrenergic stimulation of cardiomyocytes incubated with dialysates of blood samples taken before (pre) and after (post) RIC.	71
Figure 3.25: Contraction velocity at baseline and after β -adrenergic stimulation of cardiomyocytes incubated with dialysates of blood samples taken before (pre) and after (post) RIC.	71
Figure 3.26: Relaxation velocity at baseline and after β -adrenergic stimulation of cardiomyocytes incubated with dialysates of blood samples taken before (pre) and after (post) RIC.	72
Figure 3.27: Height of Ca^{2+} transients at baseline and after β -adrenergic stimulation of cardiomyocytes after hypoxia and reoxygenation.	73
Figure 3.28: Velocity of Ca^{2+} increase at baseline and after β -adrenergic stimulation of cardiomyocytes after hypoxia and reoxygenation.	73
Figure 3.29: Velocity of Ca^{2+} decrease at baseline and after β -adrenergic stimulation of cardiomyocytes after hypoxia and reoxygenation.	74
Figure 3.30: Contractile amplitude at baseline and after β -adrenergic stimulation of cardiomyocytes after hypoxia and reoxygenation.	75
Figure 3.31: Contraction velocity at baseline and after β -adrenergic stimulation of cardiomyocytes after hypoxia and reoxygenation.	75
Figure 3.32: Relaxation velocity at baseline and after β -adrenergic stimulation of cardiomyocytes after hypoxia and reoxygenation.	76
Figure 3.33: Height of Ca^{2+} transients.	77
Figure 3.34: Velocity of Ca^{2+} increase at baseline and after β -adrenergic stimulation of cardiomyocytes incubated with dialysates of blood samples taken before (pre) and after (post) RIC.	77
Figure 3.35: Velocity of Ca^{2+} decrease of cardiomyocytes incubated with dialysates of blood samples taken before (pre) and after (post) RIC.	78
Figure 3.36: Contractile amplitude of cardiomyocytes incubated with dialysates of blood samples taken before (pre) and after (post) RIC.	79

Figure 3.37: Contraction velocity of cardiomyocytes incubated with dialysates of blood samples taken before (pre) and after (post) RIC.....	79
Figure 3.38: Relaxation velocity of cardiomyocytes incubated with dialysates of blood samples taken before (pre) and after (post) RIC.....	80

10 List of Tables

Table 1: Buffers and solutions used in the measurement on isolated cardiomyocytes (isolation of cardiomyocytes)34

Table 2: Buffers used in protein analysis (preparation of heart lysates)46

Table 3: Buffers and gels used in protein analysis (gel electrophoresis)47

Table 4: Buffers and solutions used in protein analysis (Western blot)49

11 References

- [1] D. M. Bers, "Calcium cycling and signaling in cardiac myocytes," *Annual Review of Physiology*, vol. 70. 2008. doi: 10.1146/annurev.physiol.70.113006.100455.
- [2] C.J. Fearnley, H.L. Roderick, and M.D. Bootman, "Calcium signaling in cardiac myocytes," *Cold Spring Harb Perspect Biol*, vol. 3, 2011, doi: 10.1101/cshperspect.a004242.
- [3] M. Tada, M.A. Kirchberger, and H.C. Li, "Phosphoprotein phosphatase-catalyzed dephosphorylation of the 22,000 dalton phosphoprotein of cardiac sarcoplasmic reticulum," *J Cyclic Nucleotide Res*, vol. 1, no. 5, pp. 329–338, 1975, PMID: 178694.
- [4] E. G. Kranias, "Regulation of calcium transport by protein phosphatase activity associated with cardiac sarcoplasmic reticulum," *Journal of Biological Chemistry*, vol. 260, no. 20, 1985, doi: 10.1016/s0021-9258(17)39139-1.
- [5] A. D. Wegener, H. K. B. Simmerman, J. Liepnieks, and L. R. Jones, "Proteolytic cleavage of phospholamban purified from canine cardiac sarcoplasmic reticulum vesicles. Generation of a low resolution model of phospholamban structure," *Journal of Biological Chemistry*, vol. 261, no. 11, 1986, doi: 10.1016/s0021-9258(19)89227-x.
- [6] J. H. Connor, H. Quan, C. Oliver, and S. Shenolikar, "Inhibitor-1, a regulator of protein phosphatase 1 function," *Protein phosphatase protocols*, vol. 93, pp. 41–58, 1998, doi: 10.1385/0-89603-468-2:41.
- [7] J. Heijman, M. Dewenter, A. El-Armouche, and D. Dobrev, "Function and regulation of serine/threonine phosphatases in the healthy and diseased heart," *Journal of Molecular and Cellular Cardiology*, vol. 64. 2013. doi: 10.1016/j.yjmcc.2013.09.006.
- [8] J. S. K. Sham, L. Cleemann, and M. Morad, "Functional coupling of Ca²⁺ channels and ryanodine receptors in cardiac myocytes," *Proc Natl Acad Sci U S A*, vol. 92, no. 1, 1995, doi: 10.1073/pnas.92.1.121.
- [9] M. B. Cannell and C. Soeller, "Numerical analysis of ryanodine receptor activation by L-type channel activity in the cardiac muscle diad," *Biophys J*, vol. 73, no. 1, 1997, doi: 10.1016/S0006-3495(97)78052-4.
- [10] D. J. Duncker, C. L. Klassen, Y. Ishibashi, S. H. Herrlinger, T. J. Pavek, and R. J. Bache, "Effect of temperature on myocardial infarction in swine," *Am J Physiol Heart Circ Physiol*, vol. 270, no. 4 39-4, 1996, doi: 10.1152/ajpheart.1996.270.4.h1189.
- [11] D. M. Bers, "Calcium fluxes involved in control of cardiac myocyte contraction," *Circulation Research*, vol. 87, no. 4. 2000. doi: 10.1161/01.RES.87.4.275.
- [12] J. W. Bassani, R. A. Bassani, and D. M. Bers, "Relaxation in rabbit and rat cardiac cells: species-dependent differences in cellular mechanisms.," *J Physiol*, vol. 476, no. 2, 1994, doi: 10.1113/jphysiol.1994.sp020130.
- [13] T. R. Shannon and D.M. Bers, "Integrated Ca²⁺ management in cardiac myocytes," *Ann N Y Acad Sci*, vol. 1015, pp. 28–38, 2004, doi: 10.1196/annals.1302.003.
- [14] T. Guo, R. L. Cornea, S. Huke, E. Camors, Y. Yang, and E. Picht, "Kinetics of FKBP12.6 binding to ryanodine receptors in permeabilized cardiac myocytes and effects on Ca sparks," *Circ Res*, vol. 106, no. 11, pp. 1743–1752, 2010, doi: 10.1161/CIRCRESAHA.110.219816.
- [15] Y. F. Xiao *et al.*, "FKBP12.6 protects heart from AngII-induced hypertrophy through inhibiting Ca²⁺/calmodulin-mediated signalling pathways in vivo and in vitro," *J Cell Mol Med*, vol. 22, no. 7, 2018, doi: 10.1111/jcmm.13645.
- [16] Y. T. Zhao *et al.*, "Sensitized signalling between L-type Ca²⁺channels and ryanodine receptors in the absence or inhibition of FKBP12.6 in cardiomyocytes," *Cardiovasc Res*, vol. 113, no. 3, 2017, doi: 10.1093/cvr/cvw247.
- [17] M. E. Anderson, "Calmodulin kinase signaling in heart: An intriguing candidate target for therapy of myocardial dysfunction and arrhythmias," *Pharmacology and Therapeutics*, vol. 106, no. 1. 2005. doi: 10.1016/j.pharmthera.2004.11.002.
- [18] E. G. Kranias and R. J. Hajjar, "Modulation of cardiac contractility by the phospholamban/SERCA2a regulatome," *Circ Res*, vol. 110, no. 12, 2012, doi: 10.1161/CIRCRESAHA.111.259754.

- [19] Y. Kimura, K. Kurzydowski, M. Tada, and D. H. MacLennan, "Phospholamban inhibitory function is activated by depolymerization," *Journal of Biological Chemistry*, vol. 272, no. 24, 1997, doi: 10.1074/jbc.272.24.15061.
- [20] A. D. Wegener and L. R. Jones, "Phosphorylation-induced mobility shift in phospholamban in sodium dodecyl sulfate-polyacrylamide gels. Evidence for a protein structure consisting of multiple identical phosphorylatable subunits," *Journal of Biological Chemistry*, vol. 259, no. 3, 1984, doi: 10.1016/s0021-9258(17)43484-3.
- [21] M. Tada, M. Inui, M. Yamada, M. Kadoma, T. Kuzuya, H. Abe, S. Kakiuchi "Effects of phospholamban phosphorylation catalyzed by adenosine 3':5'-monophosphate- and calmodulin-dependent protein kinases on calcium transport ATPase of cardiac sarcoplasmic reticulum," *J Mol Cell Cardiol*, vol. 15, no. 5, 1983, doi: 10.1016/0022-2828(83)91345-7.
- [22] R. E. Klabunde, "Cardiac Myocytes and Sarcomeres." Accessed: Nov. 05, 2022. [Online]. Available: <https://cvphysiology.com/intro>
- [23] A. Wesley Burks, 4 - *Tropomyosin; Structure and Functions of Contractile Proteins*. Academic Press, 1966. doi: 10.1016/B978-1-4832-2912-6.50011-2.
- [24] L. M. Biga *et al.*, *Anatomy & Physiology*, 1st ed. OpenStax/Oregon State University, 2020.
- [25] S. Labeit, B. Kolmerer, and W. A. Linke, "The giant protein titin: Emerging roles in physiology and pathophysiology," *Circulation Research*, vol. 80, no. 2. 1997. doi: 10.1161/01.RES.80.2.290.
- [26] Eric H. Lee, "The Chain-like Elasticity of Titin." Accessed: Dec. 11, 2022. [Online]. Available: <https://www.ks.uiuc.edu/Research/z1z2/#:~:text=The%20soft%20elasticity%20of%20titin%20is%20also%20due%20to%20a,straight%20shape%20when%20under%20tension.>
- [27] M. Itoh-Satoh *et al.*, "Titin mutations as the molecular basis for dilated cardiomyopathy," *Biochem Biophys Res Commun*, vol. 291, no. 2, pp. 385–393, 2002, doi: 10.1006/bbrc.2002.6448.
- [28] J. G. Betts *et al.*, *Anatomy & Physiology 2e*. OpenStax, Rice University, Houston, Texas, 2020.
- [29] A. V. Gomes, J. D. Potter, and D. Szczesna-Cordary, "The role of troponins in muscle contraction," *IUBMB Life*, vol. 54, no. 6. 2002. doi: 10.1080/15216540216037.
- [30] M. Kumar, E. R. Kasala, L. N. Bodduluru, V. Dahiya, D. Sharma, V. Kumar, and M. Lahkar. "Animal models of myocardial infarction: Mainstay in clinical translation," *Regulatory Toxicology and Pharmacology*, vol. 76, 2016, doi: 10.1016/j.yrtph.2016.03.005.
- [31] C. Weber and H. Noels, "Atherosclerosis: Current pathogenesis and therapeutic options," *Nature Medicine*, vol. 17, no. 11. 2011. doi: 10.1038/nm.2538.
- [32] Institute of Medicine (US). Committee on Social Security Cardiovascular Disability Criteria, *Cardiovascular Disability: Updating the Social Security Listings*. National Academies Press, 2010. doi: 10.17226/12940.
- [33] O. J. Mechanic, M. Gavin, and S. A. Grossman., *Acute Myocardial Infarction*. StatPearls [Internet]. Treasure Island (FL): StatPearls Publishing 2023 Jan, 2022.
- [34] A. E. Moran, M. H. Forouzanfar, G. A. Roth, G. A. Mensah, M. Ezzati, A. Flaxman, C. JL Murray, and M. Naghavi, "The global burden of ischemic heart disease in 1990 and 2010: The global burden of disease 2010 study," *Circulation*, vol. 129, no. 14. 2014. doi: 10.1161/CIRCULATIONAHA.113.004046.
- [35] World Health Organization, "Top 10 causes of death" Accessed: Jan. 22, 2023. [Online]. Available: <https://www.who.int/news-room/fact-sheets/detail/the-top-10-causes-of-death>
- [36] F. Altamirano, Z. V. Wang, and J. A. Hill, "Cardioprotection in ischaemia-reperfusion injury: Novel mechanisms and clinical translation," *Journal of Physiology*, vol. 593, no. 17. 2015. doi: 10.1113/JP270953.
- [37] P. Liu, C. E. Hock, R. Nagele, and P. Y. K. Wong, "Formation of nitric oxide, superoxide, and peroxynitrite in myocardial ischemia-reperfusion injury in rats," *Am*

- J Physiol Heart Circ Physiol*, vol. 272, no. 5 41-5, 1997, doi: 10.1152/ajpheart.1997.272.5.h2327.
- [38] R. Bolli, M. O. Jeroudi, B. S. Patel, C. M. DuBose, E. K. Lai, R. Roberts, and P. B. McCay, "Direct evidence that oxygen-derived free radicals contribute to postischemic myocardial dysfunction in the intact dog," *Proceedings of the National Academy of Sciences*, vol. 86, no. 12, pp. 4695–4699, 1989, doi: 10.1073/pnas.86.12.4695.
- [39] H. M. Piper and D. García-Dorado, "Prime causes of rapid cardiomyocyte death during reperfusion," in *Annals of Thoracic Surgery*, vol. 272, no. 5, 1999. doi: 10.1016/S0003-4975(99)01025-5.
- [40] G. Heusch, "Cardioprotection: Chances and challenges of its translation to the clinic," *The Lancet*, vol. 381, no. 9861. 2013. doi: 10.1016/S0140-6736(12)60916-7.
- [41] T. Kalogeris, C. P. Baines, M. Krenz, and R. J. Korthuis, "Ischemia/Reperfusion," *Compr Physiol*, vol. 7, no. 1, 2016, doi: 10.1002/cphy.c160006.
- [42] P. Cowled, and R. Fitridge. "Pathophysiology of reperfusion injury." In: Fitridge, R. (eds) *Mechanisms of Vascular Disease*. Springer, Cham., pp. 415-440, 2020, https://doi.org/10.1007/978-3-030-43683-4_18
- [43] H. L. Wyatt, J. S. Forrester, P. L. da Luz, G. A. Diamond, R. Chagrasulis and H. J. C. Swan, "Functional abnormalities in nonoccluded regions of myocardium after experimental coronary occlusion," *Am J Cardiol*, vol. 37, no. 3, 1976, doi: 10.1016/0002-9149(76)90285-X.
- [44] P. R. Maroko, P. Libby, W. R. Ginks, C. M. Bloor, W. E. Shell, B. E. Sobel and Jr Ross., "Coronary Artery Reperfusion," *Journal of Clinical Investigation*, vol. 51, no. 10, 1972, doi: 10.1172/jci107090.
- [45] Z. Kocak *et al.*, "Modulation of oxidative–nitrosative stress and inflammatory response by rapamycin in target and distant organs in rats exposed to hindlimb ischemia–reperfusion: The role of mammalian target of rapamycin," *Can J Physiol Pharmacol*, vol. 97, no. 12, 2019, doi: 10.1139/cjpp-2019-0394.
- [46] B. A. French and C.M. Kramer, "Mechanisms of Post-Infarct Left Ventricular Remodeling. ," *Drug Discov Today Dis Mech*, vol. 4, no. 3, pp. 185–196, 2007, doi: 10.1016/j.ddmec.2007.12.006.
- [47] S. Frantz and M. Nahrendorf, "Cardiac macrophages and their role in ischaemic heart disease," *Cardiovascular Research*, vol. 102, no. 2. 2014. doi: 10.1093/cvr/cvu025.
- [48] W. W. Lee *et al.*, "PET/MRI of inflammation in myocardial infarction," *J Am Coll Cardiol*, vol. 59, no. 2, 2012, doi: 10.1016/j.jacc.2011.08.066.
- [49] C. A. Beltrami *et al.*, "Structural basis of end-stage failure in ischemic cardiomyopathy in humans," *Circulation*, vol. 89, no. 1, 1994, doi: 10.1161/01.CIR.89.1.151.
- [50] N. Ruparelía, J. E. Digby, A. Jefferson, D. J. Medway, S. Neubauer, C. A. Lygate, and R. P. Choudhury, "Myocardial infarction causes inflammation and leukocyte recruitment at remote sites in the myocardium and in the renal glomerulus," *Inflammation Research*, vol. 62, no. 5, 2013, doi: 10.1007/s00011-013-0605-4.
- [51] D. Carrick *et al.*, "Pathophysiology of LV Remodeling in Survivors of STEMI Inflammation, Remote Myocardium, and Prognosis," *JACC Cardiovasc Imaging*, vol. 8, no. 7, 2015, doi: 10.1016/j.jcmg.2015.03.007.
- [52] J. Carberry *et al.*, "Remote Zone Extracellular Volume and Left Ventricular Remodeling in Survivors of ST-Elevation Myocardial Infarction," *Hypertension*, vol. 68, no. 2, 2016, doi: 10.1161/HYPERTENSIONAHA.116.07222.
- [53] E. Murphy and C. Steenbergen, "Mechanisms underlying acute protection from cardiac ischemia-reperfusion injury," *Physiological Reviews*, vol. 88, no. 2. 2008. doi: 10.1152/physrev.00024.2007.
- [54] M. S. Mozaffari, J. Y. Liu, W. Abebe, and B. Baban, "Mechanisms of load dependency of myocardial ischemia reperfusion injury.," *Am J Cardiovasc Dis*, vol. 3, no. 4, 2013, PMID: 24224132; PMCID: PMC3819580.
- [55] S. M. Krause and D. Rozanski, "Effects of an increase in intracellular free [Mg²⁺] after myocardial stunning on sarcoplasmic reticulum Ca²⁺ transport," *Circulation*, vol. 84, no. 3, 1991, doi: 10.1161/01.CIR.84.3.1378.

- [56] S. Krause and M. L. Hess, "Characterization of cardiac sarcoplasmic reticulum dysfunction during short-term, normothermic, global ischemia," *Circ Res*, vol. 55, no. 2, 1984, doi: 10.1161/01.RES.55.2.176.
- [57] J. W. T. Fiolet and A. Baartscheer, "Cellular calcium homeostasis during ischemia; a thermodynamic approach," *Cardiovascular Research*, vol. 45, no. 1, 2000. doi: 10.1016/S0008-6363(99)00294-1.
- [58] G. W. Dorn and C. Maack, "SR and mitochondria: Calcium cross-talk between kissing cousins," *Journal of Molecular and Cellular Cardiology*, vol. 55, no. 1, 2013. doi: 10.1016/j.yjmcc.2012.07.015.
- [59] R. Zucchi *et al.*, "Sarcoplasmic reticulum calcium uptake in human myocardium subjected to ischemia and reperfusion during cardiac surgery," *J Mol Cell Cardiol*, vol. 28, no. 8, 1996, doi: 10.1006/jmcc.1996.0159.
- [60] R. Zucchi, S. Ronca-Testoni, G. Yu, P. Galbani, G. Ronca, and M. Mariani, "Postischemic changes in cardiac sarcoplasmic reticulum Ca²⁺ channels: A possible mechanism of ischemic preconditioning," *Circ Res*, vol. 76, no. 6, 1995, doi: 10.1161/01.RES.76.6.1049.
- [61] G. B. Luciani, A. D. Agnola, A. Mazzucco, V. Gallucci, and G. Salvati, "Effects of ischemia on sarcoplasmic reticulum and contractile myofilament activity in human myocardium," *Am J Physiol Heart Circ Physiol*, vol. 265, no. 4 34-4, 1993, doi: 10.1152/ajpheart.1993.265.4.h1334.
- [62] S. Chen and S. Li, "The Na⁺/Ca²⁺ exchanger in cardiac ischemia/reperfusion injury," *Med Sci Monit*, vol. 18, no. 11, 2012, doi: 10.12659/msm.883533.
- [63] A. Kronenbitter *et al.*, "Impaired Ca²⁺ cycling of nonischemic myocytes contributes to sarcomere dysfunction early after myocardial infarction," *J Mol Cell Cardiol*, vol. 119, 2018, doi: 10.1016/j.yjmcc.2018.04.004.
- [64] R. Ventura-Clapier and V. Veksler, "Myocardial ischemic contracture: Metabolites affect rigor tension development and stiffness," *Circ Res*, vol. 74, no. 5, 1994, doi: 10.1161/01.RES.74.5.920.
- [65] Y. V. Ladilov, B. Siegmund, and H. M. Piper, "Protection of reoxygenated cardiomyocytes against hypercontracture by inhibition of Na⁺/H⁺ exchange," *Am J Physiol Heart Circ Physiol*, vol. 268, no. 4 37-4, 1995, doi: 10.1152/ajpheart.1995.268.4.h1531.
- [66] B. Siegmund, R. Zude, and H. M. Piper, "Recovery of anoxic-reoxygenated cardiomyocytes from severe Ca²⁺ overload," *Am J Physiol Heart Circ Physiol*, vol. 263, no. 4 32-4, 1992, doi: 10.1152/ajpheart.1992.263.4.h1262.
- [67] D. Garcia-Dorado, J. Inserte, M. Ruiz-Meana, M. A. González, J. Solares, M. Juliá, J. A. Barrabés and J. Soler-Soler, "Gap junction uncoupler heptanol prevents cell-to-cell progression of hypercontracture and limits necrosis during myocardial reperfusion," *Circulation*, vol. 96, no. 10, 1997, doi: 10.1161/01.CIR.96.10.3579.
- [68] Z. Zhang, B. J. Biesiadecki, and J. P. Jin, "Selective deletion of the NH₂-terminal variable region of cardiac troponin T in ischemia reperfusion by myofibril-associated μ -calpain cleavage," *Biochemistry*, vol. 45, no. 38, 2006, doi: 10.1021/bi060273s.
- [69] S. Kötter *et al.*, "Titin-Based Cardiac Myocyte Stiffening Contributes to Early Adaptive Ventricular Remodeling after Myocardial Infarction," *Circ Res*, vol. 119, no. 9, 2016, doi: 10.1161/CIRCRESAHA.116.309685.
- [70] C. M. Kramer, W. J. Rogers, T. M. Theobald, T. P. Power, S. Petruolo, and N. Reichek, "Remote noninfarcted region dysfunction soon after first anterior myocardial infarction: A magnetic resonance tagging study," *Circulation*, vol. 94, no. 4, 1996, doi: 10.1161/01.CIR.94.4.660.
- [71] R. B. Stamm, R. S. Gibson, H. L. Bishop, B. A. Carabello, G. A. Beller, and R. P. Martin, "Echocardiographic detection of infarct-localized asynergy and remote asynergy during acute myocardial infarction: Correlation with the extent of angiographic coronary disease," *Circulation*, vol. 67, no. 1, 1983, doi: 10.1161/01.CIR.67.1.233.
- [72] J. J. Pilla *et al.*, "Early postinfarction ventricular restraint improves borderzone wall thickening dynamics during remodeling," *Annals of Thoracic Surgery*, vol. 80, no. 6, 2005, doi: 10.1016/j.athoracsur.2005.05.089.

- [73] B. M. Jackson, J. H. Gorman III, I. S. Salgo, S. L. Moainie, T. Plappert, M. St. John-Sutton, L. H. Edmunds Jr, and R. C. Gorman, "Border zone geometry increases wall stress after myocardial infarction: Contrast echocardiographic assessment," *Am J Physiol Heart Circ Physiol*, vol. 284, no. 2 53-2, 2003, doi: 10.1152/ajpheart.00360.2002.
- [74] B. M. Jackson, M. P. Landi, J. H. Gorman III, Y. Enomoto, H. Sakamoto, T. Plappert, M. G. St. John Sutton, I. Salgo, and R. C. Gorman, "Borderzone geometry after acute myocardial infarction: A three-dimensional contrast enhanced echocardiographic study," *Annals of Thoracic Surgery*, vol. 80, no. 6, 2005, doi: 10.1016/j.athoracsur.2005.05.103.
- [75] N. G. Frangogiannis, "The mechanistic basis of infarct healing," *Antioxidants and Redox Signaling*, vol. 8, no. 11–12, 2006. doi: 10.1089/ars.2006.8.1907.
- [76] C. P. Baines, "How and when do myocytes die during ischemia and reperfusion: The late phase," in *Journal of Cardiovascular Pharmacology and Therapeutics*, vol. 284, no. 3-4, 2011. doi: 10.1177/1074248411407769.
- [77] J. P. M. Cleutjens, J. C. Kandala, E. Guarda, R. V. Guntaka, and K. T. Weber, "Regulation of collagen degradation in the rat myocardium after infarction," *J Mol Cell Cardiol*, vol. 27, no. 6, 1995, doi: 10.1016/S0022-2828(05)82390-9.
- [78] G. Olivetti, J. M. Capasso, L. G. Meggs, E. H. Sonnenblick, and P. Anversa, "Cellular basis of chronic ventricular remodeling after myocardial infarction in rats," *Circ Res*, vol. 68, no. 3, 1991, doi: 10.1161/01.RES.68.3.856.
- [79] R. Klocke, W. Tian, M. T. Kuhlmann, and S. Nikol, "Surgical animal models of heart failure related to coronary heart disease," *Cardiovascular Research*, vol. 74, no. 1, 2007. doi: 10.1016/j.cardiores.2006.11.026.
- [80] T. O. Nossuli, V. Lakshminarayanan, G. Baumgarten, G. E. Taffet, C. M. Ballantyne, L. H. Michael, and M. L. am Entman, "A chronic mouse model of myocardial ischemia-reperfusion: Essential in cytokine studies," *Am J Physiol Heart Circ Physiol*, vol. 278, no. 4 47-4, 2000, doi: 10.1152/ajpheart.2000.278.4.h1049.
- [81] R. M. Jacoby and R. W. Nesto, "Acute myocardial infarction in the diabetic patient: pathophysiology, clinical course and prognosis," *J Am Coll Cardiol*, vol. 20, no. 3, pp. 736–744, 1992, doi: 10.1016/0735-1097(92)90033-j.
- [82] S. V. Arnold *et al.*, "Clinical Management of Stable Coronary Artery Disease in Patients with Type 2 Diabetes Mellitus: A Scientific Statement from the American Heart Association," *Circulation*, vol. 141, no. 19, 2020. doi: 10.1161/CIR.0000000000000766.
- [83] J. Cui; Y. Liu; Y. Li; F. Xu; Y. Liu, "Type 2 Diabetes and Myocardial Infarction: Recent Clinical Evidence and Perspective," *Front Cardiovasc Med*, vol. 8, 2021, doi: 10.3389/fcvm.2021.644189.
- [84] Deutsche Diabetes Gesellschaft (DDG) und diabetesDE – Deutsche Diabetes-Hilfe "Deutscher Gesundheitsbericht Diabetes 2017," Kirchheim + Co GmbH, Mainz, 2017. Available: https://www.diabetesde.org/system/files/documents/gesundheitsbericht_2017.pdf.
- [85] Y. Du, C. Heidemann, A. Göwald, P. Schmich, and C. Scheidt-Nave, "Prevalence and comorbidity of diabetes mellitus among non-institutionalized older adults in Germany - Results of the national telephone health interview survey German Health Update (GEDA) 2009," *BMC Public Health*, vol. 13, no. 1, 2013, doi: 10.1186/1471-2458-13-166.
- [86] D. Aguilar *et al.*, "Newly diagnosed and previously known diabetes mellitus and 1-year outcomes of acute myocardial infarction: The Valsartan in acute myocardial infarction (VALIANT) trial," *Circulation*, vol. 110, no. 12, 2004, doi: 10.1161/01.CIR.0000142047.28024.F2.
- [87] R. J. Stevens, R. L. Coleman, A. I. Adler, I. M. Stratton, D. R. Matthews, and R. R. Holman, "Risk Factors for Myocardial Infarction Case Fatality and Stroke Case Fatality in Type 2 Diabetes: UKPDS 66," *Diabetes Care*, vol. 27, no. 1, 2004, doi: 10.2337/diacare.27.1.201.
- [88] R. D. Abbott, R. P. Donahue, W. B. Kannel, and P. W. F. Wilson, "The Impact of Diabetes on Survival Following Myocardial Infarction in Men vs Women: The

- Framingham Study," *JAMA: The Journal of the American Medical Association*, vol. 260, no. 23, 1988, doi: 10.1001/jama.1988.03410230074031.
- [89] D. D. Belke, E. A. Swanson, and W. H. Dillmann, "Decreased sarcoplasmic reticulum activity and contractility in diabetic db/db mouse heart," *Diabetes*, vol. 53, no. 12, 2004, doi: 10.2337/diabetes.53.12.3201.
- [90] Falcao-Pires I; Hamdani N; Borbely A; Gavina C; Schalkwijk CG; van der Velden J; van Heerebeek L; Stienen GJ; Niessen HW; Leite-Moreira AF; Paulus JW, "Diabetes mellitus worsens diastolic left ventricular dysfunction in aortic stenosis through altered myocardial structure and cardiomyocyte stiffness." *Circulation*, vol. 124, no. 10, pp.1151-1159, 2011, doi: 10.1161/CIRCULATIONAHA.111.025270.
- [91] D. D. Belke, E. A. Swanson, and W. H. Dillmann. "Decreased sarcoplasmic reticulum activity and contractility in diabetic db/db mouse heart." *Diabetes*, vol. 53, no. 12, pp. 3201-3208, 2004, doi: 10.2337/diabetes.53.12.3201.
- [92] A. Norman and H. Henry, *Hormones*, 3rd ed., Academic Press (London, Oxford, Boston, New York, San Diego), 2014.
- [93] W. T. Cefalu, "Animal models of type 2 diabetes: Clinical presentation and pathophysiological relevance to the human condition," *ILAR J*, vol. 47, no. 3, 2006, doi: 10.1093/ilar.47.3.186.
- [94] "Type 2 diabetes - Symptoms and Causes." Accessed: Jul. 01, 2022. [Online]. Available: <https://www.mayoclinic.org/diseases-conditions/type-2-diabetes/symptoms-causes/syc-20351193>
- [95] M. Jackerott, A. Møldrup, P. Thams, E. D. Galsgaard, J. Knudsen, Y. C. Lee, and J. H. Nielsen, "STAT5 activity in pancreatic beta-cells influences the severity of diabetes in animal models of type 1 and 2 diabetes," *Diabetes*, vol. 55, no. 10, pp. 2705–2712, 2006, doi: 10.2337/db06-0244.
- [96] B. Goffrier, M. Schulz, and J. B. Feigenbaum, "Administrative prevalences and incidences of diabetes mellitus from 2009 to 2015," *Versorgungsatlas*, vol. 17, no. 3, 2017, doi: 10.20364/VA-17.03.
- [97] International Diabetes Federation., *IDF Diabetes Atlas*, 9th ed. 2019. Accessed: Jan. 26, 2023. [Online]. Available: www.diabetesatlas.org.
- [98] World Health Organization, "Screening for type 2 diabetes : report of a World Health Organization and International Diabetes Federation meeting," No. *WHO/NMH/MNC/CRA/03.1*, 2003.
- [99] K. Szabadfi, E. Pinter, D. Reglodi, and R. Gabriel, "Neuropeptides, trophic factors, and other substances providing morphofunctional and metabolic protection in experimental models of diabetic retinopathy," *Int Rev Cell Mol Biol*, vol. 311, pp. 1–121, 2014, doi: 10.1016/B978-0-12-800179-0.00001-5.
- [100] C. E. Alpers and L. H. Kelly, "Mouse models of diabetic nephropathy," *Curr Opin Nephrol Hypertens*, vol. 20, no. 3, 2011, doi: 10.1097/MNH.0b013e3283451901.
- [101] K. Kobayashi, T. M. Forte, S. Taniguchi, B. Y. Ishida, K. Oka, and L. Chan, "The db/db mouse, a model for diabetic dyslipidemia: Molecular characterization and effects of western diet feeding," *Metabolism*, vol. 49, no. 1, 2000, doi: 10.1016/S0026-0495(00)90588-2.
- [102] J. F. Peden and M. Farrall, "Thirty-five common variants for coronary artery: Disease: The fruits of much collaborative labour," *Hum Mol Genet*, vol. 20, no. R2, 2011, doi: 10.1093/hmg/ddr384.
- [103] M. E. Piché, P. Poirier, I. Lemieux, and J. P. Després, "Overview of Epidemiology and Contribution of Obesity and Body Fat Distribution to Cardiovascular Disease: An Update," *Progress in Cardiovascular Diseases*, vol. 61, no. 2. 2018. doi: 10.1016/j.pcad.2018.06.004.
- [104] A. B. Zhai and H. Haddad, "The impact of obesity on heart failure," *Current Opinion in Cardiology*, vol. 32, no. 2. 2017. doi: 10.1097/HCO.0000000000000370.
- [105] H. M. Dashti, T. C. Mathew, M. Khadada, M. Al-Mousawi, H. Talib, S. K. Asfar, A. I. Behbahani, and N. S. Al-Zaid, "Beneficial effects of ketogenic diet in obese diabetic subjects," *Mol Cell Biochem*, vol. 302, pp. 249–256, 2007, doi: 10.1007/s11010-007-9448-z.

- [106] S. D. H. Malnick and H. Knobler, "The medical complications of obesity," *Journal of the Association of Physicians*, vol. 99, no. 9, pp. 565–579, 2006, doi: /10.1093/qjmed/hcl085.
- [107] C. X. Fang, F. Dong, D. P. Thomas, H. Ma, L. He, and J. Ren, "Hypertrophic cardiomyopathy in high-fat diet-induced obesity: role of suppression of forkhead transcription factor and atrophy gene transcription," *American Journal of Physiology-Heart and Circulatory Physiology*, vol. 293, no. 5, pp. 1206–1215, 2008, doi: 10.1152/ajpheart.00319.2008.
- [108] D. M. Bers, "Cardiac excitation-contraction coupling," *Nature*, vol. 415, no. 6868, pp. 198–205, 2002, doi: 10.1038/415198a.
- [109] G. V. Halade, Y. Jin, and M. L. Lindsey, "Roles of saturated vs. polyunsaturated fat in heart failure survival: not all fats are created equal.," *Cardiovasc Res*, vol. 93, no. 1, pp. 4–5, 2012, doi: 10.1093/cvr/cvr298.
- [110] K. M. Jeckel, K. E. Miller, A. J. Chicco, P. L. Chapman, C. M. Mulligan, P. H. Falcone, M. L. Miller, M. J. Pagliassotti, and M. A. Frye, "The role of dietary fatty acids in predicting myocardial structure in fat-fed rats.," *Lipids Health Dis*, vol. 10, no. 1, pp. 1–11, 2011, doi: 10.1186/1476-511X-10-92.
- [111] A. P. L. Leopoldo *et al.*, "Long-term obesity promotes alterations in diastolic function induced by reduction of phospholamban phosphorylation at serine-16 without affecting calcium handling.," *J Appl Physiol*, vol. 117, no. 6, pp. 669–678, 2014, doi: 10.1152/japplphysiol.00088.2014.
- [112] Y. Cheng; W. Li; T. A. McElfresh; X. Chen; J. M. Berthiaume; L. Castel; X. Yu; D. R. Van Wagoner; M. P. Chandler, "Changes in myofilament proteins, but not Ca²⁺ regulation, are associated with a high-fat diet-induced improvement in contractile function in heart failure.," *American Journal of Physiology-Heart and Circulatory Physiology*, vol. 301, no. 4, pp. 1438–1446, 2011, doi: 10.1152/ajpheart.00440.2011.
- [113] K. M. Mellor, J. R. Bell, M. J. Young, R. H. Ritchie, and L. M. D. Delbridge, "Myocardial autophagy activation and suppressed survival signaling is associated with insulin resistance in fructose-fed mice," *J Mol Cell Cardiol*, vol. 50, no. 6, 2011, doi: 10.1016/j.yjmcc.2011.03.002.
- [114] D. Catalucci *et al.*, "Akt increases sarcoplasmic reticulum Ca²⁺ cycling by direct phosphorylation of phospholamban at Thr17," *Journal of Biological Chemistry*, vol. 284, no. 41, 2009, doi: 10.1074/jbc.M109.036566.
- [115] S. Rastogi, E. Sentex, V. Elimban, N. S. Dhalla, and T. Netticadan, "Elevated levels of protein phosphatase 1 and phosphatase 2A may contribute to cardiac dysfunction in diabetes," *Biochim Biophys Acta Mol Basis Dis*, vol. 1638, no. 3, 2003, doi: 10.1016/S0925-4439(03)00092-9.
- [116] C. E. Murry, R. B. Jennings, and K. A. Reimer, "Preconditioning with ischemia: a delay of lethal cell injury in ischemic myocardium," *Circulation*, vol. 74, no. 5, pp. 1124–1136, 1986, doi: 10.1161/01.cir.74.5.1124.
- [117] E. Braunwald, "Cardiovascular science: opportunities for translating research into improved care," *J Clin Invest*, vol. 123, no. 1, pp. 6–10, 2013, doi: 10.1172/JCI67541.
- [118] X. L. Tang, H. Sato, S. Tiwari, B. Dawn, Q. Bi, Q. Li, G. Shirk, and R. Bolli, "Cardioprotection by postconditioning in conscious rats is limited to coronary occlusions <45 min," *Am J Physiol Heart Circ Physiol*, vol. 291, no. 5, 2006, doi: 10.1152/ajpheart.00479.2006.
- [119] S. Baig, B. Moyle, K. V. S. Nair, J. Redgrave, and A. Majid, "Remote ischaemic conditioning for stroke: unanswered questions and future directions," *Stroke Vasc Neurol*, vol. 6, no. 2, pp. 298–309, 2021, doi: 10.1136/svn-2020-000722.
- [120] A. Heinen *et al.*, "The release of cardioprotective humoral factors after remote ischemic preconditioning in humans is age- and sex-dependent," *J Transl Med*, vol. 16, no. 1, 2018, doi: 10.1186/s12967-018-1480-0.
- [121] R. V. Jensen, N. B. Støttrup, S. B. Kristiansen, and H. E. Bøtker, "Release of a humoral circulating cardioprotective factor by remote ischemic preconditioning is dependent on preserved neural pathways in diabetic patients," *Basic Res Cardiol*, vol. 107, no. 5, 2012, doi: 10.1007/s00395-012-0285-1.

- [122] K. D. Hougaard *et al.*, "Remote ischemic preconditioning as an adjunct therapy to thrombolysis in patients with acute ischemic stroke: A randomized trial," *Stroke*, vol. 45, no. 1, 2014, doi: 10.1161/STROKEAHA.113.001346.
- [123] D. J. Hausenloy and D. M. Yellon, "The therapeutic potential of ischemic conditioning: an update," *Nat Rev Cardiol*, vol. 8, no. 11, pp. 619–629, 2011, doi: 10.1038/nrcardio.2011.85.
- [124] M. Totzeck, U. B. Hendgen-Cotta, B. A. French, and T. Rassaf, "A practical approach to remote ischemic preconditioning and ischemic preconditioning against myocardial ischemia/reperfusion injury," *J Biol Methods*, vol. 3, no. 4, 2016, doi: 10.14440/jbm.2016.149.
- [125] D. J. Hausenloy *et al.*, "Translating novel strategies for cardioprotection: The Hatter Workshop Recommendations," *Basic Research in Cardiology*, vol. 105, no. 6, 2010, doi: 10.1007/s00395-010-0121-4.
- [126] C. S. Carr, R. J. Hill, H. Masamune, S. P. Kennedy, D. R. Knight, W. R. Tracey, and D. M. Yellon, "Evidence for a role for both the adenosine A1 and A3 receptors in protection of isolated human atrial muscle against simulated ischaemia," *Cardiovasc Res*, vol. 36, no. 1, 1997, doi: 10.1016/S0008-6363(97)00160-0.
- [127] M. Abu-Amara, S. Y. Yang, A. Quaglia, P. Rowley, B. Fuller, A. Seifalian, and B. Davidson, "Role of endothelial nitric oxide synthase in remote ischemic preconditioning of the mouse liver," *Liver Transplantation*, vol. 17, no. 5, pp. 610–619, 2011, doi: 10.1002/lt.22272.
- [128] S. L. Page, T. B. Angoulvant, D. Angoulvant, and F. Prunier, "Remote ischemic conditioning and cardioprotection: a systematic review and meta-analysis of randomized clinical trials," *Basic Res Cardiol*, vol. 110, no. 2, pp. 1–17, 2015, doi: 10.1007/s00395-015-0467-8.
- [129] S. Y. Tsibulnikov, L. N. Maslov, A. S. Gorbunov, N. S. Voronkov, A. A. Boshchenko, S. V. Popov, E. S. Prokudina, N. Singh, and J. M. Downey, "A Review of Humoral Factors in Remote Preconditioning of the Heart," *Journal of Cardiovascular Pharmacology and Therapeutics*, vol. 24, no. 5, 2019, doi: 10.1177/1074248419841632.
- [130] N. Teramoto *et al.*, "Experimental pig model of old myocardial infarction with long survival leading to chronic left ventricular dysfunction and remodeling as evaluated by PET," *Journal of Nuclear Medicine*, vol. 52, no. 5, 2011, doi: 10.2967/jnumed.110.084848.
- [131] R. Y. Tsien, T. J. Rink, and M. Poenie, "Measurement of cytosolic free Ca^{2+} in individual small cells using fluorescence microscopy with dual excitation wavelengths," *Cell Calcium*, vol. 6, no. 1–2, 1985, doi: 10.1016/0143-4160(85)90041-7.
- [132] R. Y. Tsien, "Fluorescence ratio imaging of dynamic intracellular signals.," *Acta Physiol Scand Suppl*, vol. 582, no. 6, 1989, doi: 10.1117/12.962706.
- [133] P. Ohlmann, B. Hechler, J. P. Cazenave, and C. Gachet, "Measurement and Manipulation of $[\text{Ca}^{2+}]_i$ in Suspensions of Platelets and Cell Cultures," *Platelets and Megakaryocytes: Volume 2: Perspectives and Techniques*, pp. 229–250, 2004, doi: 10.1385/1-59259-783-1:229.
- [134] P. Taggart, P. Sutton, Z. Chalabi, M. R. Boyett, R. Simon, D. Elliott, and J. S. Gill, "Effect of adrenergic stimulation on action potential duration restitution in humans," *Circulation*, vol. 107, no. 2, pp. 285–289, 2003, doi: 10.1161/01.cir.0000044941.13346.74.
- [135] G. Heusch, "Myocardial ischaemia–reperfusion injury and cardioprotection in perspective," *Nat Rev Cardiol*, vol. 17, no. 2, pp. 773–789, 2020, doi: 10.1038/s41569-020-0403-y.
- [136] S. M. Haffner, S. Lehto, T. Rönnekaa, K. Pyörälä, and M. Laakso, "Mortality from Coronary Heart Disease in Subjects with Type 2 Diabetes and in Nondiabetic Subjects with and without Prior Myocardial Infarction," *New England Journal of Medicine*, vol. 339, no. 4, 1998, doi: 10.1056/nejm199807233390404.

- [137] J. J. M. Greer, D. P. Ware, and D. J. Lefer, "Myocardial infarction and heart failure in the db/db diabetic mouse," *Am J Physiol Heart Circ Physiol*, vol. 290, no. 1, 2006, doi: 10.1152/ajpheart.00583.2005.
- [138] F. Funk et al., "Diabetes disturbs functional adaptation of the remote myocardium after ischemia/reperfusion," *J Mol Cell Cardiol*, vol. 173, pp. 47–60, 2022, doi: 10.1016/j.yjmcc.2022.09.002.
- [139] J. M. J. Pickard, S. M. Davidson, D. J. Hausenloy, and D. M. Yellon, "Co-dependence of the neural and humoral pathways in the mechanism of remote ischemic conditioning," *Basic Res Cardiol*, vol. 111, no. 4, 2016, doi: 10.1007/s00395-016-0568-z.
- [140] N. Chitnis, S. Vooturi, and B. H. Rao, "Sudden cardiac death early after ST elevation myocardial infarction with and without severe left ventricular dysfunction," *Indian Heart J*, vol. 66, no. 6, 2014, doi: 10.1016/j.ihj.2014.10.416.
- [141] D. Hasdai, C. B. Granger, S. S. Srivatsa, D. A. Criger, S. G. Ellis, R. M. Califf, E. J. Topol, and D. R. Holmes, "Diabetes mellitus and outcome after primary coronary angioplasty for acute myocardial infarction: Lessons from the GUSTO-IIb angioplasty substudy," *J Am Coll Cardiol*, vol. 35, no. 6, 2000, doi: 10.1016/S0735-1097(00)00591-X.
- [142] W. B. Kannel and D. L. McGee, "Diabetes and glucose tolerance as risk factors for cardiovascular disease: The Framingham study," *Diabetes Care*, vol. 2, no. 2, 1979, doi: 10.2337/diacare.2.2.120.
- [143] M. R. Bristow, R. Ginsburg, W. Minobe, R. S. Cubicciotti, W. S. Sageman, K. Lurie, M. E. Billingham, D. C. Harrison, and E. B. Stinson, "Decreased Catecholamine Sensitivity and β -Adrenergic-Receptor Density in Failing Human Hearts," *New England Journal of Medicine*, vol. 307, no. 4, 1982, doi: 10.1056/nejm198207223070401.
- [144] W. G. Haynes, W. I. Sivitz, D. A. Morgan, S. A. Walsh, and A. L. Mark, "Sympathetic and Cardiorenal Actions of Leptin," *Hypertension*, vol. 30, no. 3, 1997, doi: 10.1161/01.HYP.30.3.619.
- [145] M. T. Waddingham, A. J. Edgley, H. Tsuchimochi, D. J. Kelly, M. Shirai, and J. T. Pearson, "Contractile apparatus dysfunction early in the pathophysiology of diabetic cardiomyopathy," *World J Diabetes*, vol. 6, no. 7, 2015, doi: 10.4239/wjd.v6.i7.943.
- [146] E. Aasum, A. D. Hafstad, D. L. Severson, and T. S. Larsen, "Age-dependent changes in metabolism, contractile function, and ischemic sensitivity in hearts from db/db mice," *Diabetes*, vol. 52, no. 2, 2003, doi: 10.2337/diabetes.52.2.434.
- [147] S. Z. Bai et al., "Decrease in calcium-sensing receptor in the progress of diabetic cardiomyopathy," *Diabetes Res Clin Pract*, vol. 95, no. 3, 2012, doi: 10.1016/j.diabres.2011.11.007.
- [148] H. R. Cross, E. G. Kranias, E. Murphy, and C. Steenbergen, "Ablation of PLB exacerbates ischemic injury to a lesser extent in female than male mice: Protective role of NO," *Am J Physiol Heart Circ Physiol*, vol. 284, no. 2 53-2, 2003, doi: 10.1152/ajpheart.00567.2002.
- [149] T. Dieterle, M. Meyer, Y. Gu, D. D. Belke, E. Swanson, M. Iwatate, J. Hollander, K. L. Peterson, J. Ross Jr, and W. H. Dillmann, "Gene transfer of a phospholamban-targeted antibody improves calcium handling and cardiac function in heart failure," *Cardiovasc Res*, vol. 67, no. 4, 2005, doi: 10.1016/j.cardiores.2005.04.029.
- [150] E. Murphy, H. Cross, and C. Steenbergen, "Sodium regulation during ischemia versus reperfusion and its role in injury," *Circulation Research*, vol. 84, no. 12, 1999, doi: 10.1161/01.RES.84.12.1469.
- [151] P. Thérout, B. R. Chaitman, N. Danchin, L. Erhardt, T. Meinertz, J. S. Schroeder, G. Tognoni, H. D. White, J. T. Willerson, and A. Jessel, "Inhibition of the sodium-hydrogen exchanger with cariporide to prevent myocardial infarction in high-risk ischemic situations: Main results of the GUARDIAN trial," *Circulation*, vol. 102, no. 25, 2000, doi: 10.1161/01.CIR.102.25.3032.
- [152] D. R. Laver, "Ca²⁺ stores regulate ryanodine receptor Ca²⁺ release channels via luminal and cytosolic Ca²⁺ sites," in *Clinical and Experimental Pharmacology and Physiology*, 2007. doi: 10.1111/j.1440-1681.2007.04708.x.

- [153] O. A. Alabas, M. Hall, T. B. Dondo, M. J. Rutherford, A. D. Timmis, P. D. Batin, J. E. Deanfield, H. Hemingway, and C. P. Gale, "Long-term excess mortality associated with diabetes following acute myocardial infarction: A population-based cohort study," *J Epidemiol Community Health* (1978), vol. 71, no. 1, 2016, doi: 10.1136/jech-2016-207402.
- [154] T. Omura, M. Yoshiyama, K. Takeuchi, A. Hanatani, S. Kim, K. Yoshida, Y. Izumi, H. Iwao, and J. Yoshikawa, "Differences in time course of myocardial mRNA expression in non-infarcted myocardium after myocardial infarction," *Basic Res Cardiol*, vol. 95, no. 4, 2000, doi: 10.1007/s003950070051.
- [155] Y. Yang, K. Jiang, X. Liu, M. Qin, and Y. Xiang, "CaMKII in Regulation of Cell Death During Myocardial Reperfusion Injury," *Frontiers in Molecular Biosciences*, vol. 8, 2021, doi: 10.3389/fmolb.2021.668129.
- [156] B. W. Huang, M. T. Chiang, H. T. Yao, and W. Chiang, "The effect of high-fat and high-fructose diets on glucose tolerance and plasma lipid and leptin levels in rats," *Diabetes Obes Metab*, vol. 6, no. 2, 2004, doi: 10.1111/j.1462-8902.2004.00323.x.
- [157] P. P. Freire, C. A. B. Alves, A. F. de Deus, A. P. L. Leopoldo, A. S. Leopoldo, D. C. T. da Silva, L. C. de Tomasi, D. H. S. Campos, and A. C. Cicogna, "Obesity does not lead to imbalance between myocardial phospholamban phosphorylation and dephosphorylation," *Arq Bras Cardiol*, vol. 103, no. 1, 2014, doi: 10.5935/abc.20140083.
- [158] A. D. Dobrian, M. J. Davies, R. L. Prewitt, and T. J. Lauterio, "Development of hypertension in a rat model of diet-induced obesity," *Hypertension*, vol. 35, no. 4, 2000, doi: 10.1161/01.HYP.35.4.1009.
- [159] A. S. Leopoldo *et al.*, "Involvement of L-type calcium channel and SERCA2a in myocardial dysfunction induced by obesity," *J Cell Physiol*, vol. 226, no. 11, pp. 2934–2942, 2011, doi: 10.1002/jcp.22643.
- [160] N. Hariri and L. Thibault, "High-fat diet-induced obesity in animal models," *Nutr Res Rev*, vol. 23, no. 2, 2010, doi: 10.1017/S0954422410000168.
- [161] J. F. Carroll, W. J. Zenebe, and T. B. Strange, "Cardiovascular function in a rat model of diet-induced obesity," *Hypertension*, vol. 48, no. 1, 2006, doi: 10.1161/01.HYP.0000224147.01024.77.
- [162] E. Ricci, S. Smallwood, C. Chouabe, H. C. Mertani, M. Raccurt, G. Morel, R. Bonvallet, "Electrophysiological characterization of left ventricular myocytes from obese Srague-Dwley rat," *Obesity*, vol. 14, no. 5, 2006, doi: 10.1038/oby.2006.90.
- [163] J. F. Carroll, A. E. Jones, R. L. Hester, G. A. Reinhart, K. Cockrell, and H. L. Mizelle, "Reduced cardiac contractile responsiveness to isoproterenol in obese rabbits," *Hypertension*, vol. 30, no. 6, 1997, doi: 10.1161/01.HYP.30.6.1376.
- [164] D. P. Relling, L. B. Esberg, C. X. Fang, W. T. Johnson, E. J. Murphy, E. C. Carlson, J. T. Saari, and J. Ren, "High-fat diet-induced juvenile obesity leads to cardiomyocyte dysfunction and upregulation of Foxo3a transcription factor independent of lipotoxicity and apoptosis." *Journal of hypertension*, vol. 24, no. 3, pp. 549-561, 2006, doi: 10.1097/01.hjh.0000203846.34314.94.
- [165] A. S. Go *et al.*, "Heart disease and stroke statistics-2013 update: A Report from the American Heart Association," *Circulation*, vol. 127, no. 1, 2013, doi: 10.1161/CIR.0b013e31828124ad.
- [166] P. Widimsky *et al.*, "Reperfusion therapy for ST elevation acute myocardial infarction in Europe: Description of the current situation in 30 countries," *Eur Heart J*, vol. 31, no. 8, 2010, doi: 10.1093/eurheartj/ehp492.
- [167] K. A. A. Fox *et al.*, "Prediction of risk of death and myocardial infarction in the six months after presentation with acute coronary syndrome: Prospective multinational observational study (GRACE)," *Br Med J*, vol. 333, no. 7578, 2006, doi: 10.1136/bmj.38985.646481.55.
- [168] R. Schulz, M.V. Cohen, M. Behrends, J. M. Downey, and G. Heusch, "Signal transduction of ischemic preconditioning," *Cardiovascular Research*, vol. 52, no. 2, 2001, doi: 10.1016/S0008-6363(01)00384-4.

- [169] D. M. Yellon, G. F. Baxter, D. Garcia-Dorado, G. Heusch, and M. S. Sumeray, "Ischaemic preconditioning: Present position and future directions," *Cardiovascular Research*, vol. 37, no. 1. 1998. doi: 10.1016/S0008-6363(97)00214-9.

12 Resume

Personal

Name:	Srivastava
First name:	Tanu
Date of birth:	9 February 1991
Birthplace:	Dumraon, India
Nationality:	Indian

School Education

2006 – 2008	St. Karen's School, Patna (India) Senior Secondary education
1996 – 2006	Krishna Niketan School, Patna (India) Primary and Secondary education

Academic Studies

07/2012 – 05/2014	Bharti Vidyapeeth University, Pune (India) Master of Technology (M.Tech) Specification: Nanotechnology
07/2008 – 05/2012	Banasthali University, Jaipur (India) Bachelor of Technology (B.Tech) Specification: Biotechnology

Professional Experience

04/2019 – to date	Heinrich Heine University, Düsseldorf (Germany) Institute of Pharmacology and Clinical Pharmacology Ph.D. candidate
10/2018 – 03/2019	Thermo Fisher Scientific, Regensburg (Germany) R&D Intern
06/2015 – 05/2018	Karlsruhe Institute of Technology, Karlsruhe (Germany) Research Assistant

13 Acknowledgement

The presented thesis was developed during the course of my scientific activity as a research associate at the Institute of pharmacology and clinical pharmacology supervised by Prof. Dr. Joachim Schmitt. I wish to express my sincere thanks to him for his dedicated supervision, motivation and support throughout the development of my thesis.

I would like to thank Prof. Dr. Jens W. Fischer for the opportunity to do my doctorate at his institute and for the use of the institute's infrastructure.

I would like to express my sincere gratitude to Prof. Dr. Jörg Breitzkreutz for supervising my work as a co-supervisor and for constructive discussions, ideas and his professional support for my research and writing of this thesis.

Also, I am grateful to the entire working group of Prof. Dr. Krüger for the good cooperation and continuous productive support during the research project within the SFB 1116.

I would like to thank the German Research Foundation for the financial support of my work within the framework of the funding of the Collaborative Research Center 1116.

I thank to Dr. Simone Gorreßen and Mr. Dominik Semmler for their familiarization with the ischemia and reperfusion model in closed thorax.

My colleague Dr. Florian Funk deserves my appreciation for numerous discussions to improve the output of my research results and for Western blot analyses. I would further like to thank my colleague Ms. Susanne Hölzer for genotyping the mic. I am thankful to Ms. Sandra Berger, the coordinator of the SFB 1116, who was always a great help with organizational questions and in all matters.

My deep appreciation goes to my parents for their moral support and continuous motivation during my entire education and life. I sincerely thank my family and friends for their encouragement and support during my work.

Not least, I would like to thank my husband Vivek Srivastava for his continuous support, encouragement and patience during the course of this work.

Affidavit Affirmation

I declare in lieu of an oath that the dissertation has been written by me independently and without improper outside help, in compliance with the "Principles for Ensuring Good Scientific Practice at Heinrich Heine University Düsseldorf".

I assure that I have submitted this work only to the Faculty of Mathematics and Natural Sciences of the Heinrich Heine University Düsseldorf.

Düsseldorf, 05.09.2023

Tanu Srivastava